

Bending Wave Isolation in Beams and Plates with Periodic Distributed Masses and Resonant Inserts

vorgelegt von
Dipl.-Ing.
Wolfgang Weith
aus Hechingen

Von der Fakultät V - Verkehrs- und Maschinensysteme
der Technischen Universität Berlin
zur Erlangung des akademischen Grades

Doktor der Ingenieurwissenschaften
- Dr.-Ing. -

genehmigte Dissertation

Promotionsausschuss:

Vorsitzender:	Prof. Dr.-Ing. Gerd Holbach
Gutachter:	Prof. Dr.-Ing. Michael Möser
Gutachter:	Prof. Dr. rer. nat. Michael Vorländer

Tag der wissenschaftlichen Aussprache: 14. April 2014

Berlin 2014
D 83

DECLARATION

I hereby declare that this thesis has not been previously submitted as an exercise for a degree at this or any other university. Except where otherwise acknowledged, the research is entirely the work of the author.

ABSTRACT DEUTSCH

Um bei Türen und Wänden eine hohe Schalldämmung zu erreichen, ist es meist erforderlich, eine hohe Masse in Kauf zu nehmen. Im industriellen Leichtbau (Schiffs- und Flugzeugkabinen, Auto, etc.) ist der Einsatz von Masse zur Schalldämmerhöhung aus Gewichts- und Kostengründen meistens nicht umsetzbar.

In dieser Arbeit wird untersucht, ob es möglich ist, mit dem Einsatz geringer Masse eine möglichst hohe Schalldämmung bzw. eine Beeinflussung der Schallausbreitung zugunsten einer erhöhten Schalldämmung zu erreichen.

Die Ausbreitung von BiegeWellen in sog. Kettenleitern erfolgt nach den bekannten physikalischen Gesetzmäßigkeiten, die, abhängig von den gewählten Abständen der Kettenglieder zueinander, bestimmte Frequenzbereiche von BiegeWellen reflektieren (sogenannte Sperrbänder bzw. stop-bands) und andere Frequenzbereiche unbeeinflusst durchlassen (sogenannte Durchlassbänder bzw. pass-bands).

Im Gegensatz zu solchen, in periodischen Abständen unterstützten bzw. unterbrochenen Balken- und Plattensystemen (z.B. Schiene auf Schwellen, Schiffsrumpf auf Spanten, etc.), werden in dieser Arbeit die Diskontinuitäten innerhalb der neutralen Faser eines Balkens bzw. einer Platte eingebettet.

In einem ersten Schritt wird analytisch untersucht, wie zylindrische Massen, die in periodischen Abständen innerhalb oder außerhalb der neutralen Faser eines unendlichen Balkens eingebettet sind, die Ausbreitung von erzwungen angeregten BiegeWellen beeinflussen. Es kann gezeigt werden, dass bei der Einbettung innerhalb der neutralen Faser ebenfalls Durchlass- und Sperrbereiche auftreten - analog zu den bekannten in periodischen Abständen mechanisch gestützten Kettenleitern. Werden diese Massen gleichmäßig verschoben außerhalb der neutralen Faser angeordnet, spielen hinzu kommende Moment-Reaktionen eine Rolle, die die Eigenschaften der Sperr- und Durchlassbereiche verändern.

Indem nun diese Massen in eine federnde Umgebung eingesetzt werden, lässt sich zeigen, dass überwiegend die Eigenschaften der Resonanzen dieser Masse-Federsysteme die Transfer-Admittanz beeinflussen. Somit können mit einer entsprechenden Anzahl von Massen, gefederten Massen und deren geometrischen Anordnung in oder außerhalb der neutralen Faser die Sperrbereiche im Rahmen bestimmter Grenzen verschoben und erweitert werden.

Einige dieser analytisch gewonnenen Effekte können anhand von Messungen an 5m langen Holzbalken mit in Sand eingelassenen Enden zur Simulation unendlicher Länge (oberhalb eines bestimmten Frequenzbereiches) und eingebetteten Diskontinuitäten mit hoher Wahrscheinlichkeit nachgewiesen werden.

In einem zweiten Teil werden diese analytischen und experimentellen Untersuchungen auf eine Platte erweitert.

Dafür wird zunächst in der analytischen Untersuchung eine halb unendliche Platte mittig angeregt und die Transfer-Admittanz hinter konzentrisch angeordneten Winkelsegmenten bzw. Halb-Ringen aus Massen bzw. Masse-Feder-Systemen errechnet. Hierbei zeigen sich analoge Effekte zu den eindimensionalen Berechnungen des unendlichen Balkens. Werden die Diskontinuitäten in Kreisringen um den Anregepunkt herum angeordnet, können die angeregten BiegeWellen an ihrer Ausbreitung gehindert

werden, so, dass diese reflektiert werden und innerhalb der Ringe „eingesperrt“ sind. Dabei kann gezeigt werden, dass sich diese Isolationswirkung bei einer durchmischten Anordnung von Massen und gefederten Massen auf einen verbreiterten Frequenzbereich ausweiten lässt.

Messtechnische Untersuchungen auf einer 0,8m x 1m großen Plexiglas-Platte mit ringförmig angeklebten Massen bzw. federnd gelagerten Massen zeigen teils übereinstimmende, teils aber auch indifferente Ergebnisse, welche sehr wahrscheinlich von dominierenden Plattenschwingungen überlagert sind, die durch die zusätzlichen Massen und die Reflexionen an den ungedämpften Plattenrändern entstehen.

Anhand der erzielten numerischen Ergebnisse und den experimentellen Erkenntnissen am Balken kann jedoch davon ausgegangen werden, dass die hier gezeigten Methoden eine praktische Anwendung auch bei endlichen Platten wie Türen oder Wände erlauben.

In dieser Arbeit werden demnach verschiedene Möglichkeiten aufgezeigt, wie mit Massen und Feder-Masse-Systemen und einer entsprechenden Anordnung Einfluss auf die Reflexionen der sich ausbreitenden BiegeWellen genommen werden kann, sowohl im Balken als auch in der Platte.

Der Schwerpunkt liegt hierbei in den Kombinationsmöglichkeiten der untersuchten physikalischen Einflüsse Periodizität und Resonanzen, die eine gewünschte Isolation von BiegeWellen möglich machen.

ABSTRACT ENGLISH

To achieve a high level of sound insulation in doors and walls, it is usually necessary to take a high mass into account. In lightweight industrial construction (for instance ship and aircraft cabins, car body, etc.), the use of pure mass to achieve better noise insulation is mostly not feasible due to weight and cost reasons. This work will investigate whether it is possible to achieve a high sound insulation by using less mass.

Bending waves in periodic wave-guides propagate in compliance with the well-known laws of physics, which, depending on the distance of the equidistant rigid or flexible supports, leads either to bending wave reflections at certain frequency ranges (stop-bands) or to a full transmission at other frequency ranges (pass-bands).

In contrast to structures, which are supported or interrupted in periodic distances (e.g., railway sleepers, bulkheads, etc.), this work manifests its discontinuities embedded in the material of a beam or a plate.

A first step is to analyse the propagation of forced excited bending waves at an infinite beam with cylindrical masses, embedded in periodic distances within or outside the neutral layer. It can be shown that when masses are embedded in the neutral layer, pass- and stop-bands also occur - in the same way as if the beam were supported by equidistant rigid supports. If the masses were uniformly shifted and located outside the neutral layer, additional moment reactions play a role, altering the properties of both stop- and pass-bands.

If masses are coated with a rubber material, the properties of the resonances of these spring-mass systems predominantly impact transfer mobility. Thus, the attenuation in stop-bands or resonances can be shifted to a certain limit in frequency and enlarged in its amplitude with a corresponding number of masses, spring-masses, and their geometrical arrangement in or outside the neutral axis.

Some of these effects, obtained analytically, can be demonstrated at measurements with discontinuities embedded in 5m long wooden beams, having their ends covered with sand to simulate infinite length above a certain frequency range.

In a second step, these analytical and experimental studies are extended to a plate.

In the analytic investigation, a semi-infinite plate is excited in the center and the transfer mobility is calculated behind concentrically arranged angular segments or half-rings made of masses or spring-mass systems.

Here, the observed effects correspond to the one-dimensional calculations of the infinite beam. If these discontinuities are arranged in circular rings around the excitation point, the propagating bending waves are reflected by the inserts and seem to be trapped within the rings.

Hereby, it could have been shown, that a mixed distribution of masses and spring-masses increases the effect of isolation and yield a broadened frequency range.

Measurement tests were conducted on a 0.8m x 1m plate out of acrylic glass loaded with rings of adhered masses or elastically supported masses. Results partly exhibited corresponding, but also inconclusive results. The vibrations on the plate are very likely superimposed by the impact additional mass and the reflections at the undamped plate edges.

Based on the obtained 1-D and 2-D numerical results and the experimental findings on the beam, it can be assumed that the methods shown herein allow a practical application even with finite panels, such as doors and walls.

Therefore different ways in this work show how influence can be exerted on the reflections of the propagating bending waves with masses and spring-mass systems and a corresponding location, both in the beam and in the plate.

The main focus rests on possible combinations of physical effects such as periodicity and resonances, which yield a desired isolation of bending waves.

ACKNOWLEDGEMENTS

The research presented was mainly undertaken during my employment as a research and teaching assistant under Prof. B.A.T. Petersson at the Institute of Fluid Dynamics and Engineering Acoustics (ISTA) at the Technical University of Berlin.

Fragments of this thesis were presented and published at several congresses (ISVR, NOVEM, DAGA).

First and foremost, I wish to express my gratitude and appreciation to my supervisor Prof. Björn Petersson. I want to thank him for our many enlightening discussions, his incredible ability to motivate, even when sometimes the results discussed were far away from what was expected. His support and assistance were invaluable; I never have experienced a professor whose door was so, unfailingly open.

Numerous people assisted me in the preparation of this work. First of all I want to thank my colleagues from Rolls-Royce Deutschland, especially Olaf Lemke, who showed me that it was possible to finalise a PhD while having a full-time - and sometimes very stressful - job. I also wish to thank all postgraduates at the ISTA, particularly Roman Tschakert, Michael Stütz and Dominic Gutsche, who were very helpful in answering my questions and supporting me in all issues that arose from the beginning. I also wish to thank all the technicians at the department for their assistance along the way, especially Mr Schirmeier, and to add a special thanks to our secretaries, who were always helpful, even years after my employment at the Institute.

My largest debt of thanks is owed to my parents and my brothers for their willingness to sacrifice, for their support on my way to finalizing this work, and for enabling my academic career.

In particular, I wish to thank Olha. Without her great support and patience, her critical analyses and her clear statements bringing me back to reality, this PhD thesis would never have been written. There are also my children, who suffered most during this period. My son Vadim, who once suggested I buy a shredder for my “Doktorarbeit”, is especially brave, and I’m proud of him.

Last but not least, although my work shows that *infinite* structures are better for securing sufficient results, I want to thank Prof. Michael Möser, who has overtaken the supervision of this work in the last three years. His support and openness helped me achieve my goal of bringing this thesis to a condition that is *finite*.

TABLE OF CONTENT

ABSTRACT DEUTSCH	5
ABSTRACT ENGLISH	7
ACKNOWLEDGEMENTS.....	9
TABLE OF CONTENT	10
1 AN INTRODUCTION	13
2 LIST OF SYMBOLS	20
3 ABBREVIATIONS	23
4 CALCULATIONS ON BEAMS WITH EMBEDDED RIGID OR FLEXIBLE INSERTS	24
4.1 INTRODUCTION TO THE STUDY ON BEAMS	24
4.2 FORMULATION	26
4.2.1 IMPEDANCES.....	29
4.2.2 PARAMETERS.....	31
4.3 NUMERICAL INVESTIGATION	32
4.3.1 HOMOGENEOUS INFINITE BEAM WITH MASSES IN THE NEUTRAL LAYER	32
4.3.2 HOMOGENEOUS INFINITE BEAM WITH RUBBER-COATED MASSES IN THE NEUTRAL LAYER.....	38
4.3.3 HOMOGENEOUS INFINITE BEAM WITH PURE AND RUBBER- COATED MASSES IN THE NEUTRAL LAYER	42
4.3.4 HOMOGENEOUS INFINITE BEAM WITH MASSES OUT OF THE NEUTRAL LAYER.....	47
4.3.5 HOMOGENEOUS INFINITE BEAM WITH RUBBER-COATED MASSES OUT OF THE NEUTRAL LAYER	49
4.4 SUMMARY OF THE CALCULATIONS ON A BEAM	52
5 MEASUREMENTS ON SLENDER BEAMS WITH EQUI- SPACED RIGID OR FLEXIBLE INSERTS.....	53
5.1 PREPARATION OF THE MEASUREMENTS WITH A SLENDER BEAM	53
5.1.1 PRELIMINARY INVESTIGATION OF AN APPROPRIATE RUBBER MATERIAL	53
5.1.2 PRE-TEST MEASUREMENTS WITH RUBBER-COATED MASSES EMBEDDED INTO BEAM PIECES	54
5.2 MEASUREMENTS ON A SLENDER BEAM.....	60
5.3 MEASUREMENT RESULTS OF A SLENDER BEAM.....	65
5.3.1 REPEATABILITY CHECK.....	65

5.3.2	MEASUREMENT RESULTS OF A BEAM WITH HOLES	66
5.3.3	MEASUREMENT RESULTS OF A BEAM WITH MASSES	66
5.3.4	MEASUREMENT RESULTS OF A BEAM WITH RUBBER-COATED MASSES	71
5.3.5	RESONANCE AND STOP-BAND INVESTIGATION WITH PHASES AND COHERENCES	73
5.3.6	SUMMARY OF DISCUSSED OBSERVATIONS OF TRANSFER MOBILITY, PHASES AND COHERENCES ON MEASUREMENTS WITH BEAMS	90
6	SUMMARY OF OBSERVATIONS WITH CALCULATIONS AND MEASURED RESULTS OF BEAMS	92
6.1	SUMMARY OF OBSERVATIONS WITH PURE MASSES EMBEDDED IN A BEAM	92
6.2	SUMMARY OF OBSERVATIONS WITH RUBBER-COATED MASSES EMBEDDED IN A BEAM	93
6.3	SUMMARY OF THE GENERAL OBSERVATIONS WITH INSERTS EMBEDDED IN A BEAM	95
7	CALCULATIONS ON INFINITE PLATES WITH EQUI- SPACED RIGID OR FLEXIBLE INSERTS	96
7.1	INTRODUCTION TO THE STUDY ON PLATES	96
7.2	FORMULATION FOR A PLATE WITH INSERTS	96
7.3	NUMERICAL CALCULATIONS ON PLATES WITH INSERTS	97
7.4	SUMMARY OF CALCULATIONS ON A PLATE WITH PURE MASSES AND RESONANT INSERTS	107
8	MEASUREMENTS ON A FINITE PLATE WITH MASSES AND ELASTICALLY SUPPORTED MASSES	109
8.1	PREPARATIONS OF THE MEASUREMENTS ON A PLATE	109
8.2	MEASUREMENT SET-UP OF A FINITE PLATE WITH MASSES AND ELASTICALLY SUPPORTED MASSES	113
8.3	MEASUREMENT RESULTS OF A FINITE PLATE WITH MASSES AND ELASTICALLY SUPPORTED MASSES	119
8.4	SUMMARY OF THE MEASUREMENTS ON A THIN, FINITE PLATE	128
9	CONCLUDING REMARKS	129
10	OUTLOOK	131
11	ATTACHMENTS	133
11.1	ADDITIONAL PARAMETER STUDY OF AN INFINITE HOMOGENOUS BEAM WITH INSERTS	133

11.1.1	LOSS FACTOR OF THE BEAM AND YOUNG’S MODULUS	133
11.1.2	LOSS FACTOR OF THE RUBBER COATING	134
11.1.3	IMPACT OF THE WEIGHT OF MASSES ONTO THE ATTENUATIONS IN THE TRANSFER MOBILITY	136
11.2	ERROR INVESTIGATION.....	138
12	REFERENCES	140
13	LIST OF TABLES	149
14	LIST OF FIGURES	150

1 AN INTRODUCTION

Worldwide noise pollution mainly signifies construction, motor noise, aircraft noise, and rail noise.

Airborne noise can be generated directly or indirectly. For instance, in an aircraft engine, the interaction between the wakes from a rotating Fan with the vanes of an outlet guide directly results in the propagation of airborne noise. On the other hand, many other audible sources - the neighbours' constant hammering, for example - have their roots in structure-borne sound. The vibrations resulting from the wall being pounded by your neighbour's hammer are transmitted to our room by the elements of structure in the building. The affected walls, the ceiling, and the floor in our room excite the adjacent air to vibrate as well. Finally this airborne sound propagates through the room and reaches our ears.

In cases, whether airborne sound is excited directly or indirectly, it is one of the main interests of an acoustic engineer to investigate and, accordingly, reduce the impact of the sound source itself.

Various airborne sound absorbers are available for all kinds of applications and frequency ranges. In the example of the hammering neighbours, well-defined absorbers in our room allow for a reduction of the airborne sound within certain limits.

As it is often not possible to reduce the impact of the source itself, it could be better to reduce the structure-borne sound on its way to our room.

The noise source should be insulated, which is easily accomplished by increasing the mass of the transition paths or decoupling them using 2 plasterboards sandwiched with absorption material. However, it is often not possible to increase the masses of transition paths or to use large absorption walls. Thus, such solutions might not be very welcome in many situations. Most vehicles, for instance, are designed to be as lightweight as possible. Therefore, it would be more advantageous to reflect or isolate incoming bending waves and minimise the emission of noise without increasing the space or the masses.

PERIODIC STRUCTURES

In periodic structures, e.g. railways with evenly distributed rigid supports, the propagating waves are reflected at each element and only propagate freely in certain frequency bands, while in others they decay. As pointed out by Brillouin [8] in his classic work about periodic structures, Newton [78] started the investigation of vibrational behaviour on periodic structures more than 300 years ago. He tried to derive a formula for the velocity of sound on a one-dimensional lattice. Since that time many

studies of periodicities in crystals, optics, electrical transmission lines and also in solid structures such as beams and plates have been researched¹.

Heckl [31] has shown, that “waves in periodically supported, undamped beams can only propagate freely (without decaying) in certain frequency bands”. Furthermore, “simple sinusoidal waves cannot propagate independently along multi-supported beams. Reflections occur at each support and ‘near-field’ wave effects also exist” (Mead [69] p. 182).

Mead [69] explained the existence of propagating and non-propagating waves with the phases of the vibration of adjacent bays. If there is no difference between the motions in adjacent bays or if they vibrate exactly in counter-phase, the wave is of non-propagating form. Thus, no wave energy is transmitted and the wave motion decays along the beam. Next to this frequency exists another band in which free wave propagation again is possible. These bands of propagating (pass-band) and non-propagating (stop-band) free waves are alternating, which was first described by Cremer and Leilich [13]. Mead also pointed out that “the free harmonic motion of an undamped infinite beam on regularly spaced identical supports may be regarded as a group of sinusoidal waves, travelling in different directions and at different speeds” (Mead [69] p. 196)².

Blanc [6] explained the non-propagating waves in periodic beams with standing waves: “At certain frequencies, the reflected waves interfere with the incoming waves and create a standing wave within a structural period. As a result of standing waves, energy does not propagate along the structure” (Blanc [6] p. 21). He also pointed out, that a length disorder can be used to broaden the pass-band.

DISORDERED/RANDOMISED DISTRIBUTION

Hodges and Woodhouse [40] found out in a simple experiment with a string and equally distributed masses attached to it that the phenomenon of Anderson localisation also works in an acoustical context. Moving the masses in a controlled way to provide a small irregularity leads to a reduction in the vibration level. According to Heckl [32] no pass-bands exist if the periodic system is disturbed, but therefore the nearfield decay is extended along the host structure.

Bansal [5] also investigated “the effect of different amounts of disorders on free flexural wave motion in undamped beam-type systems consisting of finite multi-span repeating units that are disordered”. He approved that “the presence of disorders normally interferes with free wave motion and narrows down the effective frequency bands of

¹ With periodic structures, it is even possible to attenuate sound in air, as Martínez-Sala et al. [66] demonstrated, obtained from a mass of trees by arranging them in a periodic lattice. Alagoz [1] used a two-dimensional sonic crystal triangular lattice made of rods to show reflective conditions in audible frequency ranges.

² This implies the side-effect, that the acoustic coincidence effect can be shifted to much lower frequencies.

free wave propagation”. But, he also explained, that “the transmission of waves can be controlled” and even the free wave propagation in certain frequency bands be broadened “by introducing appropriate disorders” (Bansal [5] p. 365).

Bouzit and Pierre [7] experimentally demonstrated “that the transmission of vibration which takes place within the frequency pass-bands of the periodic beam is greatly hindered when span length randomness is introduced” [p. 649]. In addition, they also found that at most frequencies in the pass-bands the spatial decay due to damping in the ordered beam was negligible compared to the spatial decay due to disorder in the disordered beam [p. 664].

Coming back to strictly ordered systems, “periodic beams have been a subject of special interest due to their common usage in several engineering applications. Based on the type of periodicity, they can be classified under the following two general categories: Beams with geometric/material periodicity and beams resting on equispaced supports. Most of the efforts so far to model dynamically periodic beams have been spent on the characterizations of the second category” (Hawwa [30] p. 453).

MATHEMATICAL MODELS

Heckl [31] and his daughter Maria [35] investigated the existence of different wave types in periodic structures. Maria Heckl [35] presented a mathematical model for the propagation of structural waves on an infinite long, periodically supported beam. The wave types considered were bending waves with displacements in the horizontal and vertical directions, compressional waves and torsional waves. She displayed two effects: The impact of stop- and pass-bands as well as couplings of the different waves.

A number of authors have produced various mathematical models to calculate the wave behaviour in periodic structures (e.g. Mead [68] [69] [70] [71], Mace [61]). Heckl [32] presented four different methods for the calculation of structure borne sound propagation on beams with many discontinuities. The method which is based on equivalent sources will be used in this thesis for the numerical study on a one-dimensional Euler-Bernoulli beam and on a two-dimensional thin plate (see Chap. 4 and 7). It will be shown, that this mathematical description will also work for inserts, which are embedded in the neutral layer of a beam or a plate³.

RESONANT SUPPORTS AND INSERTS

“In a typical ship, the main propulsion and auxiliary machinery, the bulkheads decks, piping, cargo, fuel, etc. comprise more than twice mass of the hull and the same is true for many aerospace mainframes. None of these substructures are attached to the main structure in a completely rigid manner and so they behave as ‘sprung masses’, each with

³ Heckl, Maria [35] used Hamilton’s principle (Cremer and Heckl [12]) to calculate the Green’s function matrix of the Timoshenko beam. According to Thompson [92] the attenuation in Timoshenko beams is slightly increased with rising frequency in comparison with Euler-Bernoulli beams. Thus, the use of an Euler-Bernoulli beam seems to be appropriate in determining attenuation with regard to a conservative appraisal.

one or more frequencies of resonance. If several of them have resonances at frequencies near the frequency of vibration, they can absorb and dissipate considerable vibratory power from the main structure” (Strasberg and Feit [89] p. 335).

Thus, it is of great interest in this thesis to involve spring-masses in the investigation of periodic structures. Furthermore, Strasberg and Feit [89] calculated the damping induced by substructures attached to an axially vibrating rod and to a flexurally vibrating beam. They reviewed the frequency dependence of the driving point impedance of a spring-mass and displayed the possibility of a “small and lightly damped spring-mass to introduce considerable damping into a much more massive structure”. This paradoxical inverse relation between the damping of the attached spring-mass-systems and the dissipation in the structure “may be understood by noting that as the damping becomes smaller, the vibratory motion of the mass and accompanying deformation of the spring become larger, for constant motion of the drive point, and the power dissipated in the spring is proportional to the square of its maximum deformation” [p. 336]. Furthermore, the impedance change at the location of the vibration absorber lead to reflected and scattered bending waves. However, the reflection or dissipation with a low damped spring-mass only works at the frequency near to resonance.

“To induce damping over a wide range of frequencies, many spring-mass frequencies distributed over that range are required” (Strasberg and Feit [89] p. 335). In their work the vibration have been limited to one direction only and effects of periodicity and moment reactions have not been considered.

Alsaif and Foda [2] developed a “method based on the dynamic Green functions to determine the optimum values of masses and/or springs on their locations on a beam structure in order to confine the vibration at an arbitrary location” [p. 629]. They verified in measurements, that the “vibrations of both simply supported and cantilevered beams can be controlled at an arbitrary location within the beam with a minimum value of attached masses or springs. The optimum locations of the masses are found to be at peaks or troughs of the flexural wave of the unloaded beam forced response” [p. 645].

Since the year 2000 a lot of research has been applied with the so called “locally resonant sonic materials”. Liu et al. [55] came up with a fabricated sonic crystals consisting of small spheres with a heavy core and a soft cladding layer. Each of these coated spheres has inherent mechanical resonance, when embedded in a matrix medium. Sound waves in the material can be totally reflected within some tuneable sonic frequency ranges, which are verified on measurements with resonances at low frequencies. According to Hirsekorn et al. [39] “sonic crystals are artificial structures consisting of a periodic array of acoustic scatterers embedded in a homogeneous matrix material, with a large impedance mismatch between the two materials” [p. 1].

“Sound transmission loss measurements on an epoxy plate containing lead spheres with a silicon-rubber coating show remarkable improvements over the mass law” (Maysenhölder [67] p. 1). These “periodic realisations of elastic heterostructures, called ‘phononic crystals’, make it possible for the achievement of complete elastic wave band gaps within which sound and vibrations are all forbidden. These new materials can be of

real interest because of the rich physics of acoustic and elastic systems, where the wave can have mixed longitudinal and transverse modes” (Wang et. al. [95] p. 1).

According to Bragg’s mechanism (having stop- and pass-bands in a periodic structure) it is “hardly to achieve low frequency band gaps with small dimensions, because the wavelength of low frequency elastic wave in common solids is long” (Wang et al. [96] p. 167). Thus, making them resonating by embedding these masses in very soft rubber, are most likely to obtain low-frequency gaps with structures of small dimension (Wang et al. [95]). The numerical study of these “locally resonant phononic crystals”, attached to the top of a beam, occurred with an Euler beam and considered flexural (bending) waves only⁴. Nevertheless, experimental results agreed very well and showed, that if the lattice constant is larger than the height and width of a beam, shearing deformation and the rotational inertia of the cross section are negligible.

In a recently published article about the coupling of resonances and Bragg scattering effects Yuan et al. [110] describe the enhancement of attenuation bands with locally resonant sonic materials, although in a low frequency region employing shear stresses.

In almost all publications of sonic crystals the resonance frequency is set below the 1st stop-band. The interaction of stop-bands within a resonance band gap or above is not investigated in detail and will be part of the observations in this work (see sub-section 4.3.2). It will be shown, that the coupling of stop-bands and resonant band gaps using a mixed lattice with masses and spring-masses increases the attenuated high frequency bandwidth at an infinite plate (see Chapter 7).

In all investigations with resonant units, the damping factor⁵ of the spring plays a major role. Conventional passive tuned vibration absorbers are mainly used to reduce motion at a certain frequency and are preferably positioned at the anti-node of the modal host structure (Jolly and Sun [44]). By increasing the damping factor of the spring, the effective magnitude at the resonance frequency is reduced, but a broader band of frequencies near the resonance can be achieved. Vibration absorbers with a low damping factor show a large attenuation in a very narrow frequency band at or near the resonance.

Hettler [38] investigated the effects of internal resonators in sandwich constructions to improve the sound insulation with the least possible mass increase. He successfully applied internal resonators to finite, lightweight double-panel structures for increasing sound reduction at low frequencies at the mass-air-mass resonance. The use of different-tuned low damped absorbers yielded a larger sound reduction than having absorbers with increased damping.

⁴ In some of the literature used the distances of phononic crystals in a lattice is called “lattice constant”. “Locally resonant phononic crystals” are sonic crystals, which become resonant by being embedded in a rubber material.

⁵ The damping factor of the spring is also called “loss factor of the spring” or “dissipation factor of the spring”.

It is obvious that this thesis should give attention to a couple of vibration absorbers with low damping factors, each tuned to a different resonance, embedded in the host structure to achieve a broadened and large attenuation band. As mentioned above, the transmitted energy in the structure is partly dissipated, but mainly damped by being reflected due to the impedance change at the vibration absorbers.

This short overview of existing literature on masses and resonant units⁶ attached or embedded in beams and plates is far from being complete. A more detailed list can be reviewed in the References (Chap. 12).

However, there is no available literature that lists the possibilities of combined effects having changed periodicity, resonances and moment reactions. Based on parameter studies and measurement results this PhD thesis will offer an overview on the effects appearing. The main focus is the following question: which combinations and distributions of embedded masses and spring-masses are sufficient to isolate bending waves in beams and plates.

STRUCTURE OF THIS THESIS

The examination begins with a numerical study of several inserts of varying impedances and positions in an infinite beam (Chap. 4).

If the calculations are made with the theory for an Euler-Bernoulli beam and the method which is based on equivalent sources (Heckl [32]), the embedded masses or spring-masses can be seen as if they were attached to the beam.

To verify the observed effects with measurements on a beam, a suitable rubber material had to be found through experimental investigation with different beam pieces. These pre-test measurements and up-following measurements on a real beam with different masses and spring-masses inserted within or out of the neutral layer are described in Chapter 5. Some of the main conclusions of the numerical study are verified by measurements on a beam with embedded inserts with damped ends (Chap. 5). Additional investigation of the measured transfer mobility at phases and coherences increases confidence in main conclusions.

All results of the numerical and experimental research at the beam with inserts are listed in Chapter 6.

Calculations on a half-infinite plate with embedded masses and spring-masses distributed in circles are described in Chapter 7. Main parts of this Chapter have been published by Weith and Petersson at the RASD conference in Southampton 2006 [98]. In Chapter 8 measurement results with masses and spring-masses attached to both sides of a finite plate suggest the complexity of a practical use.

⁶ The resonant inserts used in this thesis will be called spring-masses or spring-mass systems, independent of their locations and damping factors. As is described in this chapter, many other expressions - such as "vibration absorbers", "vibration neutralizers", "sonic crystals" or "locally resonant phononic crystals" - exist in the literature.

The main observations of the numerical study and the measurements at beams and plates are summarised in the *Concluding Remarks* (Chap. 9).

However, several ways to improve the findings of this PhD thesis are discussed in the *Outlook* (Chap. 10).

In *Attachments* (Chap. 11) additional side-effects of the material properties are displayed and an error investigation is discussed.

References are listed in alphabetical order of authors in Chapter 12. Sources, which are not referenced in this thesis, were additionally studied to create this work and may be used to provide the reader with a deeper insight and better overview of the diversity of periodic structures.

All numerical studies and appraisals of the measurement results have been conducted with MATLAB.

Although the objective of vibration damping is to reduce the sound propagation in air, calculations or measurements of the sound power transmitted from the observed host structures to the fluid have not been applied. Considering primarily investigations on infinite structures, I'd like to cite Arthur Blanc (Blanc [6] p. 21), who pointed out that "if no waves propagate in an infinite structure, no sound is radiated in the far field".

2 LIST OF SYMBOLS

UPPER CASE LATIN LETTERS

B	<i>Bending stiffness of a beam</i>
B'	<i>Bending stiffness of a plate</i>
E	<i>Complex Young's modulus</i>
E_{real}	<i>Young's modulus (real part)</i>
F	<i>Frequency</i>
F_0	<i>Excitation force</i>
F_{mass}	<i>Excitation force on a mass</i>
$F_{spring-mass\ system}$	<i>Excitation force on a spring-mass system</i>
F_r	<i>Frequency resolution</i>
F_μ	<i>Substituted force an insert</i>
F_v	<i>Resulting force on an insert</i>
$G_F(x, x_{00})$	<i>Green's function (force) of a pure beam with excitation at x_{00}</i>
$G_F(x, x_v)$	<i>Green's function (force) of a beam with inserts with excitation at x_v</i>
G_{Konst}	$G_{Konst} = \frac{\omega}{4Bk^3}$
$G_M(x, x_v)$	<i>Green's function (moment) of a beam with inserts with excitation at x_v</i>
$H_0^{(2)}$	<i>Hankel function of the second kind</i>
M_{mass}	<i>Moment of a mass</i>
$M_{spring-mass\ system}$	<i>Moment of a spring-mass system</i>
M_μ	<i>Substituted moment an insert</i>
M_v	<i>Resulting moment on an insert</i>
N	<i>Natural number</i>
X	<i>Position on a plate</i>
X_S	<i>Excitation point on a plate</i>
X_μ	<i>Distance in X-direction from excitation point to the insert on a plate</i>
X_v	<i>Distance in X-direction from excitation point to the arbitrary insert on a plate</i>

LIST OF SYMBOLS

Y	<i>Transfer mobility</i>
$Z_{F, mass}$	<i>Impedance of a mass, excitation by a force</i>
$Z_{F, spring-mass}$	<i>Impedance of a spring-mass, excitation by a force</i>
$Z_{M, mass}$	<i>Impedance of a mass, excitation by a moment</i>
$Z_{M, spring-mass}$	<i>Impedance of a spring-mass, excitation by a moment</i>
Z_{F_μ}	<i>Impedance of the substituted force of an insert</i>
Z_{M_μ}	<i>Impedance of the substituted moment of an insert</i>

LOWER CASE LATIN LETTERS

a	<i>Acceleration</i>
b	<i>Width of the beam</i>
$dist$	<i>Distance between two inserts</i>
f_{res}	<i>Resonance frequency</i>
f_λ	<i>Frequency of a stop-band</i>
h	<i>Height of the beam/plate</i>
m	<i>Mass</i>
m'	<i>Mass per unit length (beam)</i>
m''	<i>Mass per unit area (plate)</i>
n	$n=1,2,3 \dots \in N$
k	<i>Wave number</i>
r_{NL}	<i>Distance of the inserts to the neutral layer</i>
s, s_{spring}	<i>Complex stiffness of the spring</i>
s_0	<i>Stiffness of the spring</i>
v	<i>Velocity</i>
$v(x)$	<i>Velocity at position x</i>
$v(x_\mu)$	<i>Velocity of an insert</i>
w	<i>Rotational velocity</i>
$w(x)$	<i>Rotational velocity at position x</i>
$w(x_\mu)$	<i>Rotational velocity of an insert</i>
x	<i>Position x at the beam, plate</i>

LIST OF SYMBOLS

x_{00}	<i>Excitation point at the beam</i>
x_{μ}	<i>Distance in x-direction from excitation point to the insert at a beam</i>
x_v	<i>Distance in x-direction from excitation point to the arbitrary insert at a beam</i>
y	<i>Position y at the plate</i>

GREEK LETTERS

α_1, α_2	<i>Angles at both sides of ω_0 in Nyquist plot to calculate the damping factor of a spring</i>
η_{beam}	<i>Loss factor of the beam</i>
η_{plate}	<i>Loss factor of the plate</i>
η_{spring}	<i>Loss factor of the rubber coating</i>
λ_B	<i>Wavelength of the bending waves</i>
$\lambda_{stop-band}$	<i>Wavelength of the bending waves at stop-band-frequencies</i>
μ	<i>Poisson's ratio</i>
μ	<i>Index of the inserts substituted by a force and moment</i>
v	<i>Index of the arbitrary inserts</i>
ρ	<i>Density</i>
ω	<i>Angular velocity</i>
ω_0	<i>Angular velocity corresponding to the maximum sweep angular velocity (resonance in Nyquist plot)</i>
ω_1, ω_2	<i>Angular velocities in Nyquist plot to calculate the damping factor of a spring</i>

3 ABBREVIATIONS

DAGA	Tagung der Deutschen Arbeitsgemeinschaft für Akustik
DEGA	Deutsche Gesellschaft für Akustik e.V.
FTT	Fast Fourier Transformation
NOVEM	Noise and Vibration: Emerging Methods
PUR	Polyurethane (2- and 3component castable resins have been used as rubber material in beams and on a plate)
PVC foam	Polyvinyl chloride foam is a light-weight material used as a rubber material.
ISTA	Institute of Fluid Dynamics and Engineering Acoustics (ISTA), Technical University of Berlin
ISVR	Institute of Sound and Vibration Research, University of Southampton
OROS	OROS – Measuring Noise & Vibration, Data acquisition system
RASD	Recent Advances in Structural Dynamics
ShA	Shore hardness (with 2- and 3-component liquids various Shore hardness of a rubber material could have been produced)

4 CALCULATIONS ON BEAMS WITH EMBEDDED RIGID OR FLEXIBLE INSERTS

4.1 INTRODUCTION TO THE STUDY ON BEAMS

The wave propagation in beams with equi-spaced rigid or flexible supports (Figure 1) have been frequently addressed and researched (see Chap. 1)⁷.

By using evenly distributed rigid supports the waves can only propagate freely in certain frequency bands, whereas in the so called stop-bands they decay. These stop- and pass-bands alternate over the frequency.

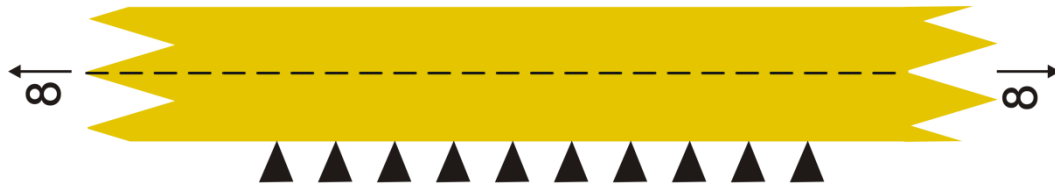


Figure 1: Infinite beam with evenly distributed rigid supports.

One of the main interests in this study is the investigation of the propagation in a homogenous slender beam with equi-spaced rigid or flexible supports, which are embedded within the beam (Figure 2). If the calculations are made with the theory of an Euler-Bernoulli-beam, the embedded inserts can be seen as were they attached to the beam.

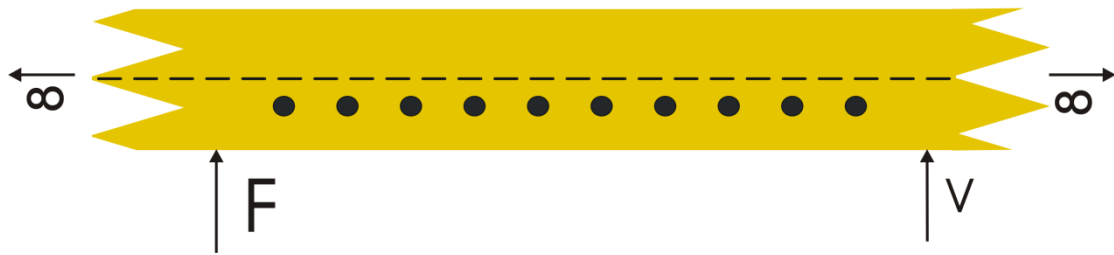


Figure 2: Infinite beam with evenly distributed embedded masses within the beam (in this case out of the neutral layer). The transfer mobility is derived by locating the driving point before the first discontinuity and registering the velocity behind the last insert.

However, bringing them into the neutral layer of the beam makes the moment reactions vanish (Figure 3).

⁷ Fragments in this chapter have been published by Weith and Petersson in [99], [101] and [102]

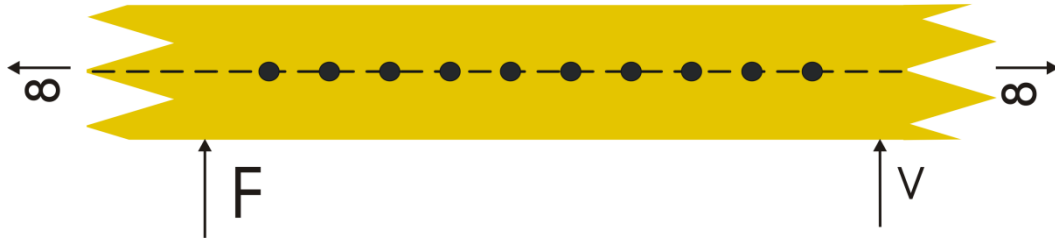


Figure 3: Infinite beam with evenly distributed embedded masses in the neutral layer.

It will be shown, that if these masses were coated with rubber (Figure 4), the attenuation at the resonance becomes in a considerable increased, whereas the stop- and pass-bands above the resonance frequency nearly vanish.

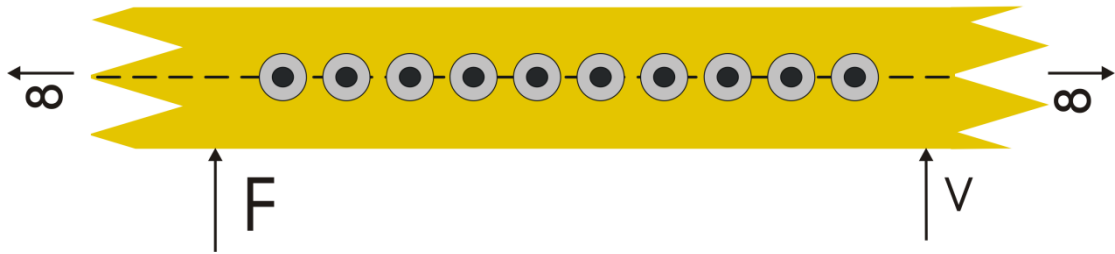


Figure 4: Infinite beam with evenly distributed rubber-coated masses in the neutral layer.

Changing the stiffness of the rubber coating of each insert broadens the attenuated frequency range (Figure 5).

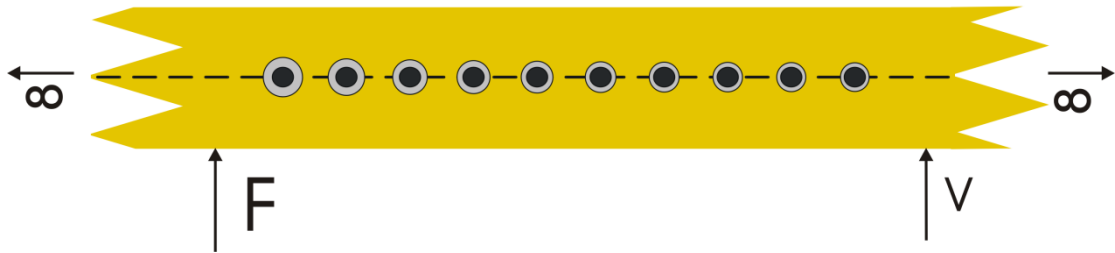


Figure 5: Infinite beam with evenly distributed rubber-coated masses with increasing stiffnesses⁸ in the neutral layer.

Bringing them out of the neutral layer, additional moment effects arise, which compromises the attenuation, but gives another opportunity to change the behaviour of the propagating bending waves (Figure 6).

⁸ In case of varying stiffness of the resonant inserts the plural of stiffness („stiffnesses“) will be used.

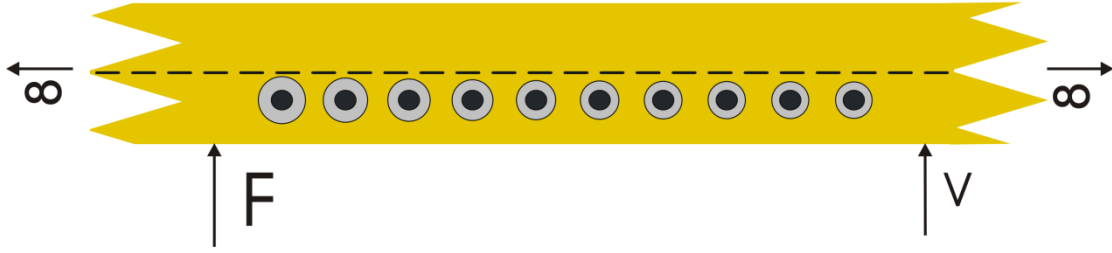


Figure 6: Infinite beam with evenly distributed rubber-coated masses with increasing stiffnesses displaced from the neutral layer.

It will be shown, that the attenuation can be influenced with the variation of following parameters:

- Weight of the masses
- Stiffness of the rubber coating
- Damping factor of the rubber coating
- Distribution of the inserts in axial direction
- Distribution of the inserts in vertical direction in distance to the neutral layer

4.2 FORMULATION

Following Cremer and Heckl [32] employing Euler-Bernoulli-theory, the governing set of equations can be written as⁹:

$$v(x) = \frac{\omega}{4Bk^3} \left[F_o G_F(x, x_{00}) - \sum_{v=1}^N F_v G_F(x, x_v) - \sum_{v=1}^N k M_v G_{F_v}(x, x_v) \right] \quad (1)$$

and

$$w(x) = \frac{\partial v(x)}{\partial x} = \frac{-\omega}{4Bk^2} \left[F_o G_{M_v}(x, x_{00}) - \sum_{v=1}^n F_v G_{M_v}(x, x_v) - \sum_{v=1}^N k M_v G_M(x, x_v) \right]. \quad (2)$$

The discontinuities are substituted by the forces and moments resulting, which are applied to the uniform beam (equation (1) and (2)). G_F , G_{F_v} , G_M and G_{M_v} are the Green's functions pertaining to the point excited, infinite beam:

⁹ In accordance to Prof. B.A.T. Petersson, who was supervising this PhD thesis, the moment reactions of the inserts in equation (1) are set to be against the initial forces. Thus, the algebraic sign of the moment reactions in equation (1) has been changed in comparison to Heckl's formulation [33].

$$G_F(x, x_v) = e^{-jk|x-x_v|} - je^{-k|x-x_v|} \quad (3)$$

$$G_M(x, x_v) = e^{-jk|x-x_v|} + je^{-k|x-x_v|} \quad (4)$$

$$G_{M_v}(x, x_v) = j(e^{-jk|x-x_v|} + e^{-k|x-x_v|}) \operatorname{sgn}(x - x_v) = -G_{F_v} \quad (5)$$

$$\operatorname{sgn}(x - x_v) = \begin{cases} -1 & \text{for } x < x_v \\ +1 & \text{for } x > x_v \end{cases} \quad (6)$$

With the responses of the possibly differing discontinuities expressed in terms of the associated impedances as

$$F_\mu = v(x_\mu)Z_{F_\mu}; \quad 1 \leq \mu \leq N \quad (7)$$

and

$$M_\mu = w(x_\mu)Z_{M_\mu}; \quad 1 \leq \mu \leq N. \quad (8)$$

The set of linear equations for the solution of the unknown auxiliary force and moments can be written as

$$\frac{F_\mu}{Z_{F_\mu}} + \frac{\omega}{4Bk^3} \left[\sum_{v=1}^N F_v G_F(x_\mu, x_v) - \sum_{v=1}^N k M_v G_{M_v}(x_\mu, x_v) \right] = F_0 \frac{\omega}{4Bk^3} G_F(x_\mu, x_{00}) \quad (9)$$

and

$$\frac{M_\mu}{Z_{M_\mu}} + \frac{-\omega}{4Bk^2} \left[\sum_{v=1}^N F_v G_{M_v}(x_\mu, x_v) + \sum_{v=1}^N k M_v G_M(x_\mu, x_v) \right] = F_0 \frac{-\omega}{4Bk^2} G_{M_v}(x_\mu, x_{00}). \quad (10)$$

By means of this set of $2N$ equations, the unknown auxiliary forces and moments can be solved for and subsequently be substituted into equations (1) and (2) to obtain the vibration field of the periodic structure:

Equation (11):

$$\begin{bmatrix} F_1 \\ F_2 \\ \vdots \\ F_\mu \\ M_1 \\ M_2 \\ \vdots \\ M_\mu \end{bmatrix} \bullet \begin{bmatrix} \frac{1}{Z_{F1}} + G_{Konst} G_F(x_1, x_1) & G_{Konst} G_F(x_1, x_2) & \cdots & G_{Konst} G_F(x_1, x_\nu) & -kG_{Konst} G_{M\nu}(x_1, x_1) & -kG_{Konst} G_{M\nu}(x_1, x_2) & \cdots & -kG_{Konst} G_{M\nu}(x_1, x_\nu) \\ G_{Konst} G_F(x_2, x_1) & \frac{1}{Z_{F2}} + G_{Konst} G_F(x_2, x_2) & \cdots & G_{Konst} G_F(x_2, x_\nu) & -kG_{Konst} G_{M\nu}(x_2, x_1) & -kG_{Konst} G_{M\nu}(x_2, x_2) & \cdots & -kG_{Konst} G_{M\nu}(x_2, x_\nu) \\ \vdots & \vdots & \vdots & \vdots & \vdots & \vdots & \vdots & \vdots \\ G_{Konst} G_F(x_\mu, x_1) & G_{Konst} G_F(x_\mu, x_2) & \cdots & \frac{1}{Z_{F\mu}} + G_{Konst} G_F(x_\mu, x_\nu) & -kG_{Konst} G_{M\nu}(x_\mu, x_1) & -kG_{Konst} G_{M\nu}(x_\mu, x_2) & \cdots & -kG_{Konst} G_{M\nu}(x_\mu, x_\nu) \\ -kG_{Konst} G_{M\nu}(x_1, x_1) & -kG_{Konst} G_{M\nu}(x_1, x_2) & \cdots & -kG_{Konst} G_{M\nu}(x_1, x_\nu) & \frac{1}{Z_{M1}} - k^2 G_{Konst} G_M(x_1, x_1) & -k^2 G_{Konst} G_M(x_1, x_2) & \cdots & -k^2 G_{Konst} G_M(x_1, x_\nu) \\ -kG_{Konst} G_{M\nu}(x_2, x_1) & -kG_{Konst} G_{M\nu}(x_2, x_2) & \cdots & -kG_{Konst} G_{M\nu}(x_2, x_\nu) & -k^2 G_{Konst} G_M(x_2, x_1) & \frac{1}{Z_{M2}} - k^2 G_{Konst} G_M(x_2, x_2) & \cdots & -k^2 G_{Konst} G_M(x_2, x_\nu) \\ \vdots & \vdots & \vdots & \vdots & \vdots & \vdots & \vdots & \vdots \\ -kG_{Konst} G_{M\nu}(x_\mu, x_1) & -kG_{Konst} G_{M\nu}(x_\mu, x_2) & \cdots & -kG_{Konst} G_{M\nu}(x_\mu, x_\nu) & -k^2 G_{Konst} G_M(x_\mu, x_1) & -k^2 G_{Konst} G_M(x_\mu, x_2) & \cdots & \frac{1}{Z_{M\mu}} - k^2 G_{Konst} G_M(x_\mu, x_\nu) \end{bmatrix} = CF_0$$

with $G_{Konst} = \frac{\omega}{4Bk^3}$. (12)

$$C = \begin{bmatrix} G_{Konst} G_{F_{\mu=1}}(x_1, x_0) \\ G_{Konst} G_{F_{\mu=2}}(x_2, x_0) \\ \vdots \\ G_{Konst} G_{F_{\mu=\mu}}(x_\mu, x_0) \\ -kG_{Konst} G_{M_{\mu=1}}(x_1, x_0) \\ -kG_{Konst} G_{M_{\mu=2}}(x_2, x_0) \\ \vdots \\ -kG_{Konst} G_{M_{\mu=\mu}}(x_\mu, x_0) \end{bmatrix} \quad (13)$$

4.2.1 IMPEDANCES

The force impedance of a pure mass in the neutral layer can be described as

$$Z_{F, mass} = \frac{F_{mass}}{v} = j \cdot \omega \cdot m. \quad (14)$$

Figure 7 depicts the masses in the neutral layer in an infinite beam.

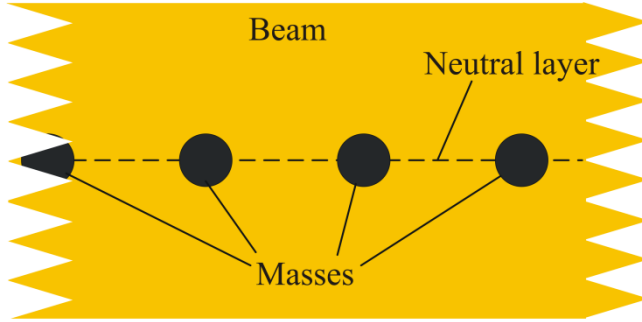


Figure 7: Embedded masses in the neutral layer.

In case of embedded rubber-coated steel balls (Figure 8), the force impedance of one discontinuity becomes

$$Z_{F, spring-mass system} = \frac{F_{spring-mass system}}{v} = \frac{m \cdot s}{j \cdot \omega \cdot m + \frac{s}{j \cdot \omega}} \quad (16)$$

and

$$s = s_0 (1 + j \cdot \eta_{spring}). \quad (15)$$

In this work castable resin will be used as a rubber material. It is expected that small vibrations yield a complex stiffness with a displacement dependent behaviour rather than to viscous damping behaviour [77]. Thus, the damping factor is used as shown in equation (15), which reflects a displacement-dependency of stiffness and damping, proportional to the excited force¹⁰.

¹⁰ By the use of viscous rubber material a velocity-dependency would have been expected.

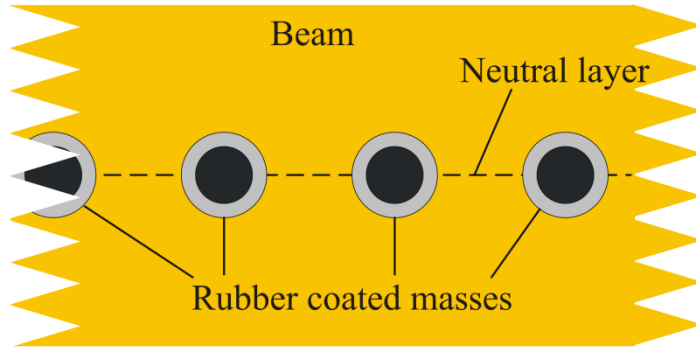


Figure 8: Rubber-coated balls in the neutral layer.

The impedances of the moment reactions depend on the distance of the masses from the neutral layer r_{NL} (Figure 9).

$$Z_{M, mass} = \frac{M_{mass}}{w} = j \cdot \omega \cdot m \cdot r_{NL}^2 \quad (17)$$

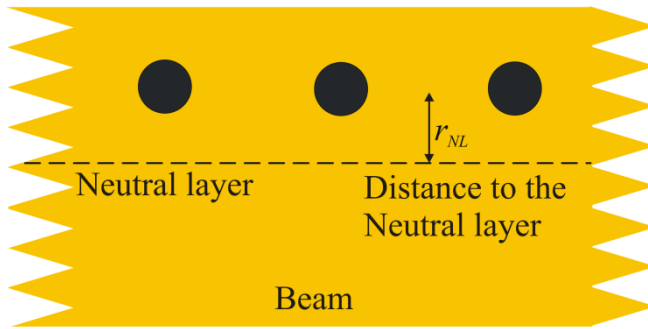


Figure 9: Masses out of the neutral layer.

If the masses were coated with rubber material, the impedance of the moment reactions also depends on the distance of the inserts from the neutral layer r_{NL} (Figure 10).

$$Z_{M, spring-mass system} = \frac{M_{spring-mass system}}{w} = \frac{m \cdot s}{j \cdot \omega \cdot m + \frac{s}{j \cdot \omega}} \cdot r_{NL}^2 \quad (18)$$

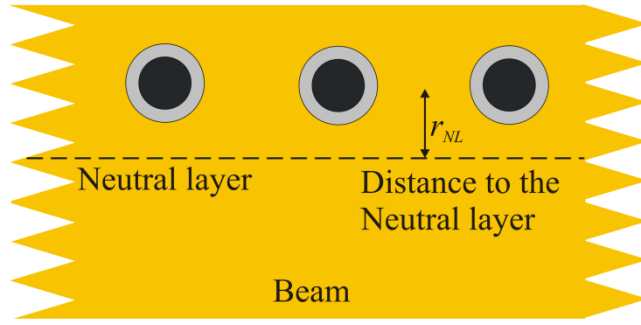


Figure 10: Rubber-coated balls at a distance from the neutral layer.

4.2.2 PARAMETERS

An infinite slender beam with 5, 10 or 20 discontinuities will be used. It is of interest to investigate such values, which are close to the parameters of real beams, masses and spring stiffnesses of the up-following measurements (see section 5.2).

The rectangular beams measure 70mm in height and 48mm in width. The loss factor of the beam is set to 0.01 and the complex Young's modulus is set to $5.6 \cdot 10^9 \cdot (1 + j \cdot \eta_{beam})$ N/m² with a damping factor of $\eta_{beam} = 0.015$. The density of the beam is set to 400 kg/m³, while the density of the inserted masses amounts to 7800 kg/m³. The complex spring stiffness of the rubber-coated balls is set to $2.5 \cdot 10^5 \cdot (1 + j \cdot \eta_{spring})$ N/m with $\eta_{spring} = 0.02$.

The inserts are distributed over different lengths with various distances each in axial direction. In case of the inserts were located out of the neutral layer, their distance amounts to 0.02m in vertical direction. The driving point force is located 0.5m before the first discontinuity and the velocity is registered 0.5m behind the last insert in most cases (Figure 11). The considered frequency range is between 10 Hz and 10 kHz.

In all investigations the limit of the simple bending wave equation has to be considered¹¹.

¹¹ In all calculations and measurements with beams, the vertical height of the beam is about $h = 80$ mm. The error of the simple bending wave equation from Euler-Bernoulli increases if the corresponding bending wave length becomes larger than 6 times that height ($\lambda > 6h$) (Cremer and Heckl [12]). Thus, transferred into a frequency, all calculated results with frequencies higher than $f = 2359$ Hz need to be considered under this condition.

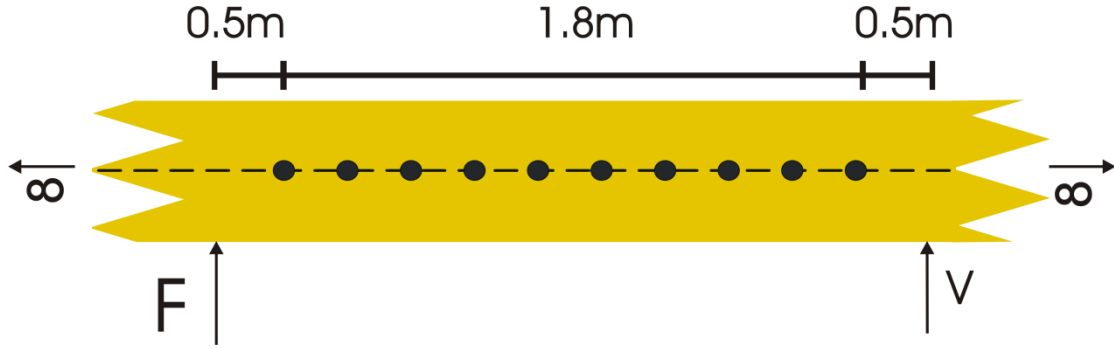


Figure 11: An infinite homogenous slender beam with inserts in the neutral layer. The inserts are distributed over various lengths. The driving point force is located 0.5m before the first discontinuity and the velocity is registered 0.5m behind the last insert.

To broaden the attenuation in the resonance area, the spring stiffness will be changed in a way that the complex spring stiffnesses of each spring-mass system are increasing in a logarithmical order, for instance, between

$$5 \cdot 10^5 (1 + j \cdot 0.02) \frac{N}{m} \leq s \leq 5 \cdot 10^6 (1 + j \cdot 0.02) \frac{N}{m}. \quad (19)$$

4.3 NUMERICAL INVESTIGATION

The following calculations show the main observations of an infinite homogenous slender beam with embedded discontinuities. These inserts consist of either pure masses or rubber-coated masses. They are distributed in the neutral layer or out of the neutral layer of the beam to study the influence of additional moment reactions¹².

In all following plots the calculations of the transfer mobility are depicted in a comparison with the same beam without inserts.

4.3.1 HOMOGENEOUS INFINITE BEAM WITH MASSES IN THE NEUTRAL LAYER

A homogeneous slender beam with evenly distributed masses in the neutral layer shows effects of stop- and pass-bands in the transfer mobility (see Figure 12). Their appearance depends on their separation. By bringing them together in always the same distance the periodic structure allows certain wavelengths to pass while other waves will be reflected.

Figure 12 shows 5 masses which are equally distributed over a length of 10m. In the double logarithmic plot the pure beam (blue curve) shows a descent at higher frequencies, which is dependent on the loss factor of the beam. The transfer mobility of

¹² In an attachment to this work (sub-sections 11.1.1 - 11.1.3) additional side effects of the main observations are depicted in order to increase confidence in the physical behaviour of the formulas used.

the beam with embedded pure masses illustrates the existence of stop- and pass-bands (red curve). The negative slopes follow from the reflections of the bending waves in these frequency ranges. These are the so called stop-bands and their occurrence is periodical due to the equi-spaced masses¹³.

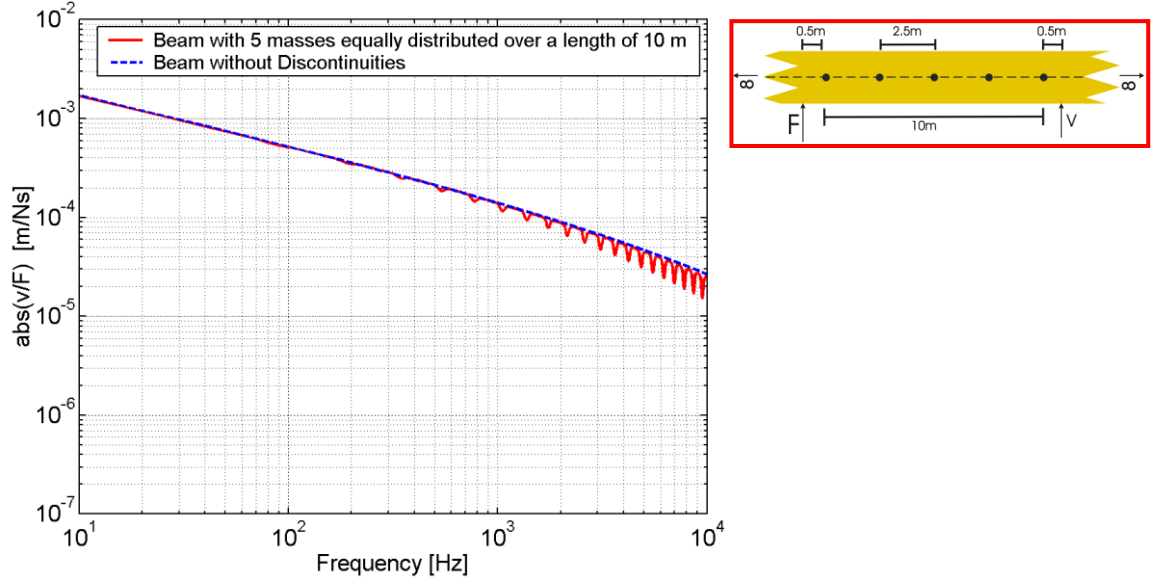


Figure 12: Transfer mobility of an infinite beam with 5 embedded masses in the neutral layer. As depicted in the sketch on the right side 5 masses are equally distributed over a length of 10m.

If now 10 masses are evenly distributed over the length of 10m (Figure 13), the distances in the frequency but also the depth and width of the stop-bands are increased.

¹³ The correlation of the distances of the masses to the frequency of the stop-bands is depicted in Table 2.

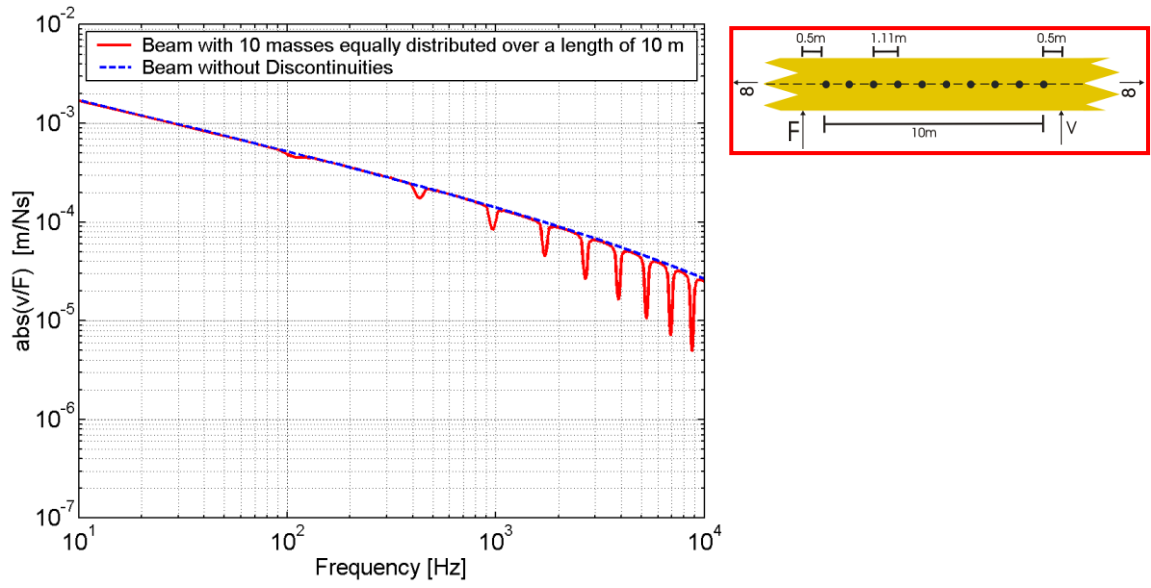


Figure 13: Transfer mobility of an infinite beam with 10 embedded masses in the neutral layer. As depicted in the sketch on the right side 10 masses are equally distributed over a length of 10m.

At the beam with 20 equally distributed masses (Figure 13) these observed effects are increased again. In the range of 10 Hz to 10 kHz only four pass-bands are visible. The smaller the distances from mass to mass the higher the stop-bands in frequency are.

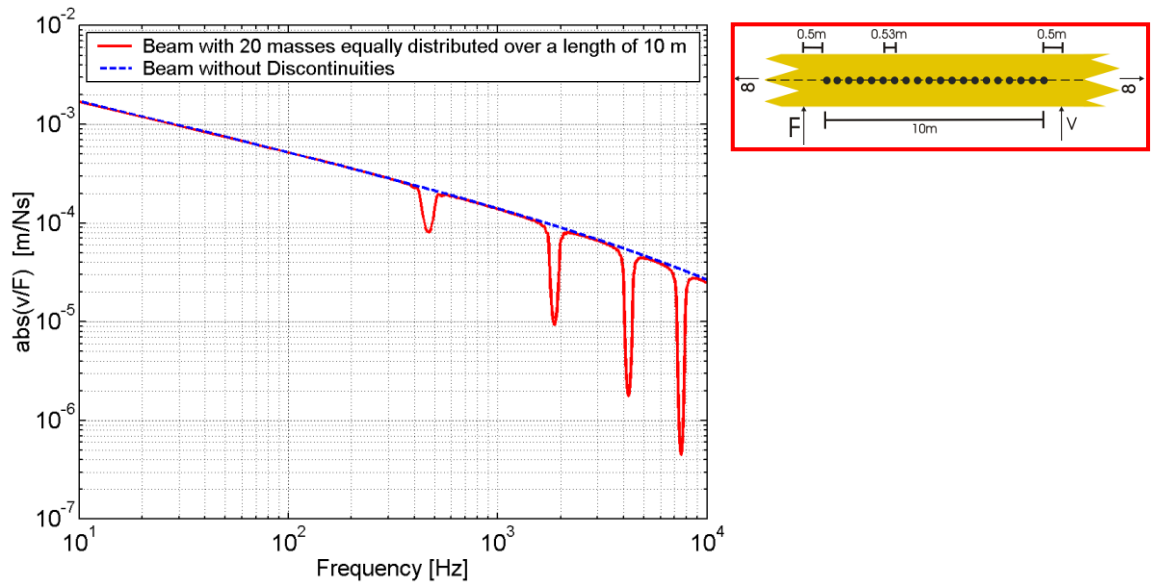


Figure 14: Transfer mobility of an infinite beam with 20 embedded masses in the neutral layer. As depicted in the sketch on the right side 20 masses are equally distributed over a length of 10m.

These observations correspond to the findings Heckl [33] and Mead et al. [70] made with beams on rigid supports.

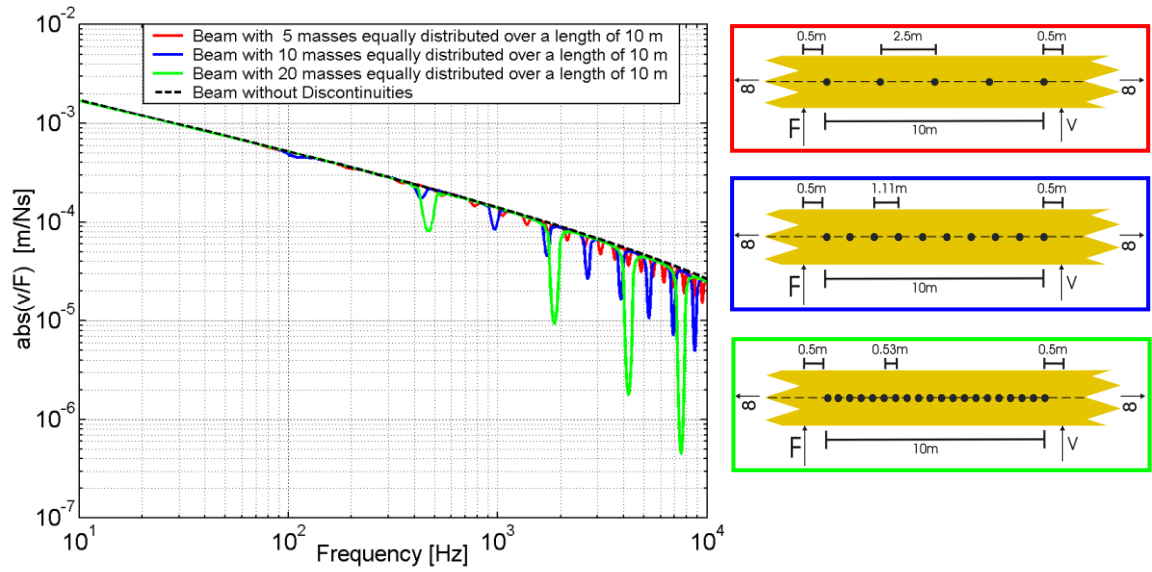


Figure 15: Transfer mobility of an infinite beam with 5, 10 and 20 embedded masses in the neutral layer. The lowest stop-bands in frequency of the beam with 5 masses are not visible in this plot. As depicted in the sketches on the left side 5, 10 and 20 masses are equally distributed over a length of 10m.

In the comparison of the three calculated types (5, 10 and 20 masses) the observed effects of increased depth and width are highlighted in Figure 15. As the distances from mass to mass per beam vary (see Table 1) the stop- and pass-bands, which are related to the wavelength, do not coincide at the same frequency ranges.

Table 1: The distances from mass to mass as depicted in Figure 15

Number of masses equally distributed over a length of 10m	Distance of mass to mass in meter
5	2.5
10	1.11
20	0.53

If the distances were all the same as depicted in Figure 16 the stop- and pass-bands coincide. The different slopes of the beams without discontinuities arise from the loss factor of the beam with regard to the different distances of the test points.

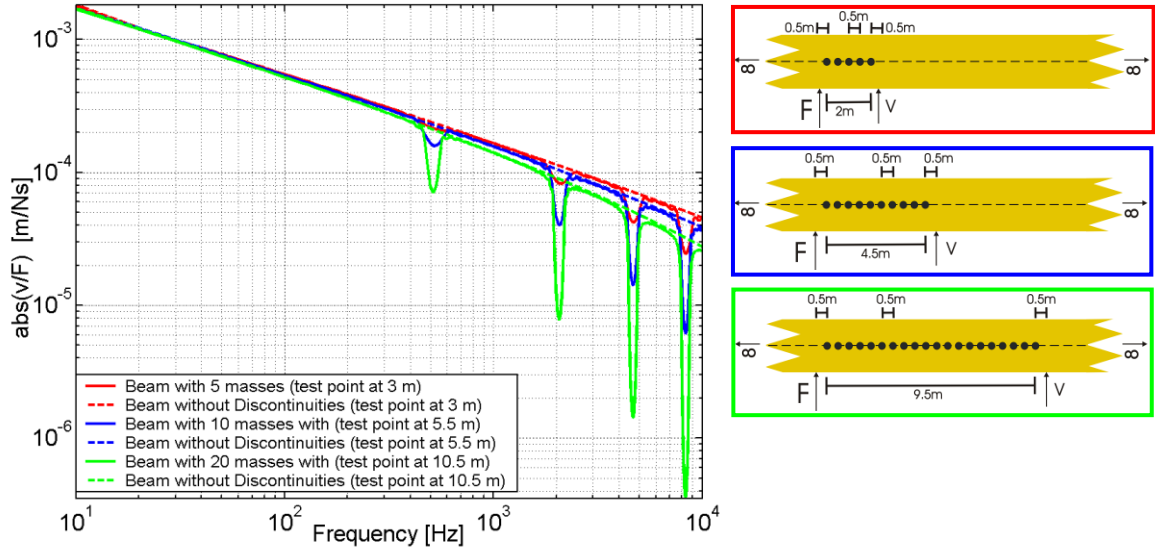


Figure 16: Transfer mobility of an infinite beam with 5, 10 and 20 embedded masses in the neutral layer with all the same distances. As depicted in the sketches on the right side 5, 10 and 20 masses are equally distributed with distances of 0.5m to each other. The test points are located 0.5m behind the last insert.

Stop-bands occur if a half of the bending wavelength or a multiple of it fits with the distances of the masses (Strasberg and Feit [89]).

$$\lambda_{stop-band} = dist \frac{2}{n}; n = 1, 2, 3, \dots \in \mathbb{N} \quad (20)$$

Their appearance in the frequency range follows from the bending wave equation

$$\lambda_B = \frac{2\pi}{\sqrt{\omega}} \sqrt[4]{\frac{B}{m'}} \quad (21)$$

and reveals in

$$f_\lambda = \frac{2\pi}{\lambda_B^2} \sqrt[4]{\frac{B}{m'}} \quad (22)$$

with

$$m' = \rho b h, \quad (23)$$

$$E = E_{real} (1 + j\eta_{beam}) \quad (24)$$

and

$$B = E b \frac{h^3}{12} . \quad (25)$$

According to these equations, there is a non-linear increase of the frequency from one stop-band to another.

The first four stop-band frequencies for different distances from mass to mass are depicted in Table 2. It can be seen that within a range of 0.2m and 2.5m distance the first stop-band varies between 22 Hz and 3.4 kHz. In the measurements at Chapter 5 the first three stop-bands of the beam with 5 masses are within the relevant frequency range from 10 Hz to 10 kHz. At the measurements with 10 masses equally distributed with distances of 0.2m to each other only one stop-band exists within this range¹⁴.

¹⁴ These observations show that very long distances are needed to achieve attenuation at lower frequencies in the audible frequency range (see also Hirsekorn [39]).

Table 2: Calculated frequencies of the first four stop-bands for beams with different distances from mass to mass

Distances from mass to mass	1 st stop-band	2 nd stop-band	3 rd stop-band	4 th stop-band	Related to
0.16m	5.302 kHz	21.21 kHz	47.72 kHz	84.84 kHz	Calculations Figure 31
0.2m	3.393 kHz	13.57 kHz	30.54 kHz	54.29 kHz	Measurements Figure 46 Figure 47 Figure 48 Figure 49
0.25m	2.172 kHz	8.687 kHz	19.55 kHz	34.75 kHz	Calculations Figure 30
0.26m	2.008 kHz	8.032 kHz	18.07 kHz	32.13 kHz	Calculations Figure 31
0.4m	848 Hz	3.393 kHz	7.635 kHz	13.57 kHz	Measurements Figure 45
0.5m	543 Hz	2.172 kHz	4.886 kHz	8.687 kHz	Calculations Figure 16 Figure 20 Figure 23 Figure 24 Figure 25 Figure 26 Figure 27 Figure 29
0.526m	490 Hz	1.96 kHz	4.41 kHz	7.84 kHz	Calculations Figure 14 Figure 15
1.053m	122.5 Hz	490 Hz	1.102 kHz	1.96 kHz	Calculations Figure 21 Figure 22 Figure 28
1.11m	109.9 Hz	439.8 Hz	989.5 Hz	1.759 kHz	Calculations Figure 13 Figure 15
2.1m	30.8 Hz	123.1 Hz	277.0 Hz	492.5 kHz	Calculations Figure 22
2.5m	21.7 Hz	86.9 Hz	195.5 Hz	347.5 Hz	Calculations Figure 12 Figure 15

4.3.2 HOMOGENEOUS INFINITE BEAM WITH RUBBER-COATED MASSES IN THE NEUTRAL LAYER

If these evenly distributed steel cylinders are coated with rubber, the effects of stop- and pass-bands diminish.

Figure 17 shows 5 masses coated with rubber, which have a complex spring stiffness of $2.5 \cdot 10^5 (1+j 0.02)$ N/m. The attenuation is dominated by the spring-mass system, albeit in a very narrow frequency band.

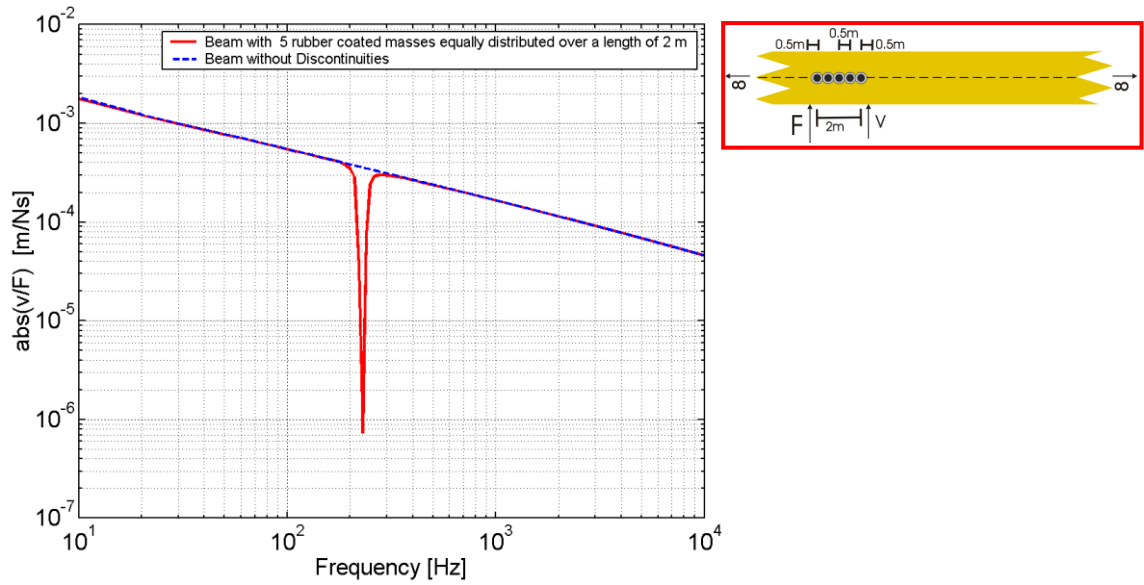


Figure 17: Transfer mobility of an infinite beam with rubber-coated masses embedded in the neutral layer. As depicted in the sketch on the right side 5 rubber-coated masses are equally distributed over a length of 2m.

The more rubber-coated masses are involved the more the transfer mobility is decreased in the resonance frequency¹⁵ (Figure 18).

$$f_{res} = \frac{1}{2\pi} \sqrt{\frac{s_{cylinder}}{m_{cylinder}}} \quad (26)$$

According to the equation of a single-degree-of-freedom spring-mass system the attenuation of the transfer mobility coincides with the resonance of that system, which is set to $f_{res} = 224$ Hz with

$$m_{cylinder} = 0.1267 \text{ kg}; \quad s_{cylinder} = 2.5 \cdot 10^5 \cdot (1 + j \cdot 0.02) \frac{N}{m} \quad (27)$$

¹⁵ The propagating bending waves are mainly reflected in the “resonance frequency” of the low damped spring-mass systems. According to the system “Infinite beam - Rubber - Mass”, this “resonance frequency” can be seen as the beam’s “anti-resonance” (see also the pre-test measurements in sub-section 5.1.1).

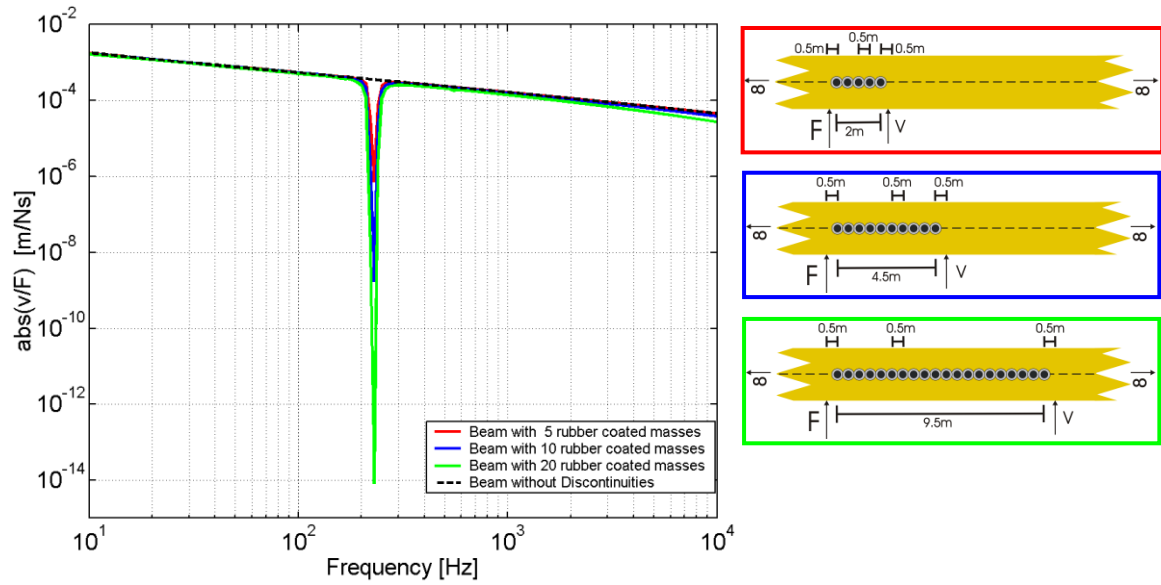


Figure 18: Transfer mobility of an infinite beam with 5, 10 and 20 rubber-coated masses embedded in the neutral layer. The transfer mobility of the beam without inserts (dashed lines) has got the same test point as the beam with 5 rubber-coated masses. As depicted in the sketches on the right side 5, 10 and 20 rubber-coated masses are equally distributed with distances of 0.5m to each other. The test points are located 0.5m behind the last insert.

In a next step the masses and stiffnesses vary in such way, that the resonances increase in a logarithmic order.

Figure 19 shows the masses being changed in a logarithmical order from $0.126 \text{ kg} \geq m \geq 0.0126 \text{ kg}$, the complex spring stiffnesses from $2.5 \cdot 10^5 \text{ N/m} \leq k \leq 2.5 \cdot 10^6 \text{ N/m}$ with a loss factor of the spring of 0.02.

It is obvious that a reduction of the masses leads to reduced attenuations while changes in spring stiffness keep the reduction in the resonances on similar levels. Thus, in order to achieve a large attenuation over a broader frequency range, the changing of the spring stiffness is more sufficient than changing the masses. Last not least, it is much easier to vary the spring stiffness with different rubber materials in comparison to embedding larger masses in the same structure. This knowledge will be applied in the measurements (Chap. 5).

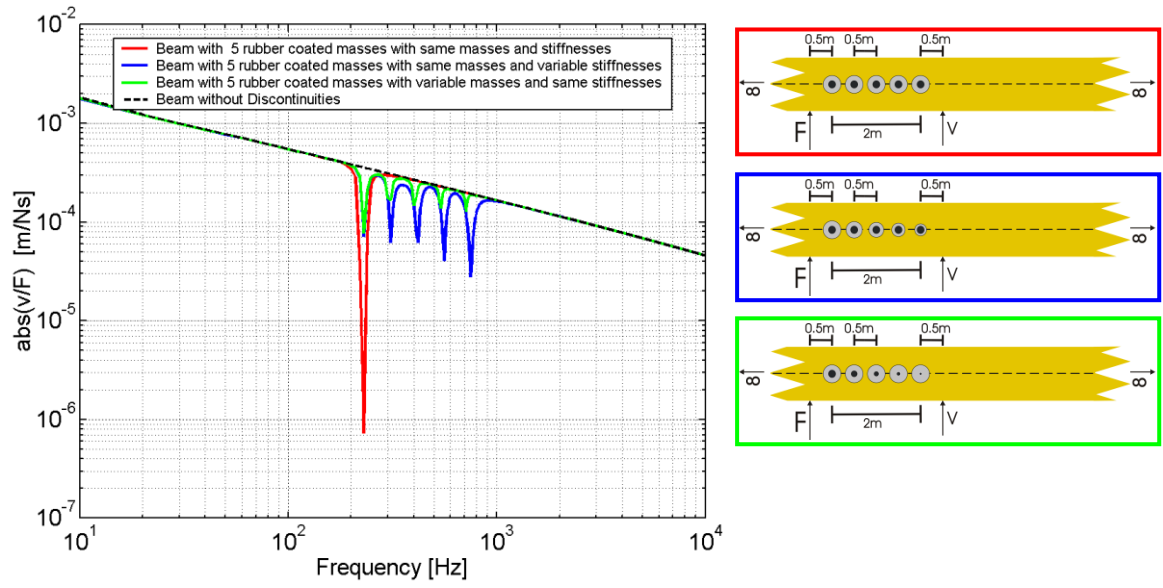


Figure 19: Transfer mobility of an infinite beam with 5 rubber-coated masses with variable masses and stiffnesses embedded in the neutral layer. As depicted in the sketches on the right side 5 rubber-coated masses with various masses or spring stiffnesses, respectively, are equally distributed with distances of 0.5m to each other.

4.3.3 HOMOGENEOUS INFINITE BEAM WITH PURE AND RUBBER-COATED MASSES IN THE NEUTRAL LAYER

An interesting effect arises if the rubber-coated masses are compared with the same number of pure masses located at the same positions. Figure 20 shows the influence of the mass-controlled stop- and pass-band onto the rubber-coated masses¹⁶. The reduction of the transfer mobility becomes smaller in the frequency range of the transition from a stop-band to a pass-band. The level of the transfer mobility of both beams is almost the same. It appears that the elastically supported masses behave like pure masses in that frequency range.

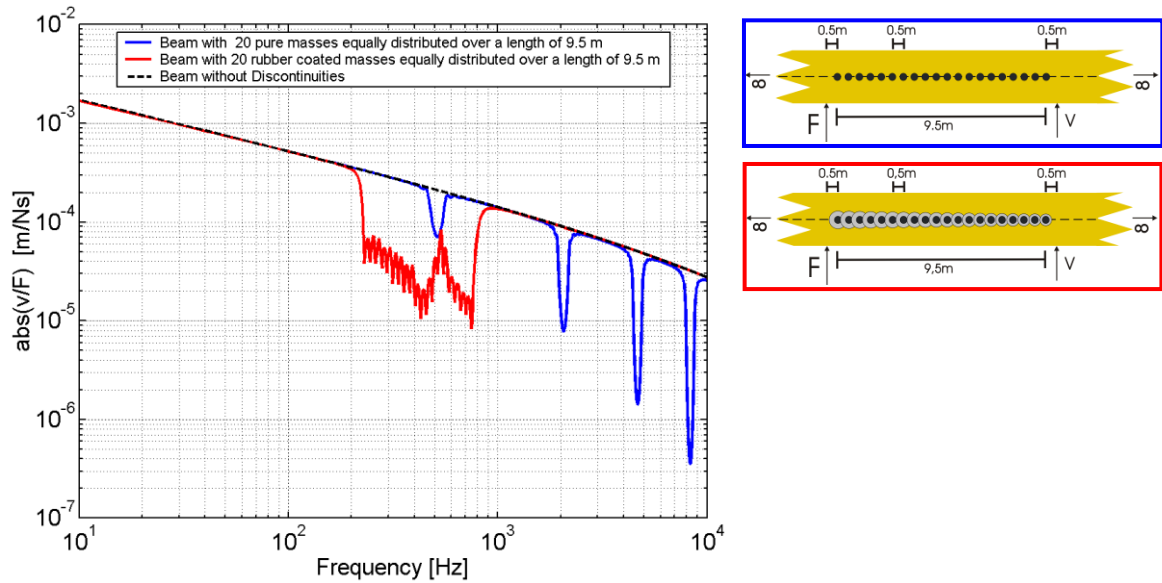


Figure 20: Transfer mobility of an infinite beam with 20 pure masses and 20 rubber-coated masses embedded in the neutral layer. As depicted in the sketches on the right side 20 masses or 20 rubber-coated masses are equally distributed with distances of 0.5m to each other. The test points are located 0.5m behind the last insert.

If the distances of the inserts were increased the first stop- and pass-band appears below the first resonance frequency of the rubber-coated masses (Figure 21). It is well-known from spring-mass-systems that below the resonance frequency the impedance of each spring-mass system is mass-controlled. Thus, in the frequency range below the lowest resonance, the 1st stop-band appears as it would be from the beam with pure masses, even with a higher attenuation.

At frequencies above the highest resonance frequency, the appearance of the stop- and pass-bands is vanished. This observation corresponds to the knowledge about spring-

¹⁶ According to Heckl, Maria [35] a support consisting of a single mass and spring has a single resonance frequency. Below this resonance frequency, each support behaves like a mass; the beam is then effectively mass-supported. Above this frequency, each support behaves like a spring; the beam is then effectively spring-supported. Directly at this resonance frequency, each support becomes rigid (if it is undamped), and the beam is effectively simply supported.

mass-systems, attached to beams, which are decoupled and solely spring controlled above their resonance frequency (Thompson [91]).

Although a small trough is visible on the 3rd stop-band the low influence reflects the spring-controlled behaviour at frequencies¹⁷, which are higher than the resonances. In the frequency range above the 3rd stop-band the transfer mobility follows the one from the beam without any inserts.

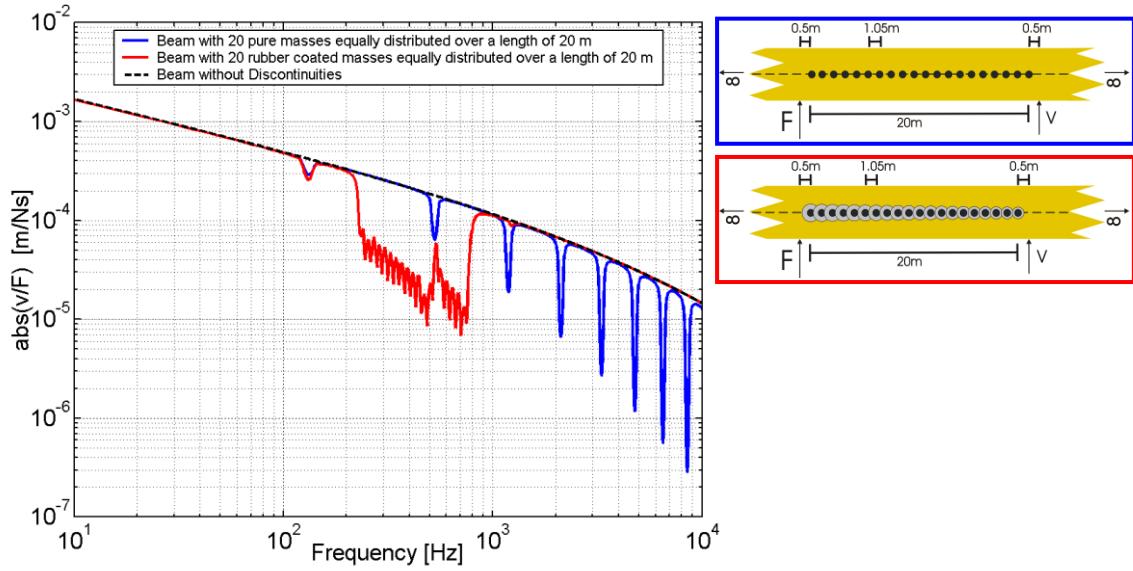


Figure 21: Transfer mobility of an infinite beam with 20 pure masses and 20 rubber-coated masses embedded in the neutral layer. As depicted in the sketches on the right side 20 masses or 20 rubber-coated masses are equally distributed with distances of 1.05m to each other. The test points are located 0.5m behind the last insert.

The observation in the following plot (Figure 22) underlines the spring- and mass-controlled behaviour above and below the resonance band. The impact of the stop-band, which reduces the attenuation of the beam with rubber inserts, is larger at stop-bands that are related to inserts with doubled distances. At the three non-common stop-bands within the resonance band (see the green curve in Figure 22), the attenuation is only reduced at the resonances of the corresponding beam (see the red dashed curve). On the other side, reductions are higher at the common stop-bands at the beam that has its inserts closer in distance (1.05m).

However, if the resonances occur in or close to a stop-band frequency, the attenuation is reduced.

With respect to the mass-controlled numbers of spring-and-mass systems, the level of reduced attenuation should be higher for the more systems involved. That means that

¹⁷ It can be seen in the following Figure 21, that a small attenuation trough is visible close to the 3rd stop-band above the highest resonance. This behaviour is possibly - although not expected - related to scattering effects in the calculations.

the stop-band that is lowest in frequency within the resonance band should have a higher impact than a stop-band on a higher frequency within the resonance band according to the number of masses that are below its own resonance and therefore still mass-controlled. In fact, this assumption is not visible in the observations of this numerical study.

As mentioned, according to Heckl, Maria [35] is the behaviour of a support consisting of a single mass and a spring rigid in its resonance, if it is undamped. Although used a low damped spring factor in these calculations, this might explain the reduced attenuation even at higher stop-bands within the resonance band.

It is even the case that the reduction induced by a stop-band occurs at frequencies that are above the highest resonance of the spring-mass systems. It is possible that the spring-mass systems still slightly act as pure masses or as “slightly rigid”; otherwise the frequency range of the mass-controlled area scatters around the resonance. The latter may explain why the reduction in the highest resonance can even occur by having only one spring-mass system above the stop-band frequency as in Figure 22 (see the red dashed curve at the highest stop-band within the resonance band)¹⁸.

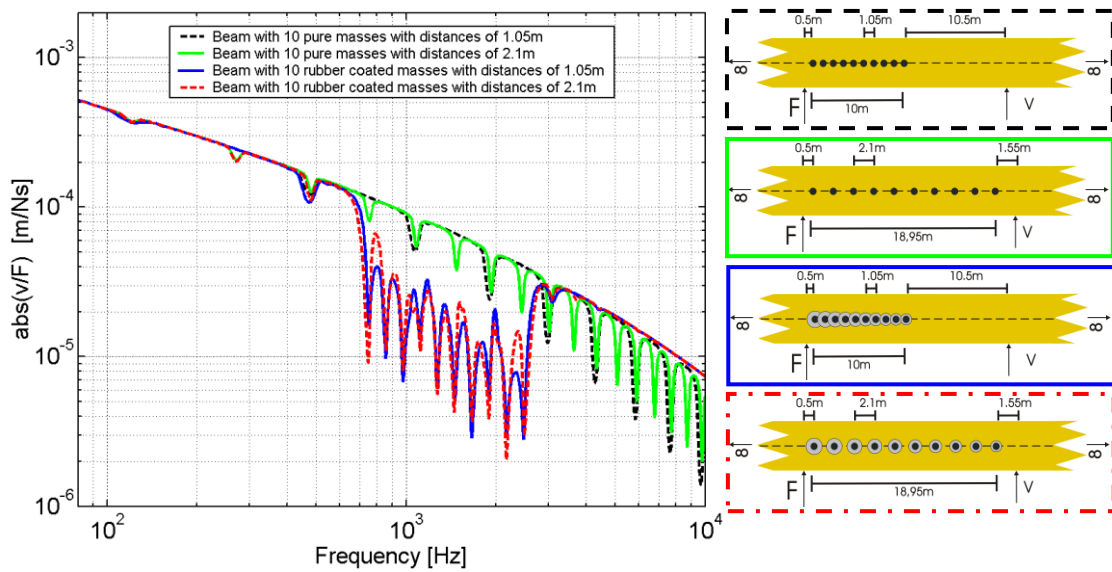


Figure 22: Transfer mobility of infinite beams with 10 pure masses and 10 rubber-coated masses embedded in the neutral layer. As depicted in the sketches on the right side 10 masses or 10 rubber-coated masses are equally distributed with distances of 1.05m or 2.1m, respectively. The test points are located 20.5m behind the first insert.

If the equidistant distribution of the pure masses is disturbed and the inserts are distributed randomly along the neutral layer, the appearance of stop-bands is

¹⁸ By having only one mass-controlled rubber-coated insert, an impact related to stop- and pass-bands of the transfer mobility is not expected. At least two masses and a “distance between them” are needed to reveal stop- and pass-band behaviour.

significantly changed (Figure 23, blue curve)¹⁹. The attenuation of the transfer mobility scatters according to the non-equal distribution.

Such random distributions have got a lower impact onto the attenuation, if resonant inserts with low stiffnesses are randomly distributed along the neutral layer. The stiffnesses of the rubber-coated masses is reduced by a factor of 100 (Figure 23, red dashed curve). The resonances occur in a frequency range below the first stop-band. Both curves, the green with inserts equally distributed and the red dashed curve with inserts randomly distributed, respectively, agree very well. Strasberg and Feit [89] also stated that the position of the spring-mass system along a beam is not relevant. In fact, as the next figure shows (Figure 24), involvement of periodic effects compromises the magnitude of attenuated resonance frequencies.

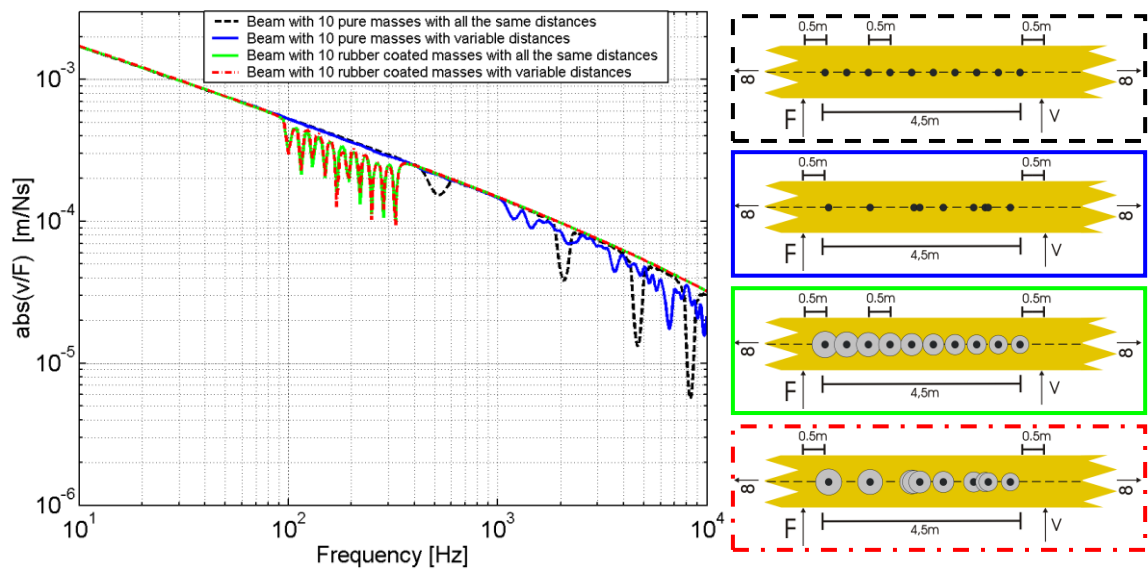


Figure 23: Transfer mobility of infinite beams with 10 pure masses and 10 rubber-coated masses with very low stiffnesses embedded in the neutral layer. As depicted in the sketches on the right side 10 masses or 10 rubber-coated masses are equally distributed with distances of 0,5m and randomly distributed, respectively. The test points are located 5.5m behind the forcing point.

If the resonances of the rubber-coated masses occur in or near a stop-band, differences in the comparison with the same rubber-coated masses, which are equally distributed along the neutral layer, are visible (Figure 24). The impact of the stop-bands or evoked attenuations deteriorates the resonance band, similar to the observations shown in Figure 22.

Furthermore, Weith and Petersson [102] have shown, that the effect of a reduced attenuation at or near by a stop-band is removed with randomised distributed spring-

¹⁹ See also Chapter 1 – Disordered/Randomised Distribution.

mass systems within the neutral layer²⁰. Thus, within certain limits, the attenuation band at resonances can be controlled with the distribution of inserts along the neutral layer.

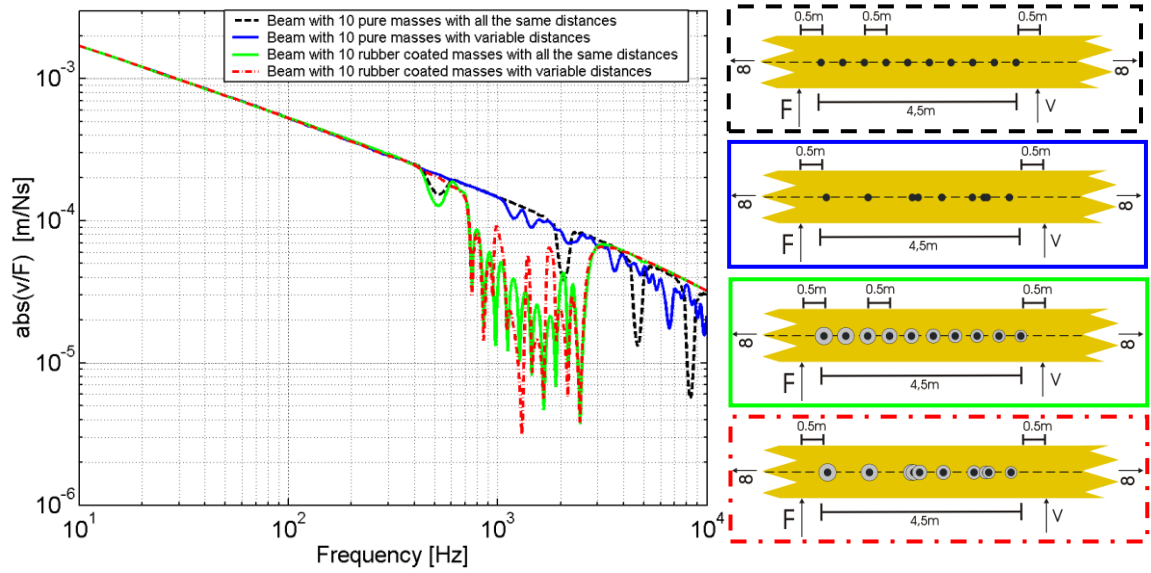


Figure 24: Transfer mobility of infinite beams with 10 pure masses and 10 rubber-coated masses with very high stiffnesses embedded in the neutral layer. As depicted in the sketches on the right side 10 masses or 10 rubber-coated masses are equally distributed with distances of 0.5m and randomly distributed, respectively. The test points are located 5.5m behind the forcing point.

²⁰ In the work of Weith and Petersson [102] 100 calculations of the Transfer mobility with randomised distributed spring-mass systems along the neutral layer have been averaged.

4.3.4 HOMOGENEOUS INFINITE BEAM WITH MASSES OUT OF THE NEUTRAL LAYER

All previous calculations have been made with inserts located in the neutral layer. Figure 25 shows a comparison of 10 masses in the neutral layer (see Figure 16) with the same 10 masses, now, displaced from the neutral layer in a distance of 0.02m. The displacement of these masses changes the transfer mobility such that the stop-bands are smeared at higher frequencies. At the 4th stop-band the transfer mobility shows higher values than the beam without any inserts.

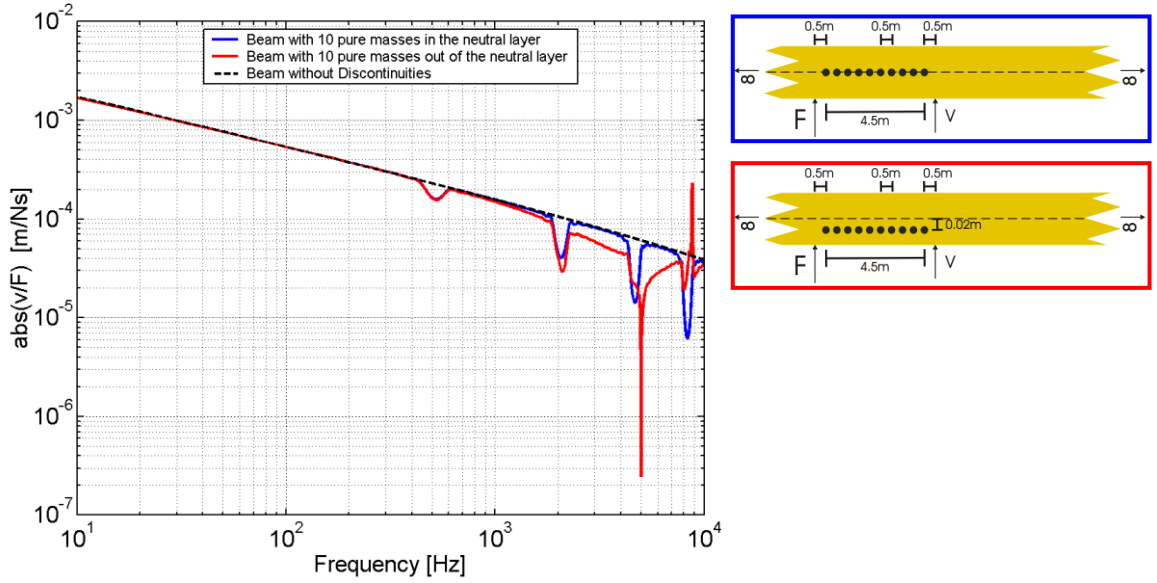


Figure 25: Transfer mobility of an infinite beam with 10 pure masses embedded in and out of the neutral layer. As depicted in the sketches on the right side 10 masses are equally distributed in and out of the neutral layer with distances in axial direction of 0.5m to each other. The test points are located 0.5 m behind the last insert.

In all four figures with 10 and 20 masses (Figure 25, Figure 26, Figure 27, Figure 28), which are distributed over two distinct distances, it can be observed that the 1st stop-band coincides in these examples. Differences occur from the 2nd stop-band on and are manifested in smeared appearances of the stop-bands as well as in an amplified behaviour. Effects of smearing and changed attenuations of the stop-bands at higher frequencies are visible. From the 2nd stop-band on, they vary such that the attenuations are lower and broadened to both sides of each stop-band. Negative peaks appear which show higher attenuations than in the beam with inserts in the neutral layer.

This behaviour reflects the observations of Mead et al. [70] and deteriorates the objective in this work of having a defined and large attenuation.

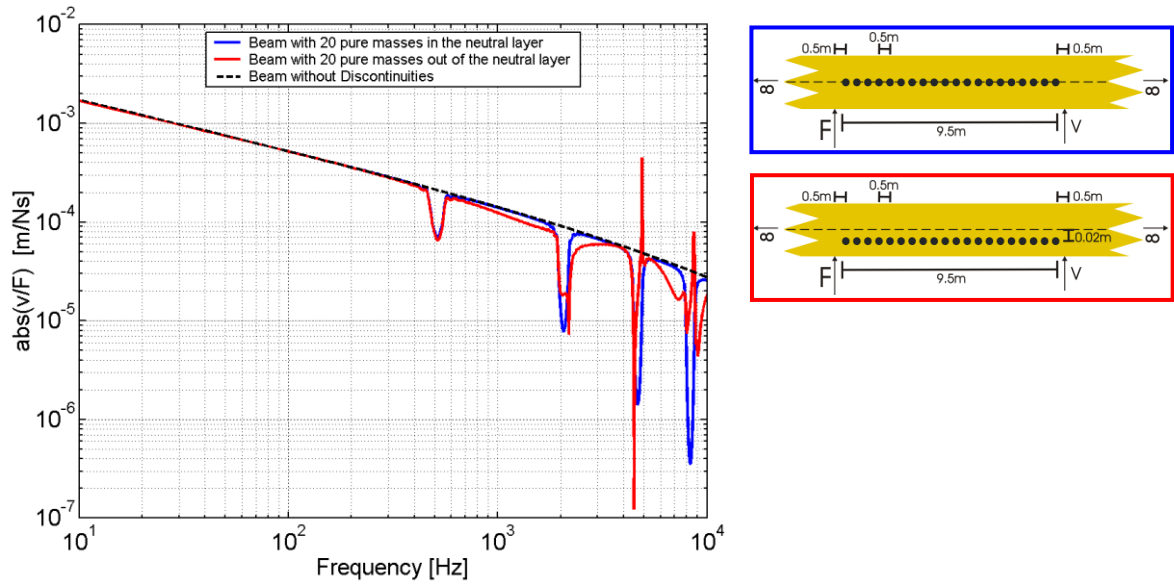


Figure 26: Transfer mobility of an infinite beam with 20 pure masses embedded in and out of the neutral layer. As depicted in the sketches on the right side 20 masses are equally distributed in and out of the neutral layer with distances in axial direction of 0.5m to each other. The test points are located 0.5 m behind the last insert.

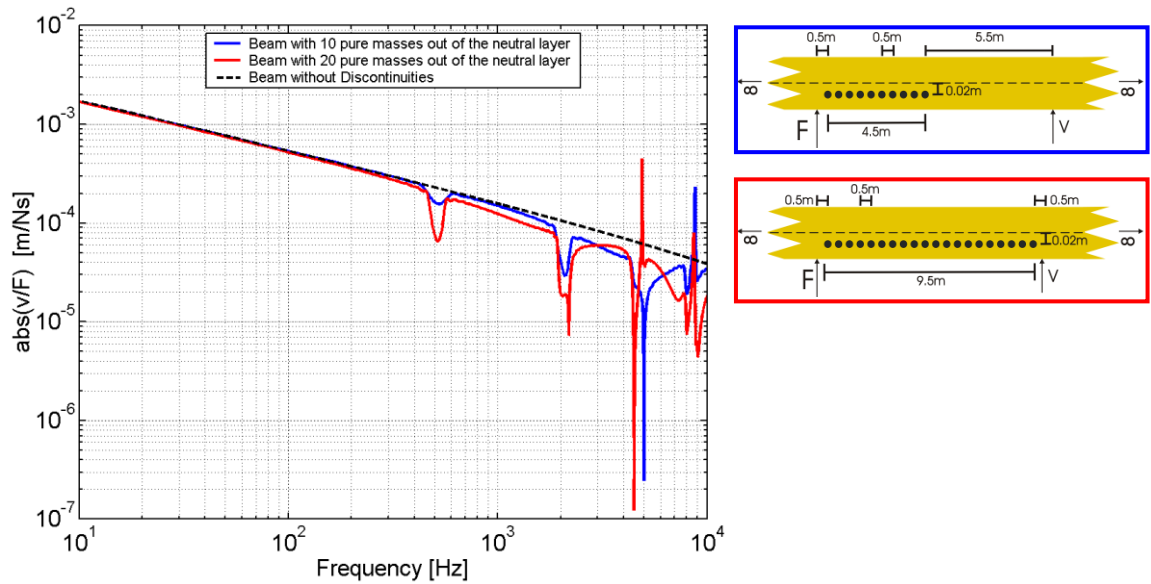


Figure 27: Transfer mobility of an infinite beam with 10 and 20 pure masses embedded out of the neutral layer with distances of 0.5m each other. As depicted in the sketches on the right side 10 and 20 masses are equally distributed out of the neutral layer with distances in axial direction of 0.5m to each other. The test points are located 10 m behind the first insert.

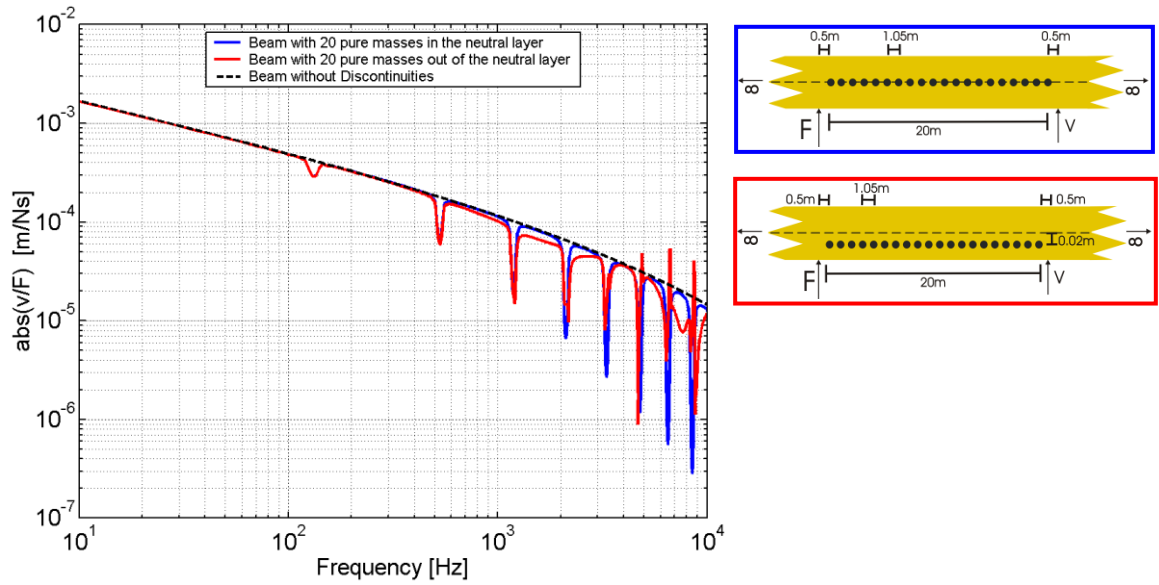


Figure 28: Transfer mobility of an infinite beam with 20 pure masses embedded in and out of the neutral layer. As depicted in the sketches on the right side 20 masses are equally distributed in and out of the neutral layer with distances in axial direction of 1.05m to each other. The test points are located 0.5 m behind the last insert.

With respect to achieving a large attenuation of the transfer mobility, a displacement of the masses from the neutral layer is not appropriate. Moment reactions reduce the attenuation even if the masses are coated with rubber, as can be observed in the following sub-section (4.3.5).

4.3.5 HOMOGENEOUS INFINITE BEAM WITH RUBBER-COATED MASSES OUT OF THE NEUTRAL LAYER

In the following the rubber-coated inserts are displaced from the neutral layer. The moment reactions slightly reduce the attenuated regions at higher frequencies (Figure 29). It can also be seen that the changed behaviour of the transfer mobility with rubber-coated masses seems to be independent of the changes with pure masses displaced from the neutral layer. The frequency ranges of the beam with pure masses and with rubber-coated masses, which are affected by the displacement (in this case approximately at and above the 2nd stop-band) are not correlating. These changes in the transfer mobility are larger at the beam with pure masses than of the beam with rubber-coated masses (see also Figure 25).

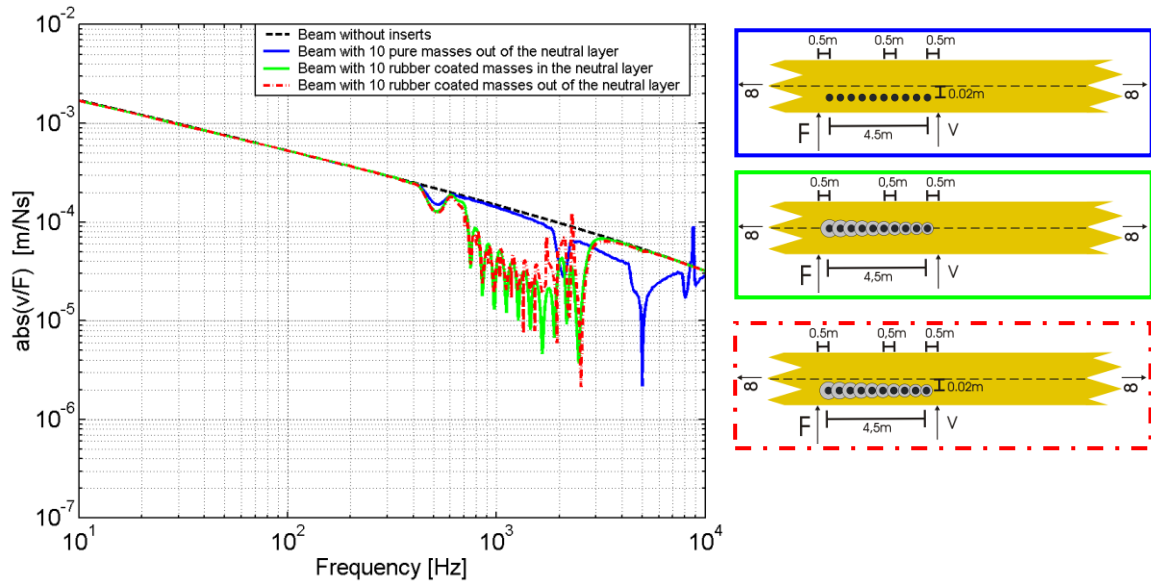


Figure 29: Transfer mobility of an infinite beam with 10 pure masses out of the neutral layer, 10 rubber-coated masses in and 10 rubber-coated masses out of the neutral layer. As depicted in the sketches on the right side 10 inserts are equally distributed in and out of the neutral layer with distances in axial direction of 0.5m to each other. The test points are located 0.5 m behind the last insert.

By doubling the number of inserts while maintaining the distances, the influence of the moment reactions becomes more visible (Figure 30). The attenuation in the resonance bands is increasing if the inserts are in the neutral layer and decreasing if they are outside it.

In the frequency range of the stop-band from the beam with pure masses, both transfer mobilities of the beam with resonant inserts show a reduced attenuation, as shown in sub-section 4.3.3. The impact of the stop-band on the inserts, which are displayed in the neutral layer, is less significant. Above the highest resonance, both curves of the beam with rubber-coated inserts again agree very well and follow the curve of the beam without any inserts.

However, in order to achieve a large attenuation with resonant inserts, it seems to be advantageous to keep them in the neutral layer.

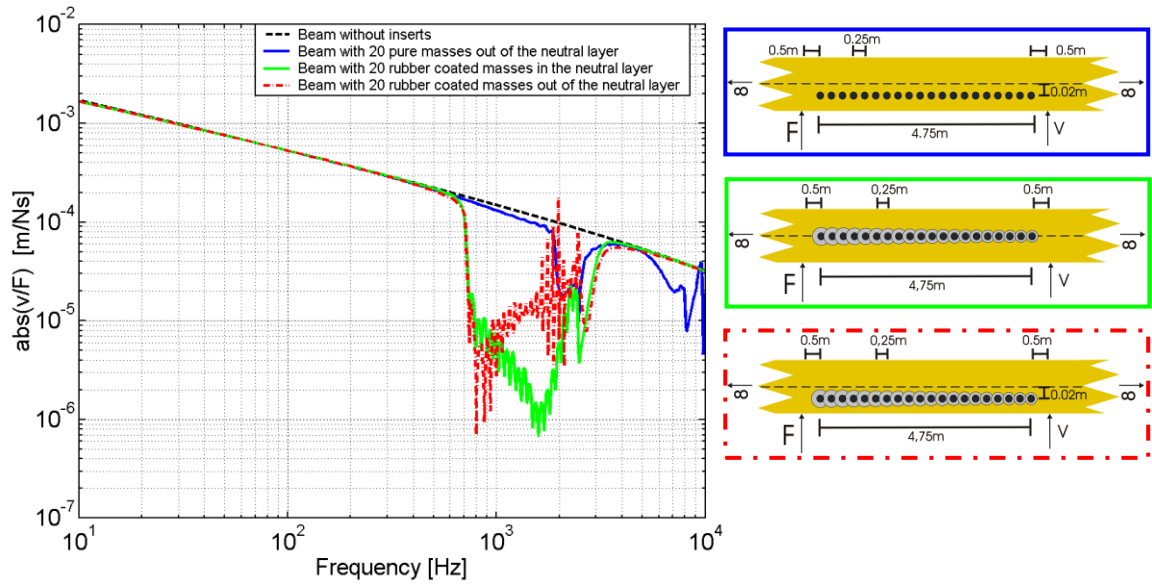


Figure 30: Transfer mobility of an infinite beam with 20 pure masses out of the neutral layer, 20 rubber-coated masses in and 20 rubber-coated masses out of the neutral layer. As depicted in the sketches on the right side 20 inserts are equally distributed in and out of the neutral layer with distances in axial direction of 0.25m to each other. The test points are located 0.5m behind the last insert.

In the following plot (Figure 31) it can be observed that there is very little influence of a stop-band on rubber-coated masses that are displayed from the neutral layer. In comparison to a beam with its inserts out of the neutral layer and distributed such that the stop-band coincides with the resonance band, there is a minor difference in the same beam with the 1st stop-band above its resonance band (compare the 1st stop-bands of the blue and black curves shown in Figure 31). Both curves of a beam with rubber-coated masses agree very well (compare the green and red dashed curves shown in Figure 31).

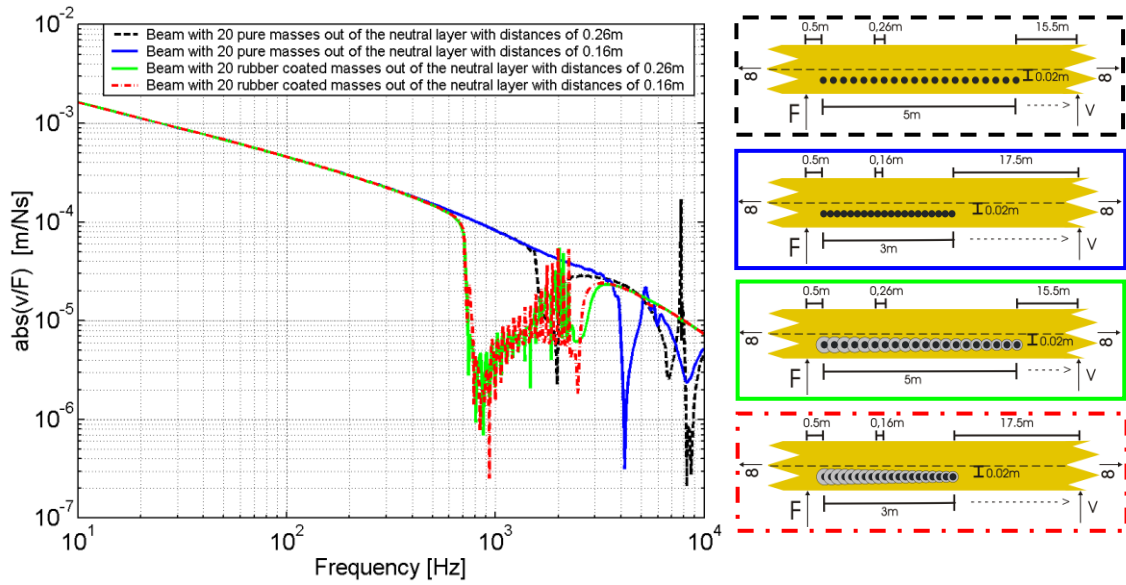


Figure 31: Transfer mobility of an infinite beam with 20 pure masses and 20 rubber-coated masses out of the neutral layer, with different equally distributed distances. As depicted in the sketches on the right side 20 inserts are equally distributed out of the neutral layer with distances in axial direction of 0.16m and 0.26m, respectively. The test points are located 20.5m behind the first insert.

Furthermore, according to Weith and Petersson [102] it could have been shown that the reduced attenuation at rising frequency with the rubber-coated masses out of the neutral layer can be minimised by distributing the inserts in randomised distances to the neutral layer.

That means that a randomised distribution of the inserts in vertical as well as in axial directions at a beam (see sub-section 4.3.3) may be helpful in controlling the attenuation.

4.4 SUMMARY OF THE CALCULATIONS ON A BEAM

All these numerical observation with masses and rubber-coated masses embedded into an infinite beam show, that there are several possibilities influence the propagating bending waves within certain limits.

As some of the effects from the numerical study can be verified with a high confidence on measurement results of a beam with ends placed in sand (see Chap. 5), all the observations of the numerical and experimental results on a beam are summarised in Chapter 6.

5 MEASUREMENTS ON SLENDER BEAMS WITH EQUI-SPACED RIGID OR FLEXIBLE INSERTS

5.1 PREPARATION OF THE MEASUREMENTS WITH A SLENDER BEAM

For the measurements with beams, a set of five beams with lengths of 5m and widths and heights of 60x80mm were purchased in order to run the investigations with various inserts²¹.

Cylindrical steel cylinders with a length of 60mm, a diameter of 16mm and a weight of 0.1267 kg had been produced by the in house workers of the Acoustic Institute of the Technical University of Berlin. The holes in the beam were drilled with a diameter of 16mm inserting the pure cylinders or with a diameter of 20mm embedding the cylinders in a suitable rubber material. Thus, the radial layer thickness of the rubber material is set to 2mm.

5.1.1 PRELIMINARY INVESTIGATION OF AN APPROPRIATE RUBBER MATERIAL

A large effort and many trials with different materials were necessary to discern a suitable rubber material, which lead to measurement results in the frequency ranges of interest. Main objective with these measurements was to show the influences by stop-bands and resonances. Hereby, low damped spring behaviour is favoured with respect to a better distinction of both conditions. Commercial silicone did not show appropriate results as the damping factor of the spring appeared too large²². At the end a special elastically Polyurethane castable resin (PUR-CR) from a specialised dealer for sculpture was most sufficient [73]. It was even possible to vary the shore hardness using a hardener (2- or 3-component liquids) within a range from ShA 40 to ShA 80.

²¹ Due to the limited number of beams available, it was not possible to explore each observation that follows from the results in the numerical study.

²² In a very early trial with silicone rubbered masses embedded in one of the wooden beams, significant resonance behaviour could not been measured (Stütz [90]). Commercial silicone appeared to have large damping properties, which vary by the time. As discussed in Chapter 1 and shown in sub-section 11.1.2, it is useful to obtain a significant attenuation at the resonances of the rubber-coated masses by keeping the loss factor of the springs as low as possible.

5.1.2 PRE-TEST MEASUREMENTS WITH RUBBER-COATED MASSES EMBEDDED INTO BEAM PIECES

In pre-test measurements small pieces were cut from a wooden beam to lengths of 50 mm and filled with a mass coated with rubber material. To assess the appropriate material conditions, measurements with a shaker have been carried out.

Therefore such a piece of a beam with the length of 50mm and an embedded steel cylinder coated in the PUR has been screwed onto a shaker. Acceleration sensors were placed to both sides of the mass and onto the top of the beam (see Figure 32). The excitation by the shaker happened vertically.

Three samples of the polyurethane castable resin were mixed with shore hardness of ShA 40, 60 and 80. An amplified white noise signal has been used to excite the beam piece by the shaker (Figure 32).

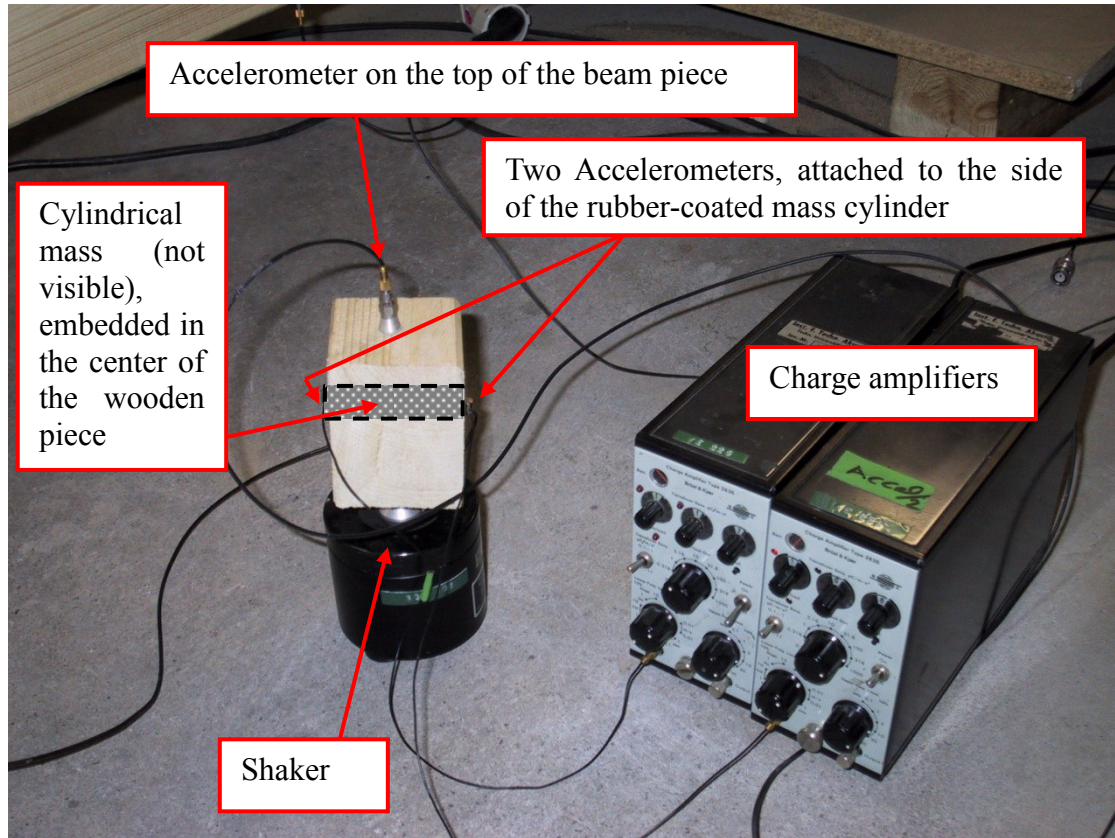


Figure 32: Measurement set-up with a small piece of the wooden beam, filled with a rubber-coated mass, which was vertically driven by a shaker. To assess an appropriate material, measurements with a shaker, excited by white noise, have been carried out.

The measurement system used has been a 16-Multi-channel acquisition system by OROS. The sampling rate was set to 20 kHz with a 6400 FFT size. Thus, according to Nyquist the frequency resolution F_r of all measurements amounts to

$$F_r = \frac{10000 \text{ Hz}}{6400} = 1.625 \text{ Hz} \quad (28)$$

The frequency responses of each accelerometer placed on the sides of a mass to the accelerometers on the top of the length of beam are shown in Figure 33. The magnitude shows a minimum between 1 kHz and 2 kHz on the left side of the masses with ShA 40 and ShA 80 and a maximum between 2 kHz and 3.5 kHz on both sides of the masses. The beam piece with the rubber layer with ShA 60 only shows a smoothed frequency response without significant extremes and may not be appropriate for use with the following measurements.

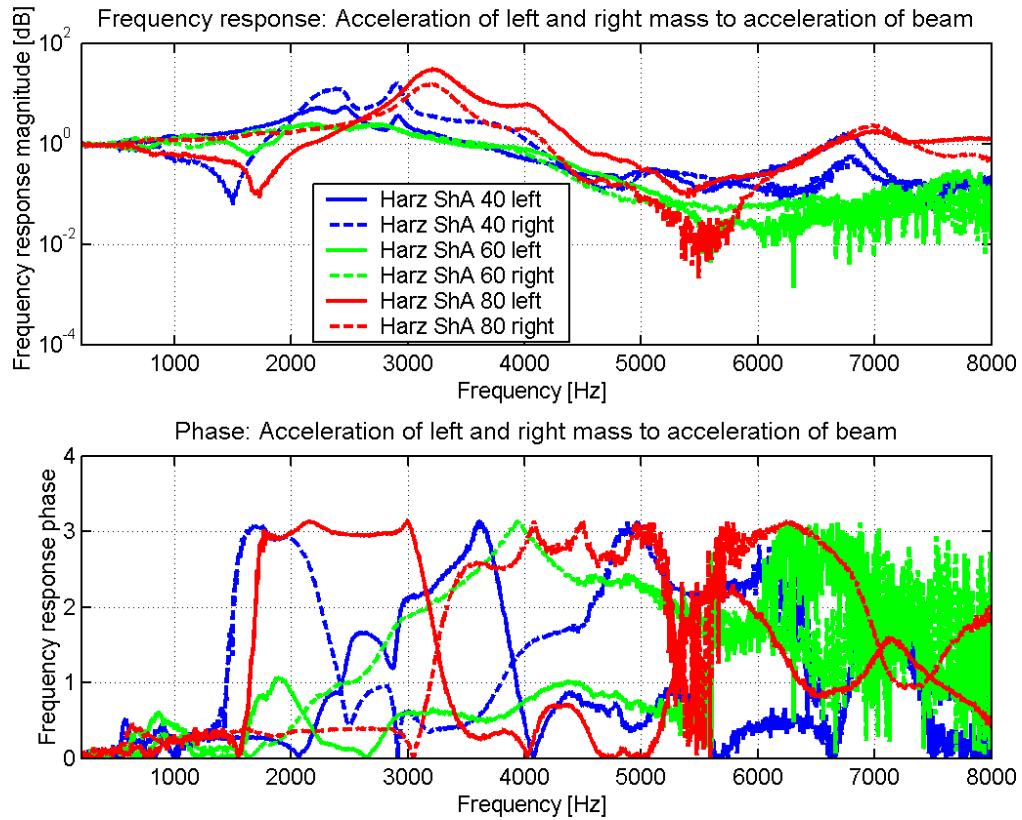


Figure 33: Frequency response of three beam pieces with embedded rubber-coated masses. The Shore hardness of the pieces is set to ShA 40, 60 and 80. Accelerometers are placed on each side of a mass and on the top of the beam piece.

The results show that the movement of the mass cylinder obviously varies over its cylindrical length. The minimum and maximum of the frequency response are visible either on the left or on the right side of the mass. The phases of the two minimum accelerations (ShA 40 and ShA 80 at frequencies about 1.5 kHz and 1.8 kHz) correspond very well. Phase changes of the pieces with a Shore hardness of ShA 40 and ShA 80 corresponds to the maxima of the mass vibrations.

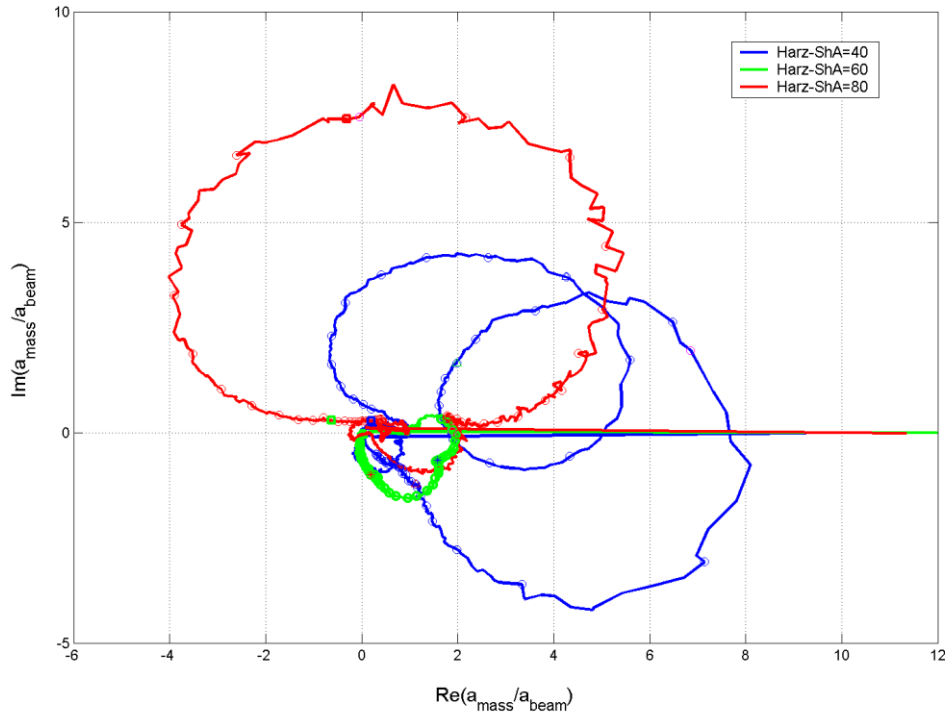


Figure 34: Three beam pieces with embedded rubber-coated masses. The Nyquist plot shows the real and imaginary part of the mean of the accelerations on the sides of the masses to the acceleration of the top of the beam piece. The Shore hardness of the pieces is set to ShA 40, 60 and 80.

The frequency responses of the two accelerometers on the sides of the top accelerometer reveals information about the resonance and damping conditions of this system. The Nyquist plots of the three different Shore hardnesses (Figure 34) show that rubber-embedded masses react differently. The resulting circles of ShA 40 and ShA 80 have larger diameters than those with a Shore hardness of ShA 60. The larger the diameter of the circles in a Nyquist plot, the lower the damping factor or the spring is²³.

These observations led to the decision to use the mixture of PUR with a Shore hardness of ShA 40 for a lower resonance frequency and ShA 80 for a higher resonance frequency in the measurements with a beam.

In addition it is of interest, which impact these observations will have onto the transfer mobility of a real beam with rubber-coated inserts. As we have seen in the calculations a large attenuation in the transfer mobility at the spring-mass resonances is to be expected (see Figure 17).

²³ In the measurements on a piece of beam with Shore hardness of ShA 40 two different resonances in the Nyquist-plot are visible (Figure 34). The doubled circles correspond to the two maxima arising at different frequencies in Figure 33.

In the following figures (Figure 35 and Figure 36) the magnitudes of the velocity are shown. On the beam piece with a Shore hardness of ShA 40 one side of the mass show a minimum velocity between 1 kHz and 2 kHz (see the orange circle in Figure 35). The same behaviour can be seen at the four pieces with a Shore hardness of 80 ShA, whereas the other side follows the vibrations of the entire beam piece (Figure 36).

In the frequency ranges between 2 kHz and 3 kHz (ShA 40) respectively 2 kHz and 5 kHz (ShA 80) the mass vibrations reach maximum values. Close to these frequencies the entire beam piece shows a minimum (see the brown circles). It is very likely that the largest reflection of bending waves in an entire beam, embedded with such rubber-coated inserts, happens in this frequency region, when the beam vibration is minimised and the rubber-coated masses are resonating. Thus, this frequency range can be declared in the system beam-rubber-mass as the “anti-resonance” of the beam piece.

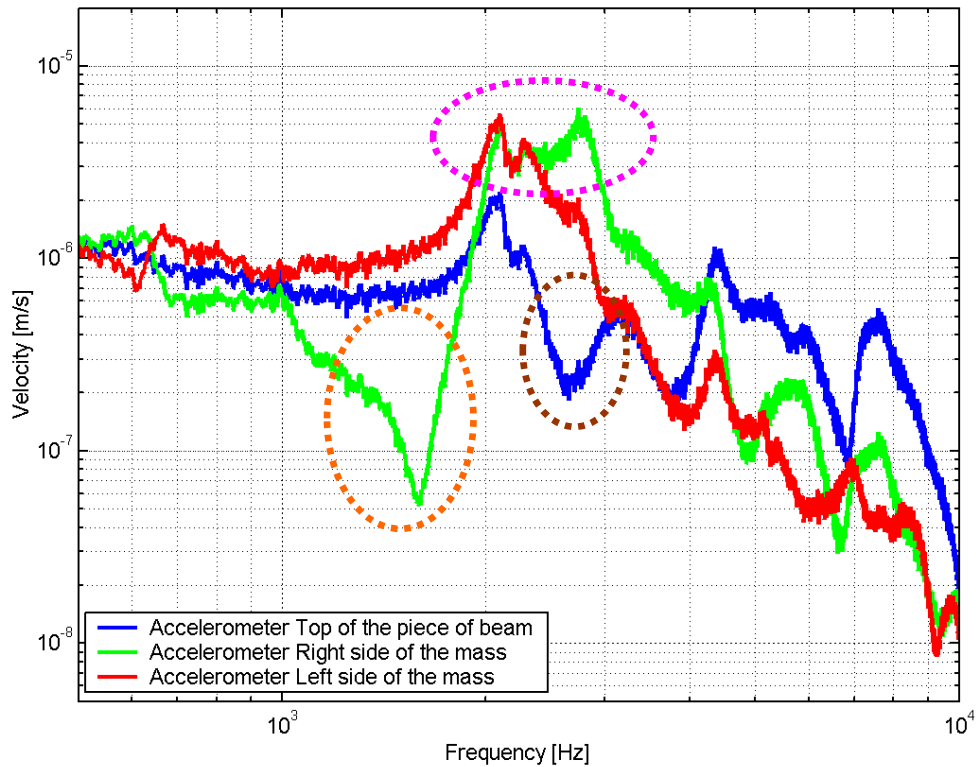


Figure 35: Velocity of a beam piece with masses embedded in rubber coating with the Shore hardness of ShA 40. Accelerometers are placed on each side of a mass and on the top of a piece. The orange dotted circle denotes a velocity minimum of one side of the masses, the pink coloured dotted circle the maximum of it. The brown dotted circle highlights a minimum vibration of the entire beam piece, which is possibly the anti-resonance.

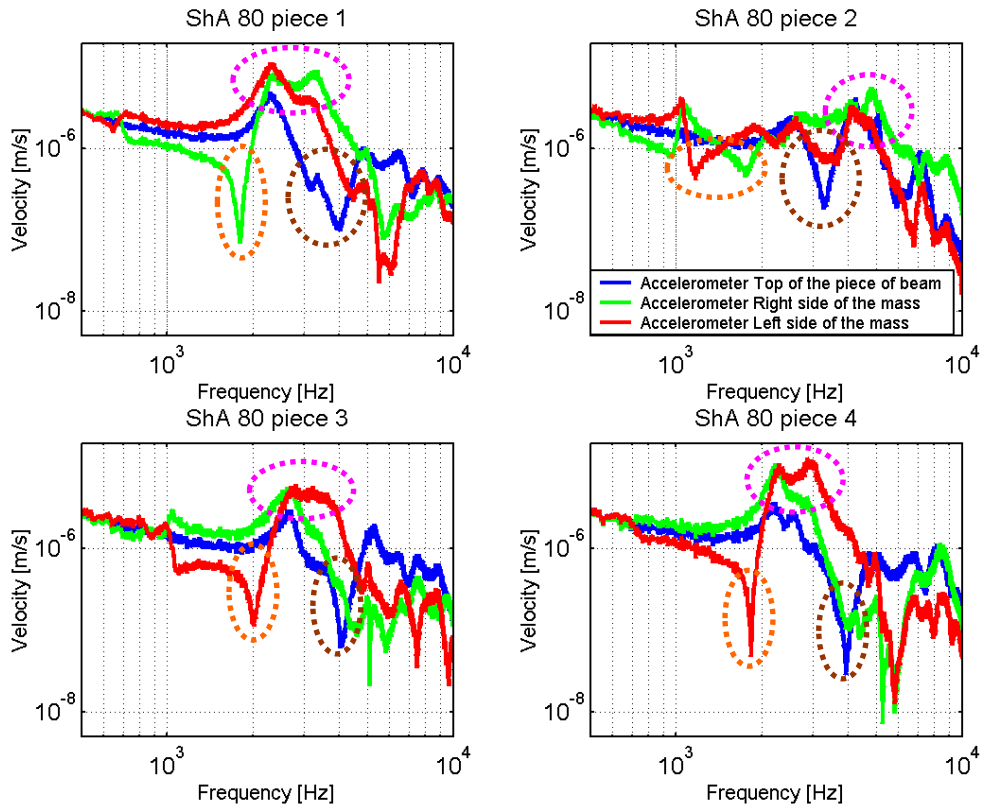


Figure 36: Velocity of 4 beam pieces with masses embedded in rubber coating with a Shore hardness of ShA 80 each. *Accelerometers are placed on each side of a mass and on the top of each piece. The orange dotted circle denotes a velocity minimum of one side of the masses, the pink coloured dotted circle the maximum of it. The brown dotted circle highlights the minimum vibration of the entire beam piece.*

The scattering of the resonances is very likely related to the sensible filling procedure of the PUR. It is obvious that the masses do not vibrate as one mass point. Varying thicknesses of the layers come along with varying stiffnesses along the cylindrical axis and in radial directions. This may explain the scattering in resonances and an asymmetric shaking cylinder²⁴.

However, within certain frequency ranges (1 kHz to 3 kHz with ShA 40 and 1 kHz to 5 kHz with ShA 80), a reduced vibration of either the masses or the entire beam piece is to be expected. It is necessary to investigate if the vertical vibrations of the shaker onto the beam piece are directly comparable to the propagating bending waves induced by a shaker on one end of a beam (see section 5.2). Furthermore, the reflections of the

²⁴ Maysenhölder [67] experimentally investigated rubber-coated lead spheres in a rigid frame and explained the existence of two maxima with the thickness resonances of the elastic layer. Maria Heckl [35] proved the existence of two different resonance frequencies for bending waves and torsional waves exciting a rubber-coated mass. In this measurement set-up - with a vertical excitation of a small wooden piece - torsional vibrations are not expected, but they may need to be considered in the measurements with beams.

bending waves in a beam with inserts are not measurable in these pre-tests with a “one-dimensional” beam piece.

Therefore, the existence of three different observed conditions of velocity needs to be considered in the following assessment of the measurement results on real wooden beams:

1. The minimum velocity of one side of the mass.
2. The “real resonance” with a maximum velocity of the cylindrical mass.
3. The “anti-resonance”, since the vibration of the beam piece is considerably reduced²⁵.

It will be shown in the investigation on a real beam with 5 or 10 embedded spring-mass systems, that the beam with inserts and a castable resin with a Shore hardness of ShA 40 has its minimum at a frequency that appears in the range of the minimum velocity of one side of the mass of the beam piece (compare Figure 35 and Figure 50 in sub-section 5.3.4).

On the other hand, it makes sense to imagine ideal reflections of bending waves evoked by the resonance of the rubber-coated masses while the entire beam is stationary. Furthermore, a large impedance change might be “seen” by the bending wave, when the mass is vibrating in maximum.

However, in the numerical study the attenuation peaks of the transfer mobility are related to the maximum acceleration of the cylindrical mass. Thus, these pre-test measurements show the complexity of real conditions such as diverting vibrations of cylindrical masses, the presence of inhomogeneous and non-isotropic wooden beams, scattering damping factors of the spring, etc.

Nevertheless, it will be shown, that some of the observed effects in the calculations can be determined with “real conditions” as well.

Finally, as a result of the pre-test measurements, the castable resin with a Shore hardness of ShA 40 for rubber with a low stiffness and ShA 80 for rubber with a high stiffness seems to be most appropriate for taking measurements on the beams.

²⁵ It is assumed that the resulting resonance frequencies of the “real resonance” and this “anti-resonance” coincide within a small range at measurements on beams. In all further discussions with the infinite or 5m long beams this “anti-resonance” will be called “resonance” for short.

5.2 MEASUREMENTS ON A SLENDER BEAM

For measurements on real beams, the same system and FFT settings used for the pre-test measurements has been employed²⁶. The shaker has been driven by an impulse, which triggers the start of the recording of the OROS measurement system. The inserts, the shaker and the sensors were set up in the same way as described for the numerical study. The shaker excited the beam with impulses. The force transducer was located between the shaker and the beam.

The general test set-up of the beams was as follows:

- Both ends of the beams were embedded into sand in a depth of 0.5m to reduce reflections.
- In 1.25m distance to one end of a beam the excitation point was located.
- In 1.25m distance to the other end of a beam the measurement point with an accelerometer was located.
- 5 or 10 discontinuities were placed on positions starting in 0.35m distance to the excitation point. The distances from mass to mass were set to 0.4m (5 discontinuities) or 0.2m (10 discontinuities) to each other.

Figure 37 shows the general measurement set-up.

²⁶ See sub-section 5.1.2

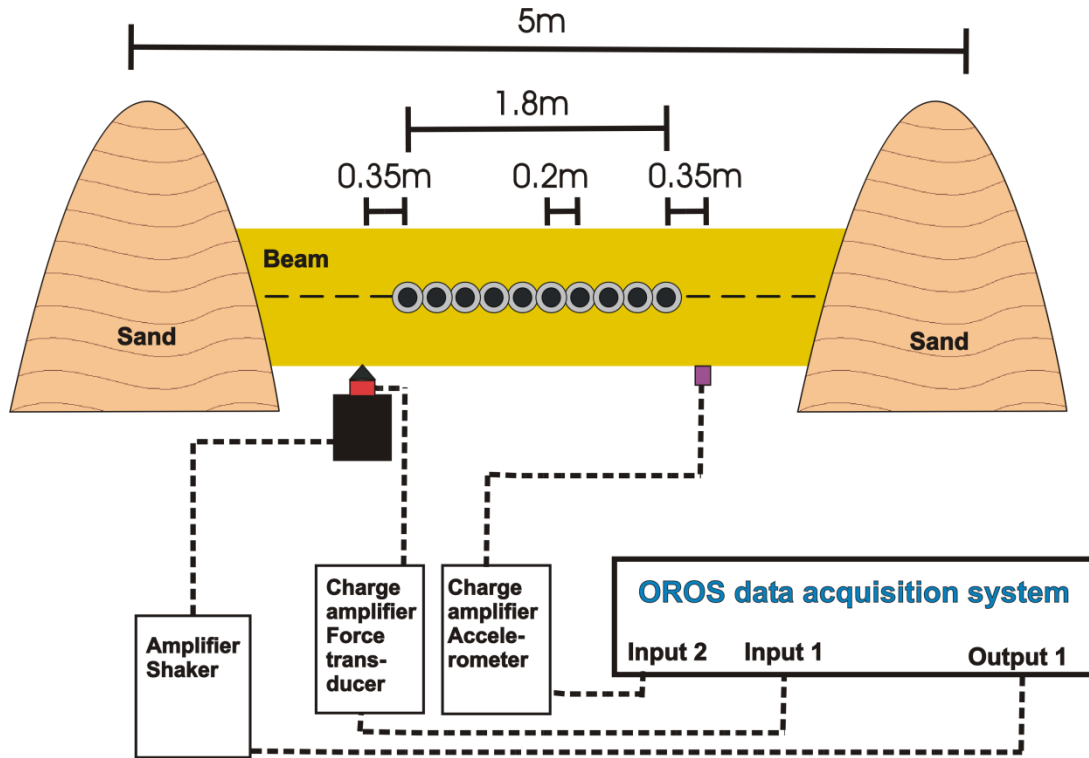
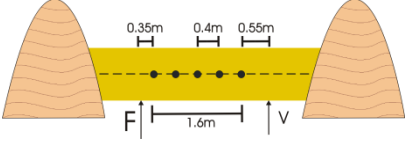
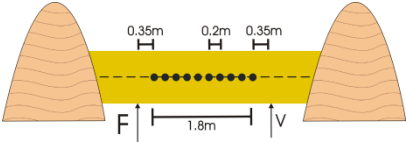
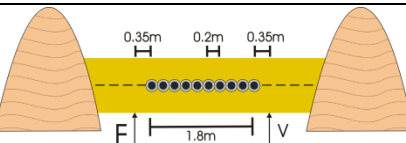
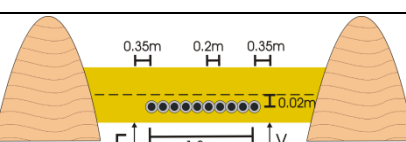
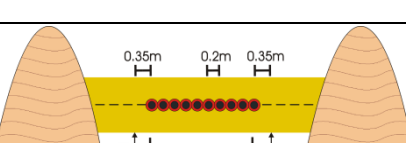
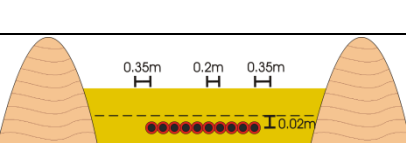


Figure 37: Basic measurement set-up of a slender beam with discontinuities embedded in the neutral layer. Both ends of the beam with a length of 5m are covered by sand to reduce reflections. The excitation happened on the left side of the 1st insert with a shaker and a force transducer connected. Data evaluation happened with an accelerometer placed on the right side of the inserts. Data acquisition and analysis were performed using a multi-channel data acquisition system from OROS. For the measurements either 5 or 10 insert were used. These consist of pure masses or rubber-coated masses with two different shore hardness and had been placed within the neutral layer or shifted by 20mm out of the neutral layer.

In the following Table 3 the six measurement configurations are shown:

Table 3: Six configurations with beams and inserts have been measured

	5 pure masses in the neutral layer
	10 pure masses in the neutral layer
	10 rubber-coated masses in the neutral layer (low stiffness, Shore hardness of ShA 40)
	10 rubber-coated masses in the neutral layer (high stiffness, Shore hardness of ShA 80)
	10 rubber-coated masses out of the neutral layer (low stiffness, Shore hardness of ShA 40)
	10 rubber-coated masses out of the neutral layer (high stiffness, Shore hardness of ShA 80)

The beam was excited with a short impulse on the driver point. Accelerometers were placed on the half way in the middle of the beam and in 1.85m distance to the other end of the beam (0.35m distance to the 10th inserts by using 10 discontinuities or 0.55m distance to the last insert, if 5 discontinuities were only used).

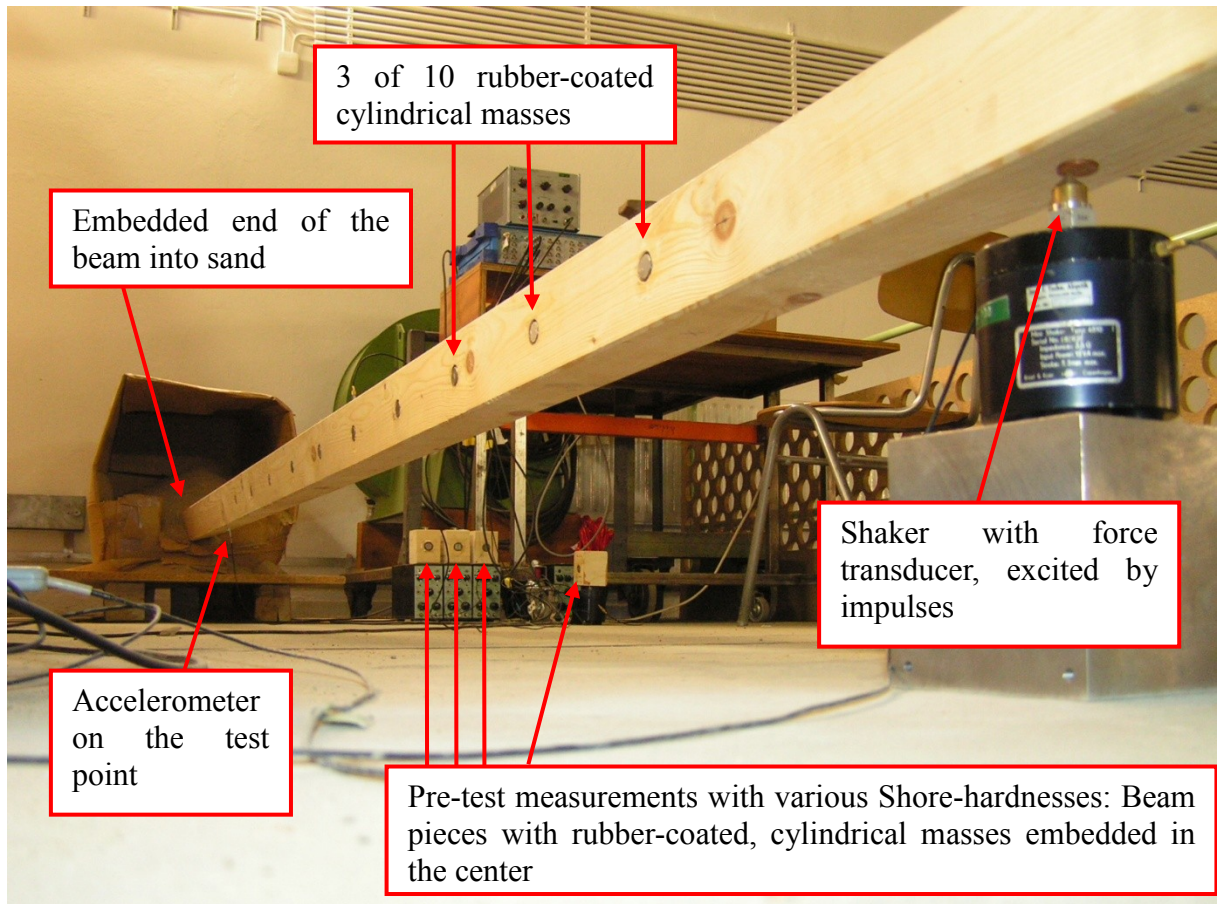


Figure 38: Measurement set-up of a slender beam. Both ends of the beam are embedded into sand to reduce reflections. 10 rubber-coated masses are equally distributed in the neutral layer. In the foreground the shaker unit is shown, which is placed on a metal cube to adjust the optimised distance to the beam (for the up following measurements the tip of the shaker has been placed centrically to the metal coin). In the background the pre-test measurement set-up with four pieces of a beam with rubber-coated masses embedded is visible.

A detailed picture of the shaker unit is displayed in Figure 39. To increase the initial energy into the beam, the shaker was driven by a short impulse induced over a metal tip on the shaker and a metal coin, which was bonded on the bottom side of the beam. The force transducer is rigidly screwed between the shaker excitation unit and this metal tip.

In Figure 40 the rubber coated area of a spring-mass is highlighted.



Figure 39: Measurement equipment of a slender beam with the excitation point of the shaker in 1.25m distance to one end of the beam.

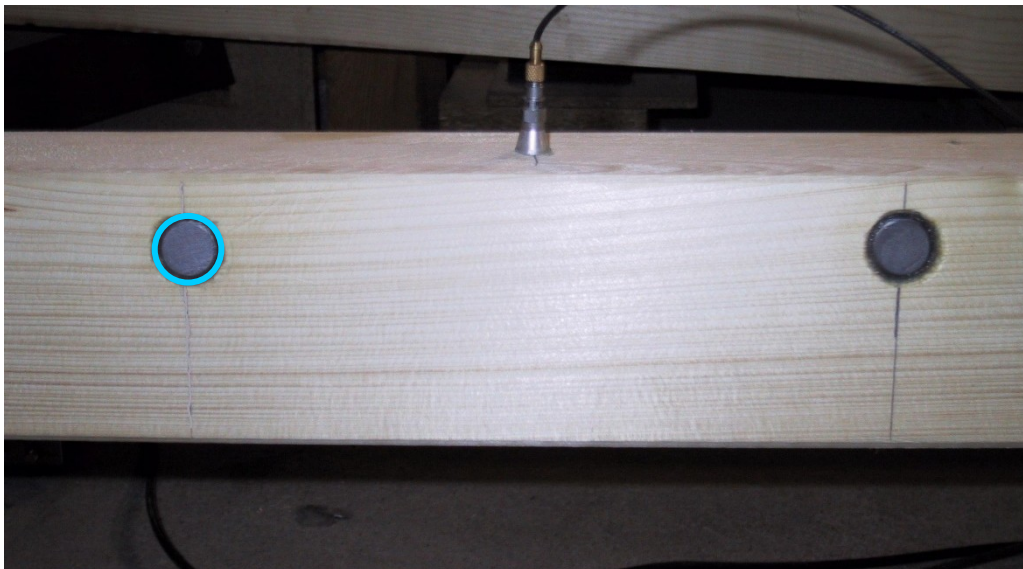


Figure 40: The 5th and 6th position of rubber-coated masses out of the neutral layer on a slender beam. The green circle highlights the rubber area of the embedded steel cylinder on the left side of the picture. The accelerometer in the middle of the inserts on the top of the beam has been used for control reasons.

5.3 MEASUREMENT RESULTS OF A SLENDER BEAM

5.3.1 REPEATABILITY CHECK

For each configuration five measurements have been carried out. In Figure 41 the transfer mobility of a pure beam (without any holes or inserts) shows a high repeatability of the five measurements. In the frequency range below 200 Hz reflections from the ends are very likely the reasons for the peaks. The damping effect of the embedded ends into sand does not represent ideal non-reflecting conditions. In all measurement results it has to be considered that the wooden beam out of pine cannot be treated as entirely isotropic and homogenous.

Additionally some of the beams were slightly drilled in axial direction, which could influence the bending waves leading in torsional vibration.

The weight of the beams also scatters, which has an impact to the densities and varying bending wave speeds.

Nevertheless, we will see that the measurements of the wooden beam with different configurations are sufficient to detect some of the effects observed in the numerical study (section 4.3).

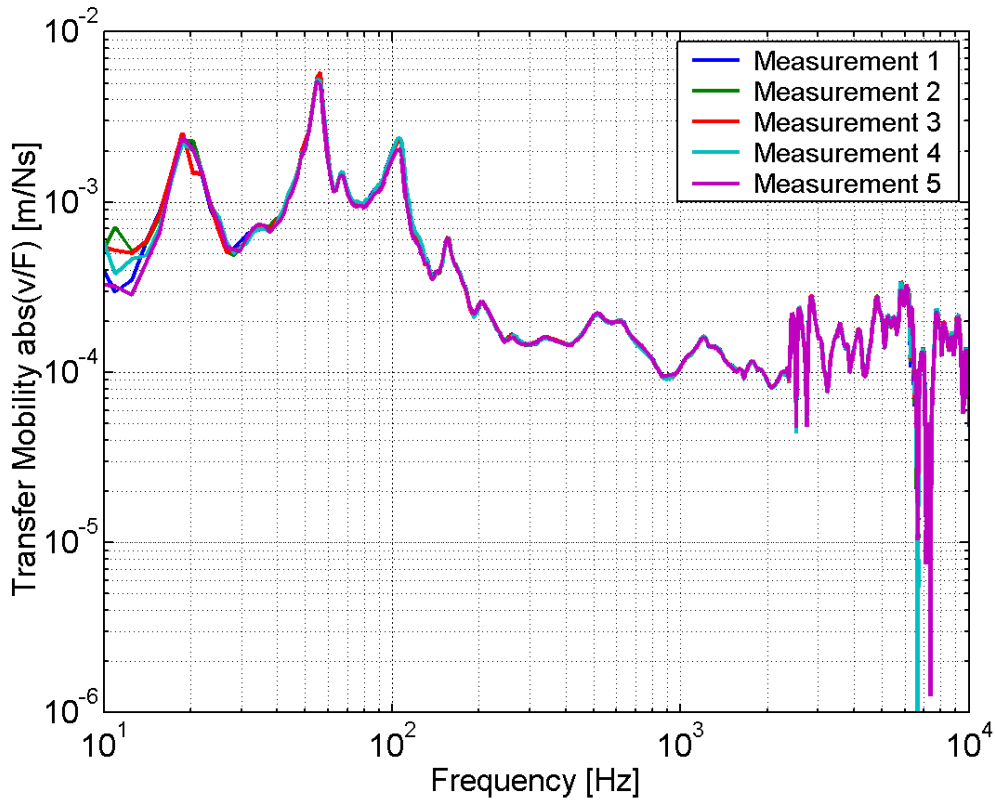


Figure 41: Transfer mobility of 5 measurements carried out on a pure beam within one test sequence. The various curves overlay very well and underline a high repeatability of the test runs.

5.3.2 MEASUREMENT RESULTS OF A BEAM WITH HOLES

In Figure 42 the transfer mobilities of the pure beam and the same beam with drilled holes are depicted. In the interesting frequency range between 200 Hz and 5 kHz slight differences are visible. As the configurations with embedded inserts will be normalised later on to be comparative with the measured test results, one of the wooden beam with only holes has been used as a baseline for further comparisons²⁷.

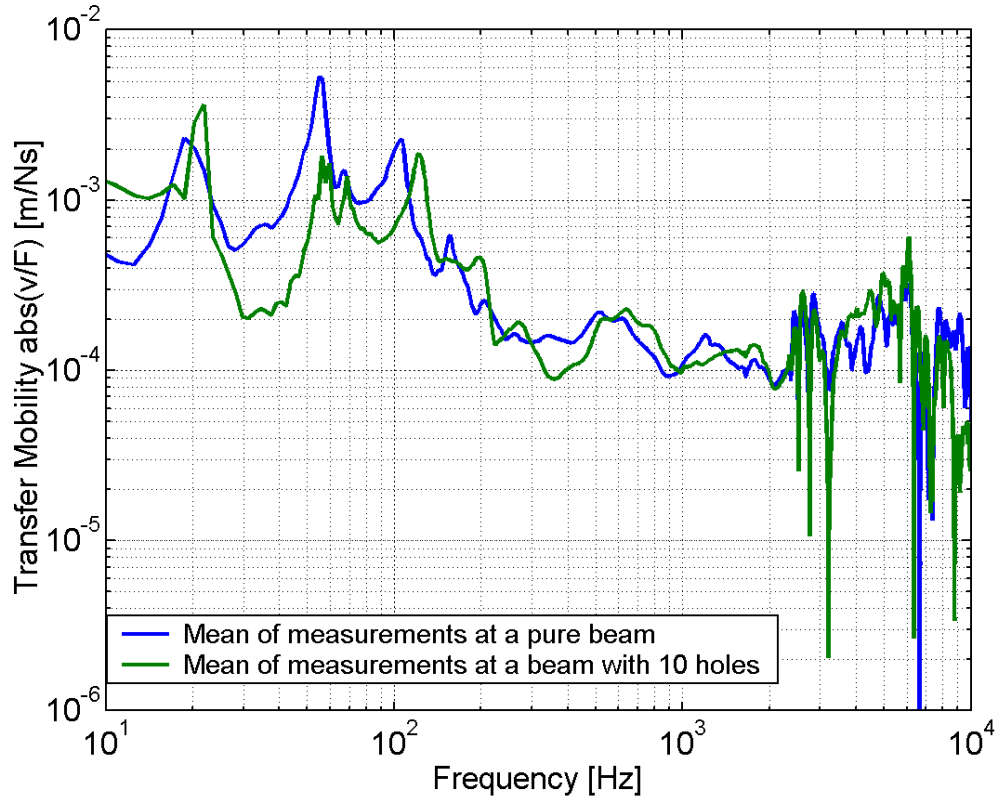


Figure 42: Transfer mobilities of the mean of 5 measurements carried out on a pure beam and on the same beam with 10 holes.

5.3.3 MEASUREMENT RESULTS OF A BEAM WITH MASSES

In the following figures the measurement results are compared with the results of the calculations.

To be able to compare the measurements with the calculations the ratio of the transfer mobilities of the beam with discontinuities to the beam without discontinuities

²⁷ Five beams had been available for this measurement series. It turned out that the properties of these beams with respect to their isotropic and homogeneous behaviour differ. Thus, it has to be considered, that each of these beams reveals in slightly varying transfer mobilities. Due to the large effort of measuring the transfer mobility of a beam, the decision was made using one of the beams with only holes as a baseline. Thus, not every beam has been measured in its form with only holes and therefore the ratios of the transfer mobilities are affected by the different conditions of each beam.

(calculations) and to the beam with only holes (measurements), respectively, will be shown. Thus, a ratio smaller than unity displays attenuation in the transfer mobility.

The measurements were undertaken with a resolution of 1.625 Hz, such that the results could be smoothed, employing a moving average.

To get an impression of expected results, Figure 43 illustrates the ratios of the transfer mobility of beams with 5 and 10 masses from the calculations done in Chapter 4. The stop-bands of the beam with 5 masses and with 10 masses are clearly depicted. The 1st stop-band of the beam with 10 masses coincides with the 2nd stop-band of the beam with 5 masses and shows a larger attenuation.

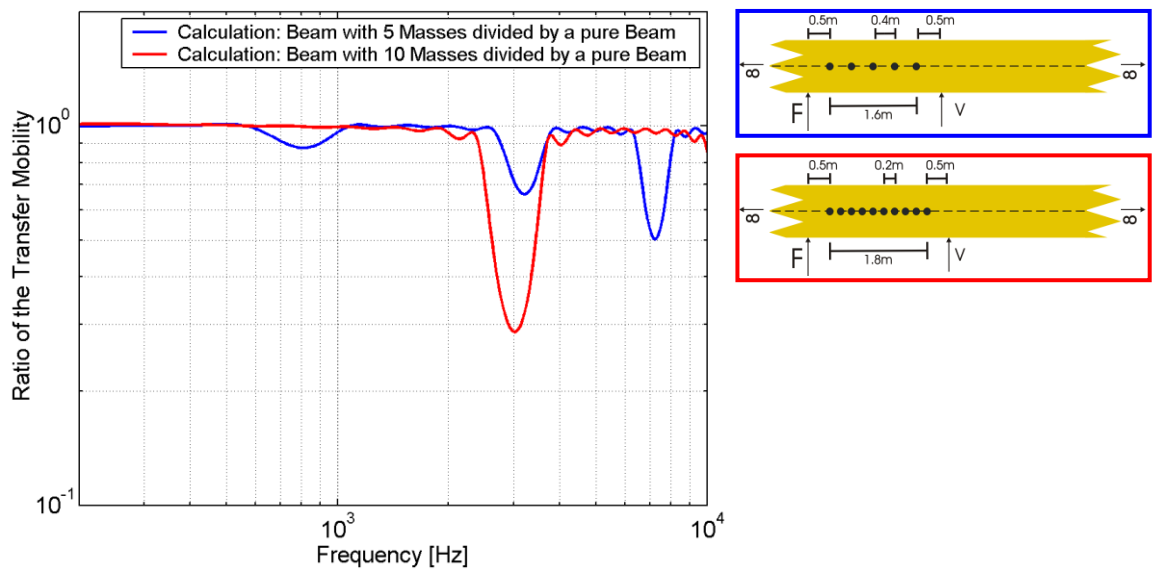


Figure 43: Calculated ratio of the transfer mobility of a beam with 5 masses (distances 0.4m) and a calculated beam with 10 masses (distances 0.2m), normalised with the same beam without any inserts. As depicted in the sketches on the right side the masses are equally distributed in the neutral layer. The test points are located 0.5m behind the last insert.

Figure 44 shows the first comparison of a measured beam with 5 masses (0.4m distances) and 10 masses (0.2m distances). The ratio of the transfer mobility measured on beams with 5 and 10 pure masses in the neutral layer illustrates the influence of the periodically distributed masses.

As expected the possible 1st stop-band of the 5 masses in the frequency range of about 848 Hz (see Table 2) does not exist at the beam with 10 masses²⁸. The 2nd stop-band of the beam with 5 masses, expected at a frequency of 3.93 kHz, coincides very well with the 1st stop-band of the beam with 10 masses. The attenuation of the beam with 10 masses is increased and has a broader frequency range than the beam with 5 masses.

²⁸ The measured attenuations at the beam with pure masses are very likely related to real existing stop-bands.

As has been shown in sub-section 4.3.1, the effect of a reflection of bending waves is higher and broader the more discontinuities are used.

Now it is interesting, what happens with the 3rd stop-band of the beam with 5 masses, which is expected to be at a frequency of 7.67 kHz (see Table 2). There is a decreased area of the transfer mobility at the frequency range around 6 kHz visible (see the blue curve and blue arrow in Figure 44), which might be the measured 3rd stop-band. On the other side a similar effect can be seen at a slightly lower frequency range at the beam with 10 masses, which is not expected due to the calculations (the 2nd stop-band of the 10 masses should be beyond the measurement upper limit of 10 kHz). Thus, at higher frequencies a significant conclusion becomes difficult.

However, the observed conditions at the measurement with the masses show a good agreement with the calculations at frequencies up to 4 kHz.

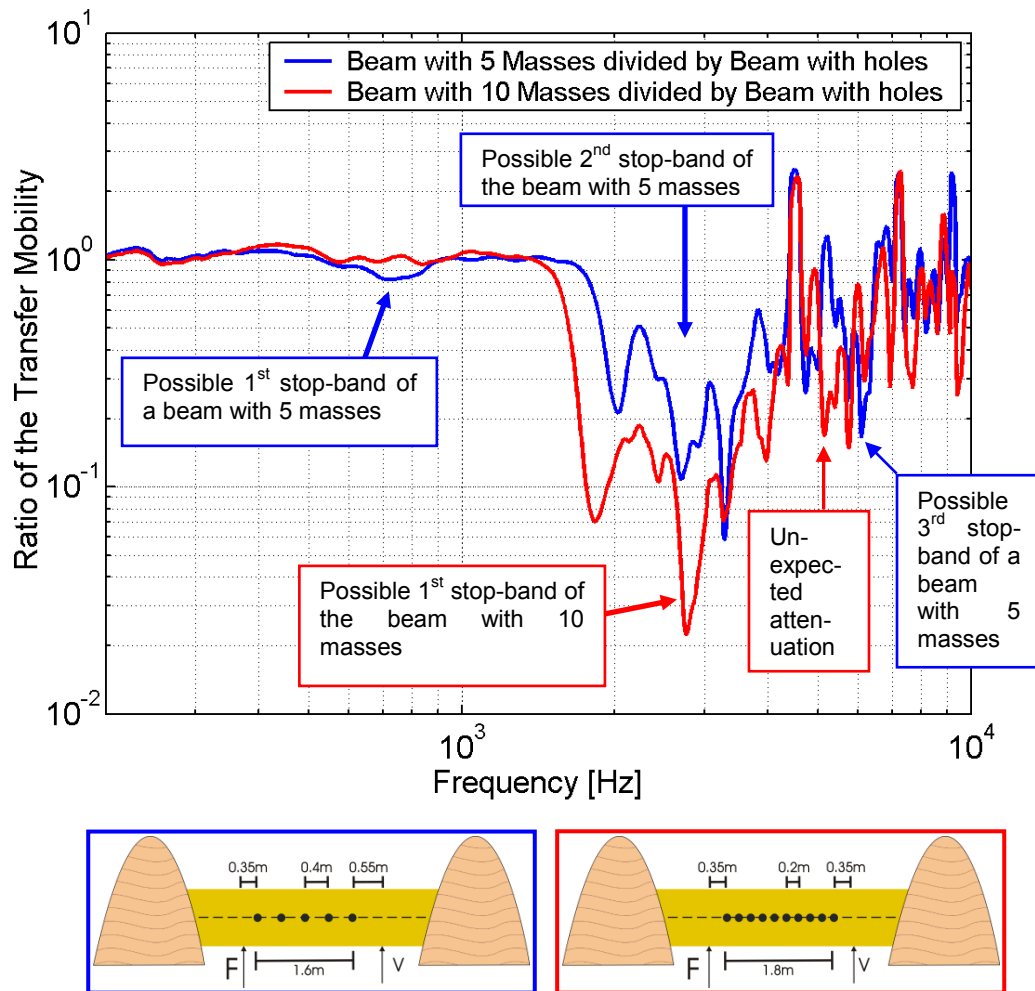


Figure 44: Measured transfer mobility of a beam with 5 and 10 masses (distances 0.2 m and 0.4 m), normalised with the same beam with only holes. As depicted in the sketches on the bottom side both ends of the beams are embedded into sand to simulate infinite conditions. Possible stop-bands are highlighted.

If we compare now the ratio of the transfer mobility of a beam with 5 masses again, but with the calculated results (Figure 45), the influence of the periodically distributed masses is obvious. The measurement curve shows a higher and broader attenuation in the first three stop-bands and the center frequency seems to be higher in compare with the calculated result. As it was observed in the parameter study of the loss factor of the beam and the Young's modulus (Sub-section 11.1.1, Figure 84), such variations might be put down to discrepancies of these values in real conditions.

At low frequencies both curves agree very well (Figure 45). The first stop-band, which is located in the frequency range of 500 Hz to 600 Hz is slightly visible.

The 3rd stop-band in the range of 6 kHz of the measured beam was expected to have a larger attenuation than the 2nd stop-band in the range of 2 kHz to 4 kHz (see the blue curve of the calculated beams). This is not the case and might be put down to inhomogeneous and non-isotropic conditions of the wooden beam and increased measurement errors at higher frequencies. Influences of differing Young's modulus in the real beam might be responsible for the slightly shifted stop-bands in frequency. In addition, the in-situ stiffnesses of the masses might have an influence to the results.

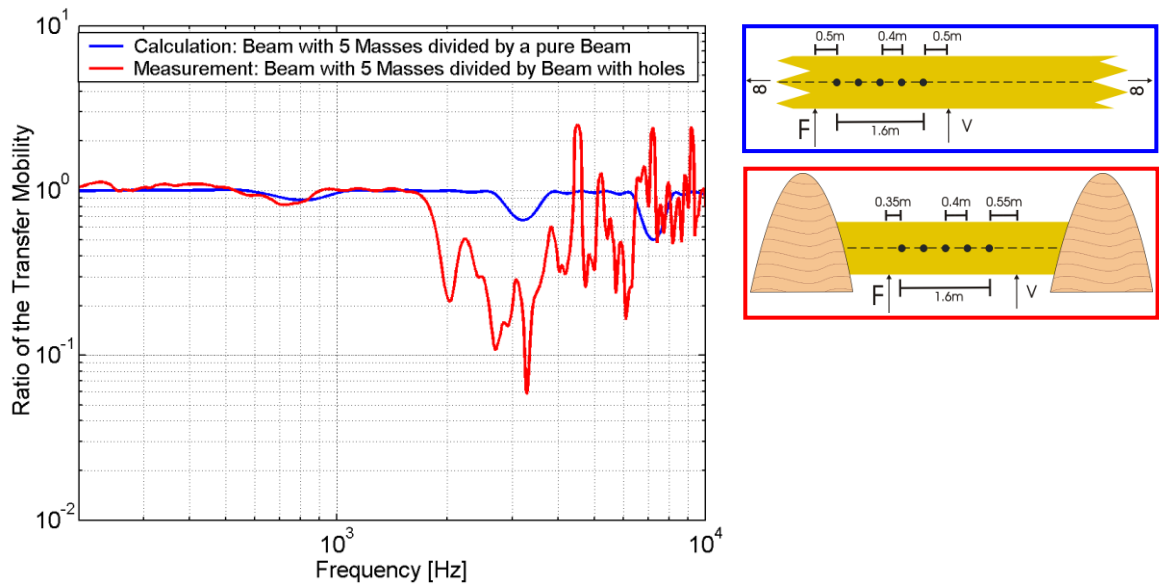


Figure 45: Ratio of the transfer mobility of beams with 5 masses (distances 0.4m). The normalisation happened with a beam without any inserts (calculation) and with the same beam with only holes (measurement), respectively. As depicted in the sketch on the right bottom side, both ends of the measured beam are embedded into sand to simulate infinite conditions. The test points are located 0.5m (calculation) and 0.55m (measurement) behind the last insert.

The same comparison with 10 masses shows similar effects at the stop-band (Figure 46). The attenuation of the transfer mobility is broader and increased at the measured beam. At frequencies from 4 kHz on variations are visible, which do not coincide with the measurement result. These differences as mentioned before might be put down to inhomogeneous and non-isotropic conditions of the wooden beam.

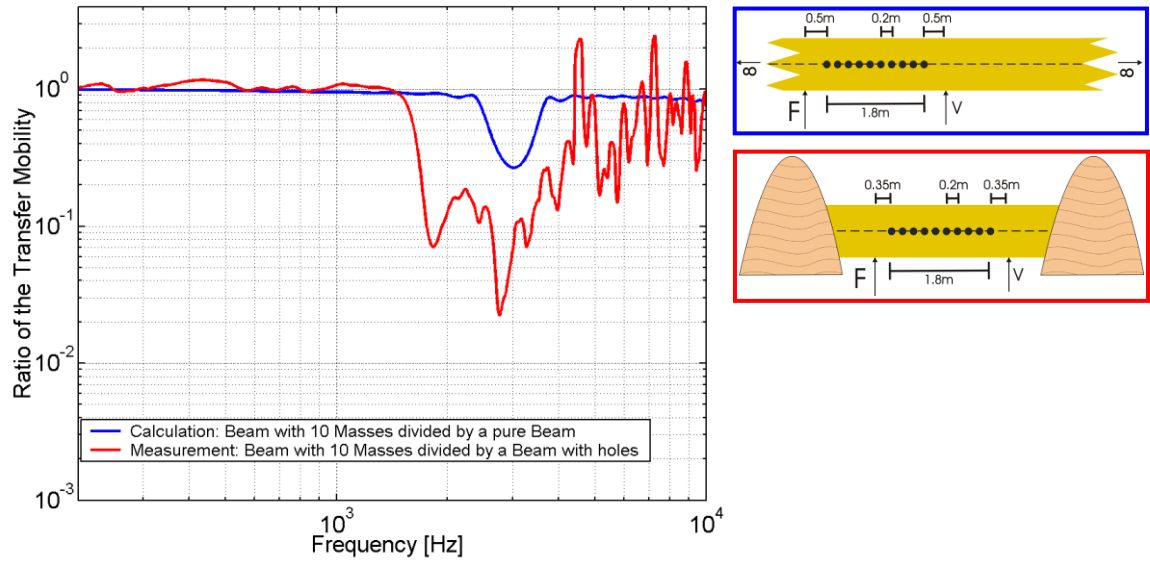


Figure 46: Ratio of the transfer mobility of a beam with 10 masses (distances 0.2m). The normalisation happened with a beam without any inserts (calculation) and with the same beam with only holes (measurement), respectively. As depicted in the sketch on the right bottom side, both ends of the measured beam are embedded into sand to simulate infinite conditions. The test points are located 0.5m (calculation) and 0.35m (measurement) behind the last insert.

Summarised, the results of the measurements on beams with 5 and 10 masses embedded in the neutral layer show that the 1st stop-band of both types arise at the frequency range as expected, although with a broader and increased attenuation of the transfer mobility. At higher frequencies differing results appeared. These could be attributed to the limits of the Euler-Bernoulli beam and real existing other wave types, which are not considered in the numerical study²⁹.

²⁹ On rails Maria Heckl [35] has shown different stop- and pass-bands in terms of whether the other wave types exist.

5.3.4 MEASUREMENT RESULTS OF A BEAM WITH RUBBER-COATED MASSES

If the embedded masses are coated with rubber, each represents a spring-mass system distributed along the beam in the neutral layer.

As we have seen in the numerical investigation (Chap. 4.3), the stop-bands vanish by coating the masses with a rubber material and the attenuation at the resonance of these spring-mass systems appears instead (Figure 17). Thus, this resonance attenuation dominates in comparison with the attenuation of a stop-band in the calculations.

Figure 47 shows the comparison of a beam with 10 rubber-coated masses with shore hardness of 40 ShA and the beam with 10 pure masses. On the first view it is not quite clear, which attenuation in the transfer mobility represents the “resonances” as expected from the calculations. A larger attenuation band is visible between 800 Hz and 2 kHz, two others at about 300 Hz and 5 kHz.

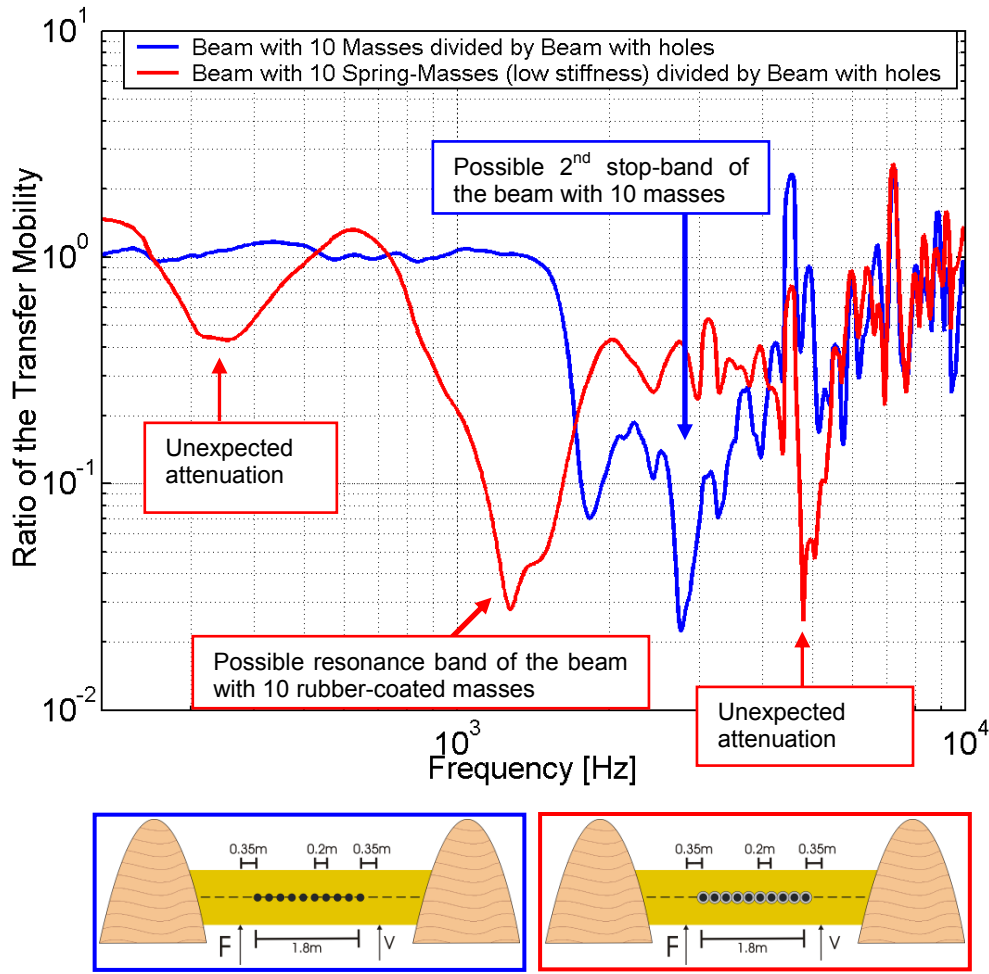


Figure 47: Ratio of the transfer mobility of a beam with 10 masses (distances 0.2m) and 10 spring-masses, respectively. The normalisation happened with the same beam with only holes. As depicted in the sketches on the bottom both ends of the measured beams are embedded into sand to simulate infinite conditions. The test points are located 0.35 m behind the last insert.

In pre-test measurements with only one rubber-coated mass embedded in a beam piece (Figure 35), it was observed that there were two suspicious frequency ranges resulting in attenuated vibrations. One of those appeared at approximately 1.5 kHz (one accelerometer on one side of the mass), the other at about 2.5 kHz (accelerometer on the top of the beam piece). In addition, it resulted that the appearance of these resonances belied a large scattering.

However, it is very likely, that the attenuated transfer mobility between 800 Hz and 2 kHz indicates the resonance band of the rubber-coated masses with low stiffness (Shore hardness of ShA 40).

To emphasize this assumption and to increase the confidence of having “real” resonances and stop-bands, it makes sense to include the results of the phases and coherences, respectively.

5.3.5 RESONANCE AND STOP-BAND INVESTIGATION WITH PHASES AND COHERENCES

The transfer mobility of the beam with 10 rubber-coated masses in Figure 47 gives reason to assume that a resonance band is located in the frequency range between 800 Hz and 2 kHz. However, this is only an assumption, which needs to be investigated by having a closer look onto the phases and the coherences³⁰.

It would have been a large undertaking to measure the resonance of each spring-mass system by fixing accelerometers on the sides of each mass (as has been done on the beam pieces for pre-test purposes in sub-section. 5.1.1).

Thus, the behaviour of the transfer mobility in the frequency range between 400 Hz and 10 kHz has been investigated by observing the behaviour of the phase and coherence of the transfer mobility of each beam with inserts. It has been examined, if one of the following conditions possibly exists:

- Stop-band of pure masses
- Resonance area of rubber-coated inserts

Changes in the phases and a reduction in the coherences in comparison with the behaviour of the beam without any inserts can be indications for being a stop-band or a resonance area³¹.

The measurements also reveal that coherence is reduced in a resonance when the input and output signal are - disturbed by a reflection and a phase shift, respectively - no longer in a fixed relation³².

In the following plots (Figure 48 and Figure 49) all measurements with rubber-coated masses are depicted and put into relation with the measurements of a pure beam and of a beam with 10 pure masses, respectively.

³⁰ Usually the resonance of a spring-mass system can be determined by searching for zero-crossings of the imaginary part of the transfer mobility. In this case, various investigations of the results have shown that this method is not conclusive and cannot be applied. Consequently, changes in phase and troughs in coherence will be explored to achieve the frequencies of possible resonances.

³¹ The phase of the transfer mobility v/F on an infinite beam changes according to the run-time of the propagating bending waves between the excitation and test points (see Figure 48). In a similar measurement set-up with a continuous elastic beam with periodically attached oscillators Wang et al. [96] demonstrated phase shifts in the resonance frequencies. That means, slight changes in the phase of the transfer mobility are to be expected when bending waves are delayed, crossing spring-mass systems on their way. Slight changes in phase are also assumed for reflections evoked by stop-bands.

³² The coherence indicates relationship between the propagating input and output signal in the beam, which is very likely reduced if the signal is deteriorated by reflections or delays.

It is obvious that in the frequency range between 1 kHz and 7 kHz the assumed mean of the transfer mobilities from all beams with inserts is below the value 1 and therefore a reduction in propagating bending waves can be adduced (see the pink colored circle on the left side plots in Figure 48 and Figure 49).

It is now left to determine which effects cause this attenuation. Are the reasons related to the impact of stop-bands or of resonances, or even influenced by other issues?

Figure 48 and Figure 49 show the behaviour of the beams with 10 masses, 10 rubber-coated masses in and 10 rubber-coated masses out of the neutral layer with the transfer mobility, the phases and coherences. As it is very difficult to see the behaviour in the phase and the coherence over the entire frequency range, a detailed investigation with zoomed frequency ranges has been made.

The focus will be on the following conditions, if applicable:

- Resonances
- Stop-bands
- Moment reactions

The relevant frequency ranges on the plots with transfer mobilities are highlighted. All measurement results in this investigation are shown over a non-logarithmic frequency range on the x-axis, as it is easier to see any influence of phases and coherences.

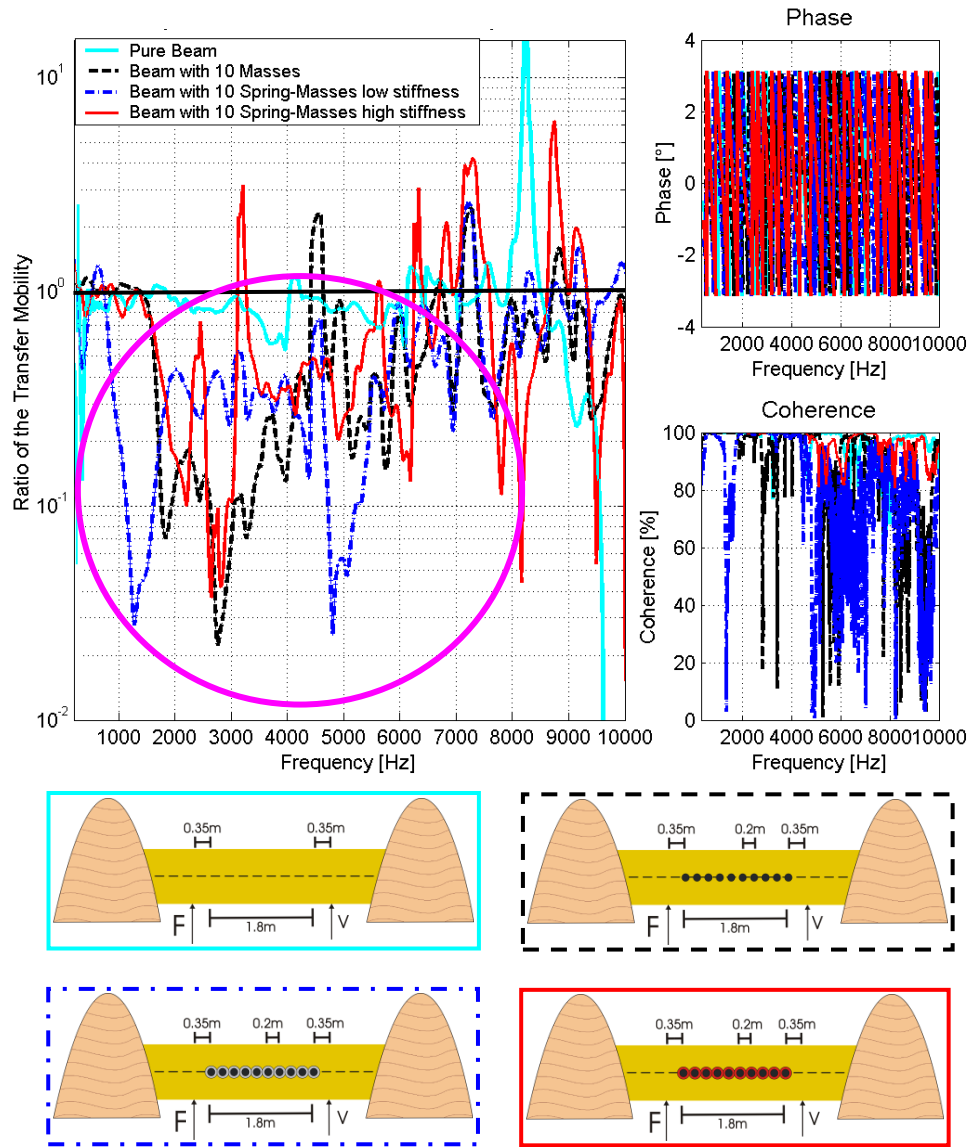


Figure 48: 400 Hz to 10 kHz: Measurement results from the ratio of the transfer mobility, phase and coherence of measured beams without discontinuities, with 10 pure masses and with 10 low stiffened (sketch in the bottom left) and 10 high stiffened (sketch in the bottom right) rubber-coated masses. The beams with inserts are located in the neutral layer and the ratios are normalised to the beam with only holes. As depicted in the sketches, both ends of the measured beams are embedded in sand to simulate infinite conditions. The test points are located 0.35 m behind the last insert. The black line denotes the ratio 1. All curves below that line represent reduced vibrations on the position of the accelerometer (see the pink colored circle).

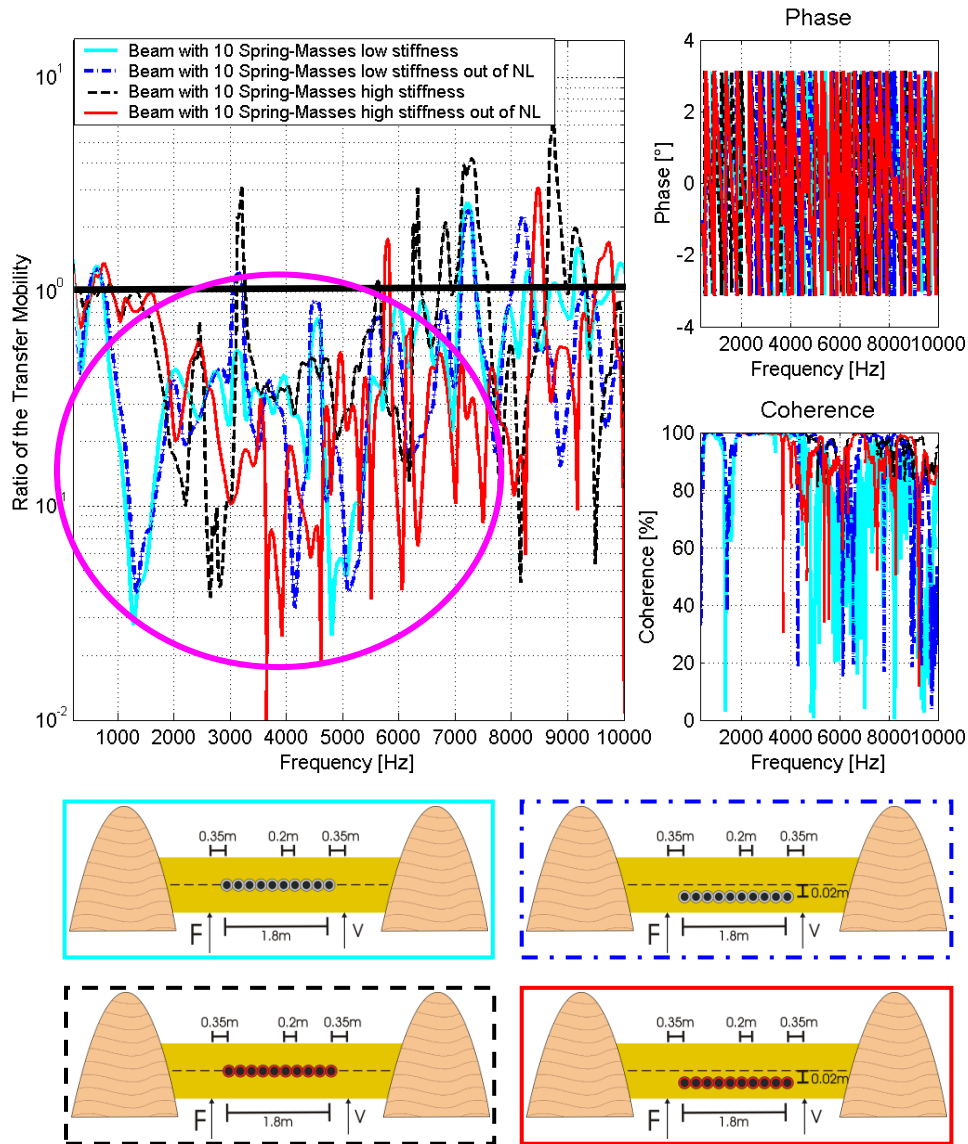


Figure 49: 400 Hz to 10 kHz: Measurement results from the ratio of the transfer mobility, phase and coherence of 4 beams with 10 rubber-coated masses with low stiffness (sketches in the top) and high stiffness (sketches at the bottom), distributed in and out of the neutral layer (all ratios are normalised with the beam with only holes). As depicted in the sketches both ends of the measured beams are embedded into sand to simulate infinite conditions. The test points are located 0.35 m behind the last insert. The black line denotes the ratio 1. All curves below that line represent reduced vibrations on the position of the accelerometer (see the pink colored circle).

Possible resonance area of the beam with 10 low stiffened rubber-coated inserts in the neutral layer at 400 Hz to 2 kHz:

The beam with 10 rubber-coated masses with a low stiffness (ShA 40) shows a significant trough in the frequency range of 1.5 kHz to 2 kHz. As the phases and coherence are significantly differing in comparison to the pure beam, this area very likely shows the resonances of the 10 rubber-coated inserts (see Figure 50). Changes in

the phase are visible in the frequency range of 1.4 kHz, which supports the assumption of real resonances in this area. In the frequency range 1.7 kHz and below, a large reduction in coherence can be observed, which underlines the assumption of real resonances.

Thus, it is very likely that the main number of rubber-coated masses is responsible for the trough in the transfer mobility in that frequency region.

As the filling procedure of the holes with rigid resin comes along with variations in coat thicknesses, different resonance frequencies within one beam are to be expected. Thus, the strong likelihood of a broader band of different resonance frequencies has to be considered.

According to the pre-test measurements employing a beam piece and a Shore hardness of ShA 40 (see sub-section 5.1.1, Figure 35), the resonance of the coated masses with the maximum acceleration appeared in the frequency range of approximately 2 kHz to 3 kHz. In these pre-test measurements, the acceleration of one side of a mass has its minimum at about 1.5 kHz. It is possible that this attenuation at the beam is related to this condition rather than to the resonating effects of spring-mass systems.

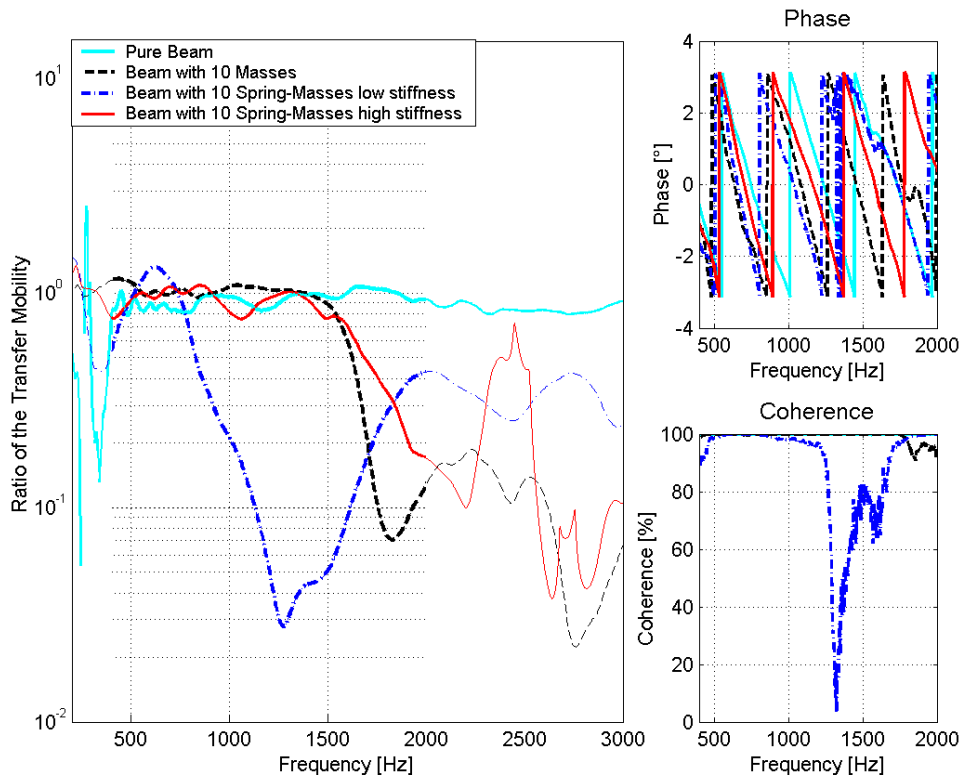


Figure 50: 400 Hz to 2 kHz: Measurement results from the ratio of the transfer mobility, phase and coherence of measured beams without discontinuities, with 10 masses and with 10 high and low stiffened rubber-coated masses. All discontinuities are located in the neutral layer and the ratios are normalised with the beam with only holes.

Possible resonance area of the beam with low stiffened rubber-coated inserts out of the neutral layer at 400 Hz to 2 kHz:

The beam with 10 rubber-coated masses with a low stiffness out of the neutral layer shows a significant trough in the same frequency ranges (1.5 kHz to 4 kHz) as the beam with inserts located in the neutral layer (see Figure 51). As the phase and the coherence also coincide with the beam with the low stiffened rubber-coated masses in the neutral layer, it is very likely that this area also shows the resonances of the 10 rubber-coated inserts.

There are no indications of having an impact of moment reactions. The reason therefore might be related to the findings in the numerical study, which shows the moment reactions becoming dominant at higher frequency range (see sub-section 4.3.4.).

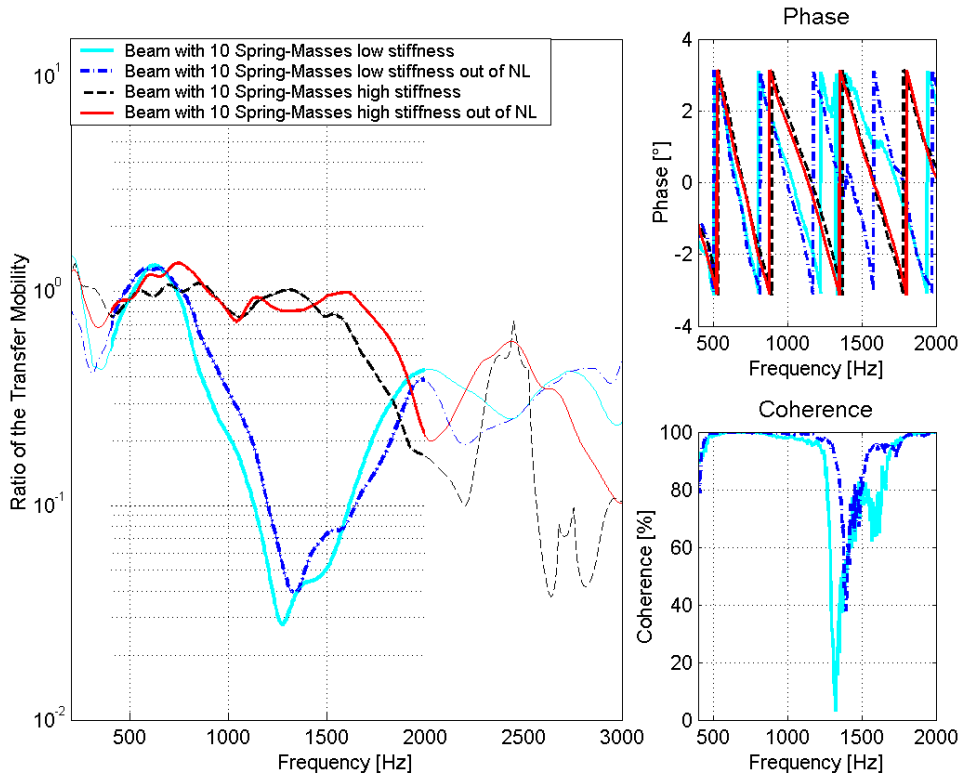


Figure 51: 400 Hz to 2 kHz: Measurement results from the ratio of the transfer mobility, phase and coherence of 4 beams with 10 rubber-coated masses. The discontinuities are located either in or out of the neutral layer and with high or low stiffened rubber material.

Possible 1st stop-band area of the beam with 10 masses in the neutral layer at 1.5 kHz to 3 kHz:

With regard to the divergence of the phase and coherence to the other three beams it is very likely that in the frequency range between 1.5 kHz and 3 kHz the 1st stop-band of the beam with 10 masses in the neutral layer is visible (Figure 52). Especially in the

frequency range between 2.5 kHz and 3 kHz a large attenuation in the transfer mobility and a significantly reduced coherence underlines the assumption of having a stop-band.

According to the calculations the 1st stop-band is expected at a frequency of 3.4 kHz. With respect to the scattering and non-ideal conditions at a real beam a high confidence of having a real stop-band in the measurements can be applied.

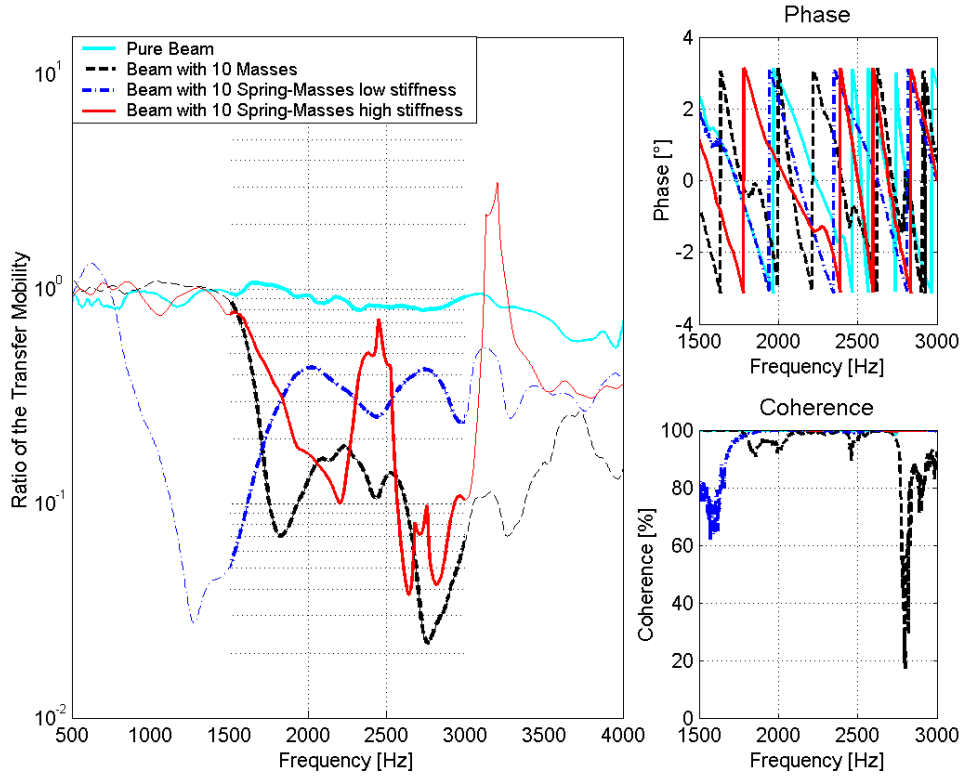


Figure 52: 1.5 kHz to 3 kHz: Measurement results from the ratio of the transfer mobility, phase and coherence of measured beams without discontinuities, with 10 masses and with 10 high and low stiffened rubber-coated masses. *All discontinuities are located in the neutral layer and the ratios are normalised with the beam with only holes.*

Possible 1st stop-band area of the beam with 10 rubber-coated masses with high stiffness in the neutral layer at 1.5 kHz to 3 kHz:

The beam with 10 rubber-coated masses with high stiffness located in the neutral layer shows a significant trough in the same frequency ranges (1.5 kHz to 4 kHz) as the beam with pure masses located in the neutral layer (Figure 52). This gives reason to assume that this area is the 1st stop-band or the resonance area.

If the assumption about a resonance area in the frequency range at 1.5 kHz of the beam with inserts of low stiffness (see Figure 51) were true, here the same reduction in coherence would have been expected. However, this is not observed: the coherence is almost unchanged. A slightly changed phase variation is visible at frequencies between 2 kHz and 2.5 kHz, signifying that in a range where attenuation is reduced the influence of the stop-band dominates.

On the other hand the beam with pure masses shows a similar significant behaviour at the phase and the coherence in compare with the beam with low stiffened inserts, although in another frequency range.

According to the pre-test measurements (see 5.1.2), we expect the 1st resonances of the beam with high stiffened coated masses in the frequency ranges between 2 kHz and 4 kHz.

However, it is difficult to determine, if these troughs of the transfer mobility really represent the 1st stop-band. With respect to the results in the calculation (see sub-section 4.3.3) a beam with resonant inserts only has stop-bands in the mass controlled frequency range, which is below the 1st resonant frequencies.

It will be shown in sub-section 4.3.5 that the 1st resonance area appears to be at a higher frequency range. Thus, it is very likely that the beam with high stiffened inserts is mass controlled in the frequency range from 1.5 kHz to 4 kHz and shows the appearance of the 1st stop-band, although this is not reflected in the behaviour of the coherences.

Possible 1st stop-band area of the beam with 10 rubber-coated masses with high stiffness in and out of the neutral layer at 1.5 kHz to 3 kHz:

The transfer mobilities of the beams with highly stiffened inserts, which are out of the neutral layer follow the curves of the same beams having inserts within the neutral layer, although with less reduced transfer mobility (Figure 53).

According to the numerical study in sub-section 4.3.5, stop-band influence is low in resonance bands when they appear at lower frequencies. Thus, it is to be expected that the beam with high-stiffened inserts outside the neutral layer also follows the trough of the 1st stop-band with respect to the given assumptions. Differences between calculations for the beam with rubbered inserts outside the neutral layer and those for the beam with them inside the neutral layer included a reduced attenuation within a resonance band and a lower impact of stop-bands on the transfer mobility. The attenuation of the beam with inserts outside the neutral layer is lower than that of the beam with inserts inside the neutral layer (Figure 53). This is a slight indication of the impact of the moment reactions, which must be considered under the given explanation.

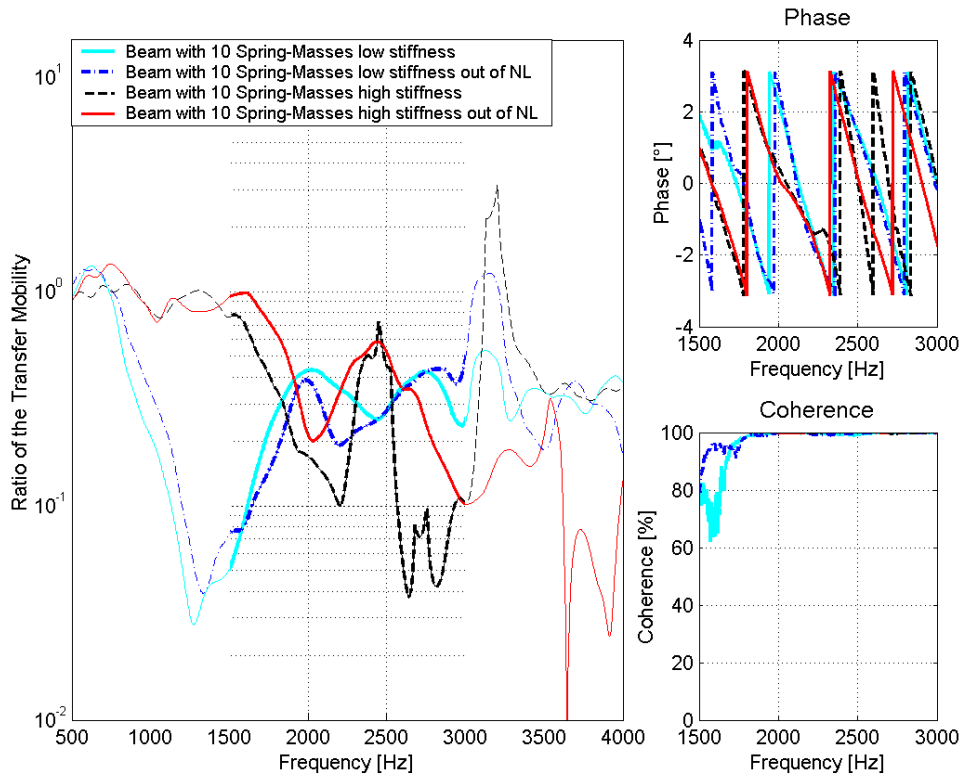


Figure 53: 1.5 kHz to 3 kHz: Measurement results from the ratio of the transfer mobility, phase and coherence of 4 beams with 10 rubber-coated masses. The discontinuities are located either in or out of the neutral layer and with high or low stiffened rubber material.

Continuation of the possible 1st stop-band area of the beam with 10 masses and of the 10 rubber-coated masses with high stiffness in the neutral layer at 2.5 kHz to 4 kHz:

In order to the transfer mobility and the coherence the frequency range between 2.5 kHz and 4 kHz shows the continuation of the 1st stop-band (Figure 54). The same behaviour is visible at the beam with 10 resonant inserts of high stiffness. As discussed above it is not quite certain if we really see a stop-band in this frequency range, as the coherence remains the same, whereas the beam with resonant inserts shows large troughs. As evidenced by the calculations (see Table 2), the centre of the stop-band is expected to occur at a frequency range of 3.4 kHz. In the measurement results the maximum reduction is visible at around 2.8 kHz, whereas the entire stop-band area is very wide and ranges from 1.5 kHz to 3.5 kHz.

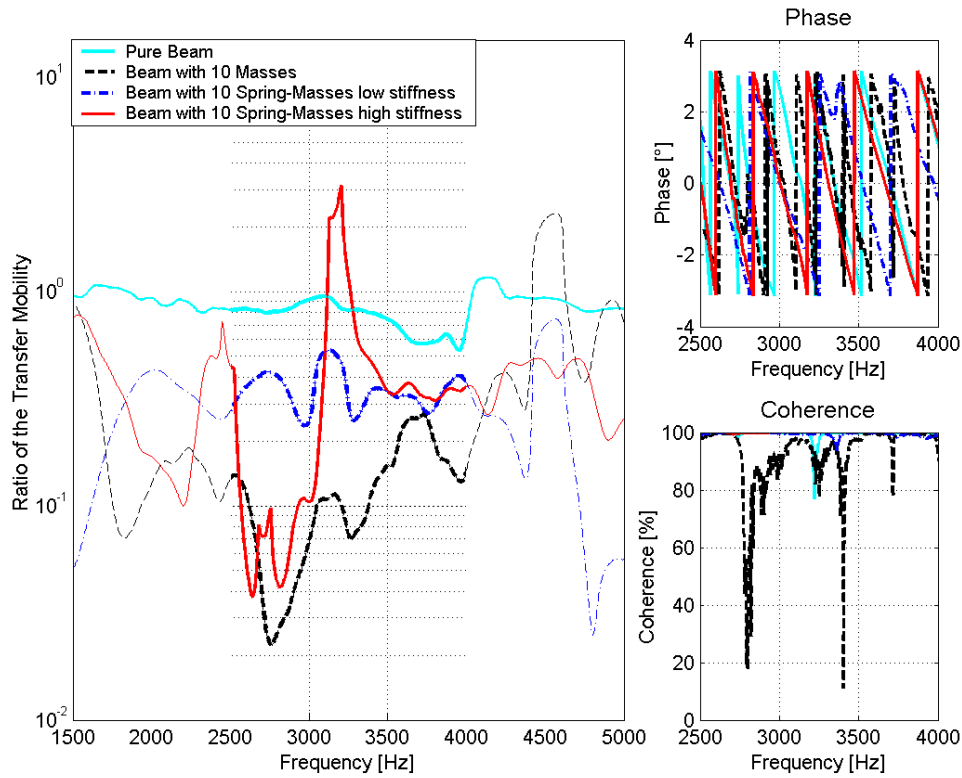


Figure 54: 2.5 kHz to 4 kHz: Measurement results from the ratio of the transfer mobility, phase and coherence of measured beams without discontinuities, with 10 masses and with 10 high and low stiffened rubber-coated masses. All discontinuities are located in the neutral layer and the ratios are normalised with the beam with only holes.

Continuation of the possible 1st stop-band area of the beam with 10 masses in the neutral layer at 2.5 kHz to 4 kHz:

It appears to be the continuation of the 1st stop-band of the beam with 10 rubber-coated masses with high stiffness, which is visible in the frequency range from 2.5 kHz to 3.5 kHz (Figure 55). In the frequency range at 3.2 kHz increased transfer mobility is visible, which seems to be related to the behaviour of the pure beam with only holes. In the evaluation of this work this divergence will not be considered.

Possible resonance area of the beam with 10 rubber-coated masses with high stiffness in and out of the neutral layer at 2.5 kHz to 4 kHz:

At 3.7 kHz on the beam with the high stiffened inserts out of the neutral layer it is very sensible that the 1st trough of the resonance is visible (Figure 55). The change in the phase and the reduction in the coherence underline this assumption.

The beam with the highly stiffened inserts in the neutral layer does not show any hints of resonance in phases or coherence in the frequency range 2.5 kHz to 4 kHz. The trough in attenuation between 2.5 kHz and 3 kHz cannot therefore be applied to a specific effect.

There are also not any indications visible on the beams with low stiffened inserts.

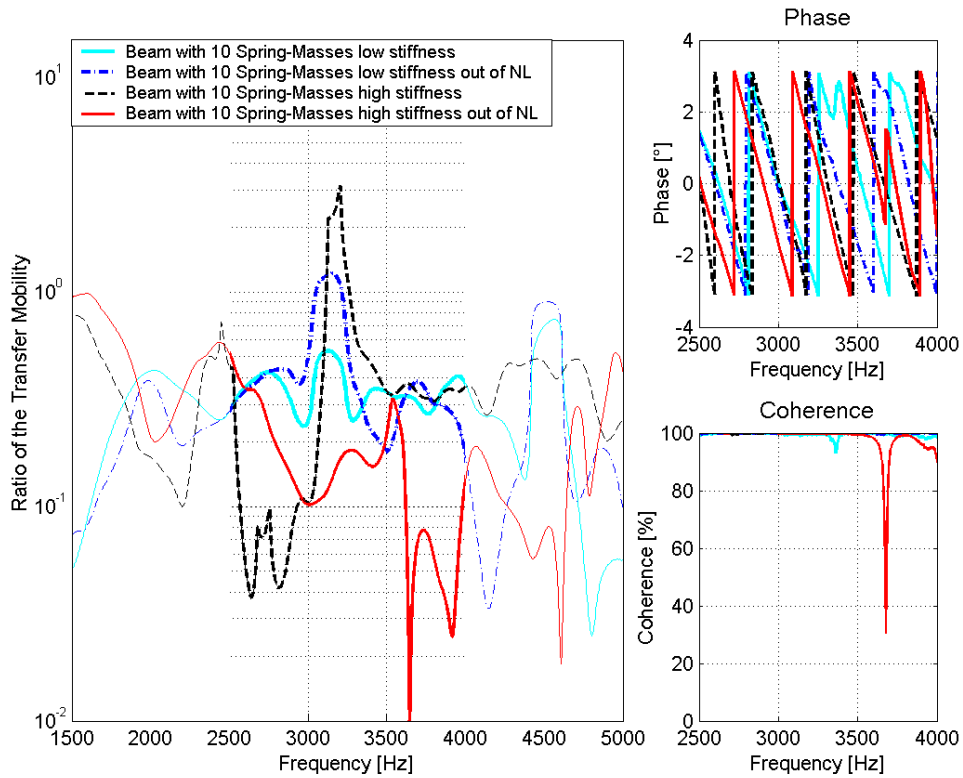


Figure 55: 2.5 kHz to 4 kHz: Measurement results from the ratio of the transfer mobility, phase and coherence of 4 beams with 10 rubber-coated masses. The discontinuities are located either in or out of the neutral layer with high and low stiffened rubber material.

Possible resonance area of the beam with 10 rubber-coated masses with low stiffness in and out of the neutral layer at 3.5 kHz to 5 kHz:

In the frequency range from 3.5 kHz to 5 kHz the attenuation of the transfer mobility of the beams with low stiffened inserts is increased, although in very narrow frequency bands (Figure 56). The behaviour in phases and coherences is changed as well and gives reason to assume another resonance frequency herein. Because the resonance band was discovered at a lower frequency range, this behaviour was not expected. However, because of the sensitive filling procedure for castable resin, it is possible that layer thickness varies and increases stiffness, as a higher resonance in one or more inserts reveals.

It is also interesting to note that the beam with the low-stiffened masses, which are outside the neutral layer, shows a negative attenuation in the stop-band. Considering that not all spring-mass systems are above their resonance, this behaviour coincides very well with the numerical study observations.

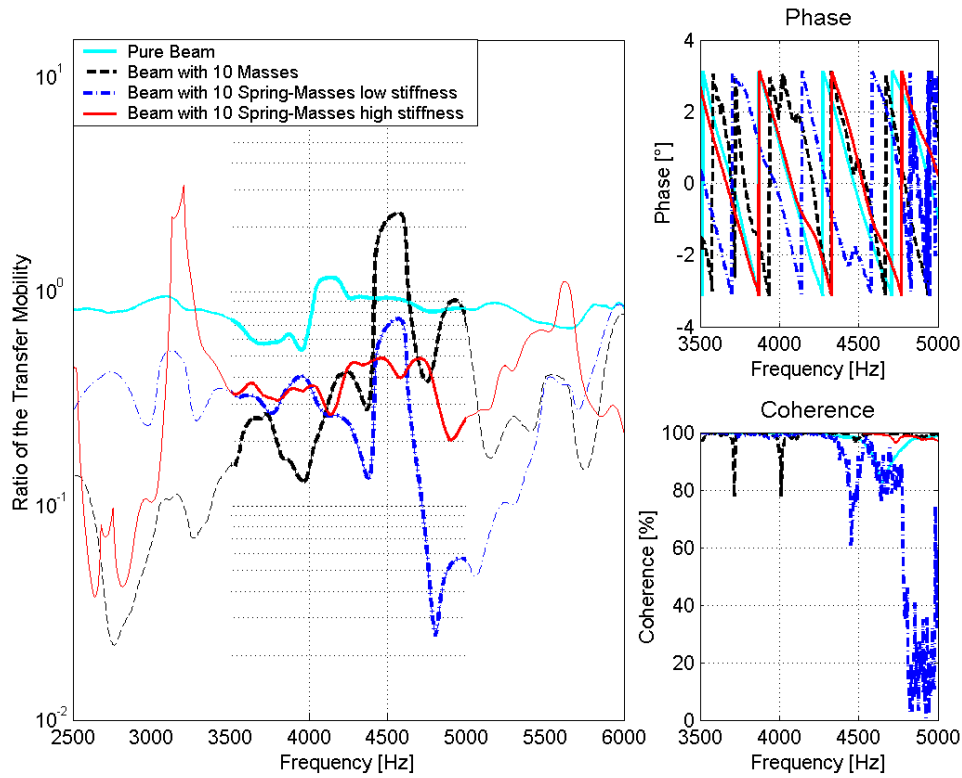


Figure 56: 3.5 kHz to 5 kHz: Measurement results from the ratio of the transfer mobility, phase and coherence of measured beams without discontinuities, with 10 masses and with 10 high and low stiffened rubber-coated masses. All discontinuities are located in the neutral layer and the ratios are normalised with the beam with only holes.

Possible resonance area of the beam with 10 rubber-coated masses with high stiffness in and out of the neutral layer at 3.5 kHz to 5 kHz:

In the frequency range from 3.5 kHz to 5 kHz it is obvious that a possible resonance area at the beam with highly stiffened inserts is visible (Figure 57). If these inserts are out of the neutral layer various troughs in the transfer mobility at 3.6 kHz and above are visible. At the beam with the rubber-coated inserts within the neutral layer only one trough at 4.2 kHz arises.

These reduced transfer mobilities are visible in the phases and the coherences as well. Thus, it is very likely to see particular resonance areas for different inserts.

Due to the indifferent kind of filling the holes with Polyurethane and centring the masses a scattered appearance of the resulting resonance frequencies is very likely.

However, assuming the resonances of the highly stiffened inserts at a beam with the inserts in the neutral layer to appear in the frequency range of 3.5 kHz to 5 kHz according to the pre-test measurements (see sub-section 5.1.2), this effect is not reflected in the measurement results.

It is very likely to observe some resonances at the beam with high-stiffened rubber-coated masses located outside the neutral layer, whereas this does not seem to be the case in the beam with the same inserts inside the neutral layer.

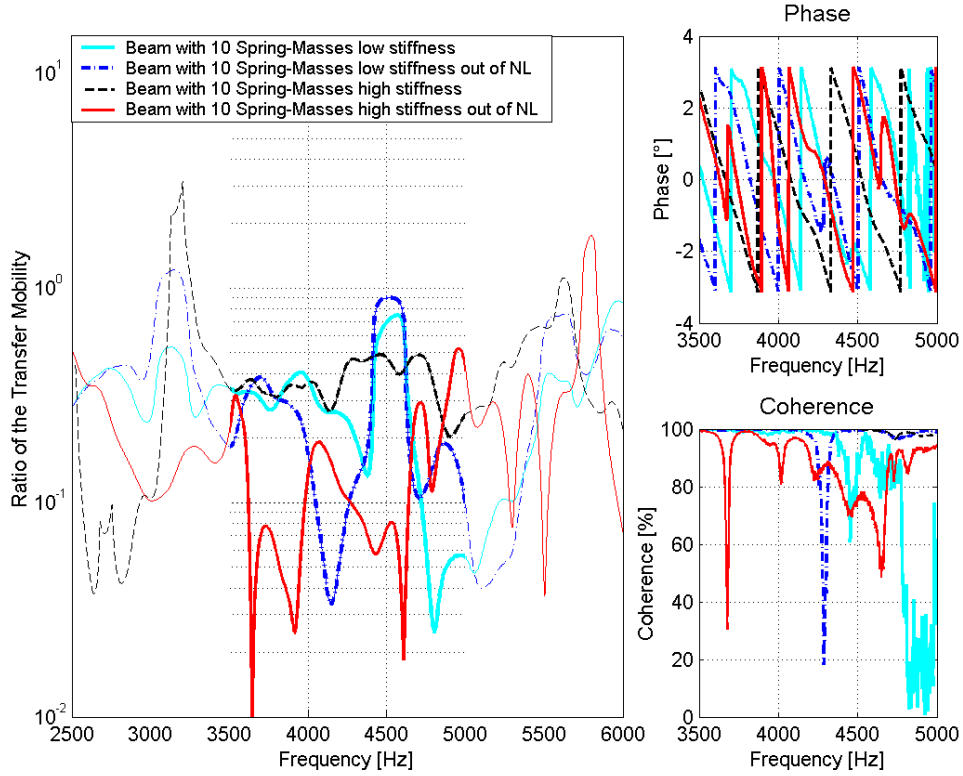


Figure 57: 3.5 kHz to 5 kHz: Measurement results from the ratio of the transfer mobility, phase and coherence of 4 beams with 10 rubber-coated masses. The discontinuities are located either in or out of the neutral layer and with high or low stiffened rubber material.

Possible resonance area of the beam with 10 rubber-coated masses with high stiffness out of the neutral layer at 4.5 kHz to 6 kHz:

The trough in the transfer mobility of the beams with 10 low-stiffened spring-masses is possibly indicative of higher-order resonances (Figure 58). The coherence and the phase underline this assumption. However, it was not expected to observe either resonances or stop-bands above the lower resonance band at 2 kHz; therefore it is difficult to judge these observations.

The beam with the high stiffened resonant inserts within the neutral layer does not show significant hints for a resonance area in this frequency range.

Possible resonance area of the beam with 10 rubber-coated masses with low stiffness in the neutral layer at 4.5 kHz to 6 kHz:

As is described in the frequency band from 2.5 kHz to 5 kHz it looks as if the trough in the frequency ranges of 4.5 kHz to 6 kHz is caused by higher resonances of the lower

stiffened beam (Figure 58). A reduced coherence and changes in the phases underlines this assumption.

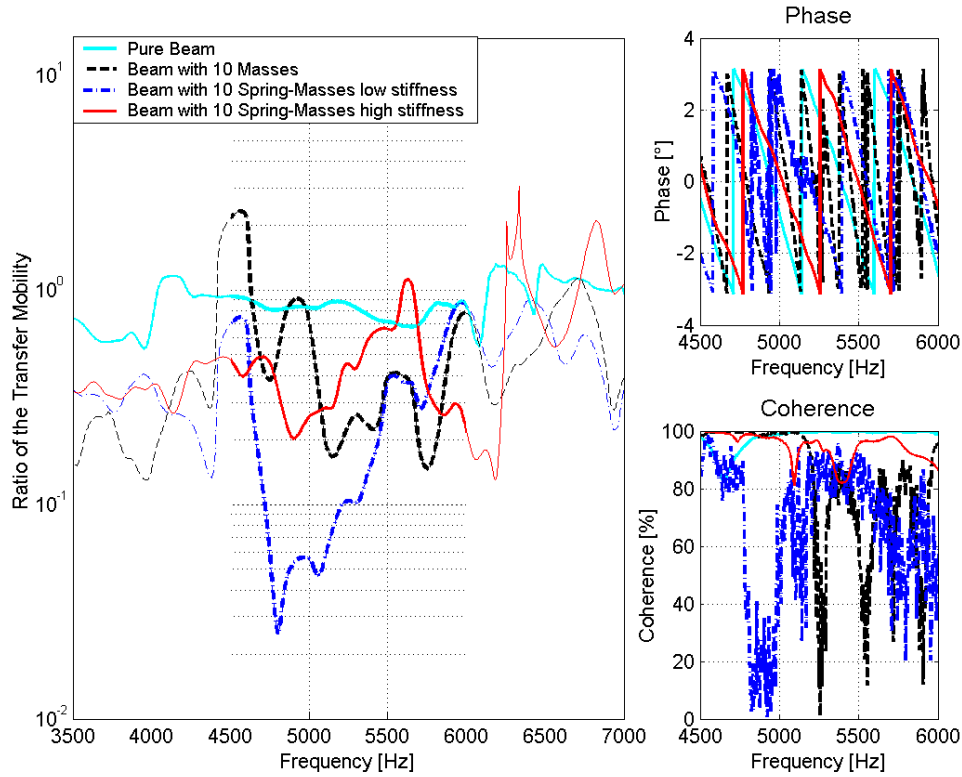


Figure 58: 4.5 kHz to 6 kHz: Measurement results from the ratio of the transfer mobility, phase and coherence of measured beams without discontinuities, with 10 masses and with 10 high and low stiffened rubber-coated masses. All discontinuities are located in the neutral layer and the ratios are normalised with the beam with only holes.

Undefined area of the beam with 10 rubber-coated masses with high stiffness in the neutral layer at 4.5 kHz to 6 kHz:

Although a very low trough just below 5 kHz is visible it is not sure, if this is a resonance. The phase and the coherence do not show significant hints (Figure 59).

Possible resonance area of the beam with 10 rubber-coated masses with high stiffness out of the neutral layer at 4.5 kHz to 6 kHz:

It is the beam with high-stiffened inserts outside the neutral layer that gives us reason to assume small resonance areas in the frequency range 4.5 kHz to 6 kHz, and especially at 5.4 kHz and above 5.5 kHz (Figure 59). The phases and coherences bolster this assumption.

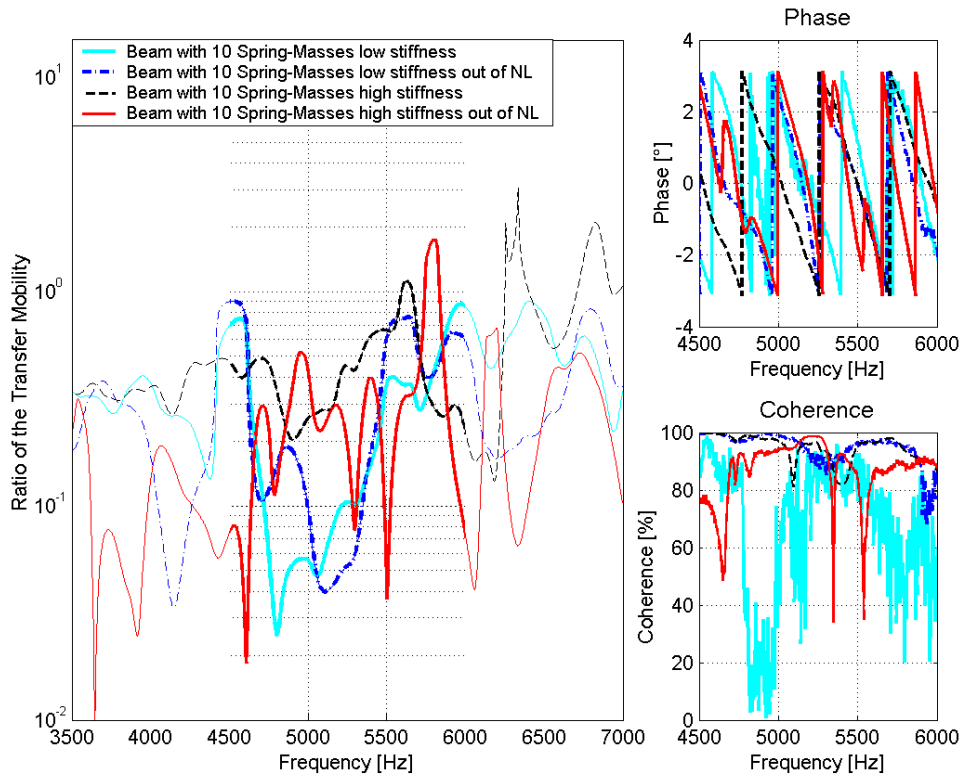


Figure 59: 4.5 kHz to 6 kHz: Measurement results from the ratio of the transfer mobility, phase and coherence of 4 beams with 10 rubber-coated masses. The discontinuities are located either in or out of the neutral layer and with high or low stiffened rubber material.

Possible resonance area of the beam with 10 rubber-coated masses with high stiffness in the neutral layer at 5.5 kHz to 7 kHz:

In the range 6 kHz and above, a resonance area in the beam with high-stiffened inserts within the neutral layer is very likely, albeit with lower characteristics in comparison to the resonances observed at the other beams (Figure 60). Changes in phase and a reduced coherence amplify this assumption.

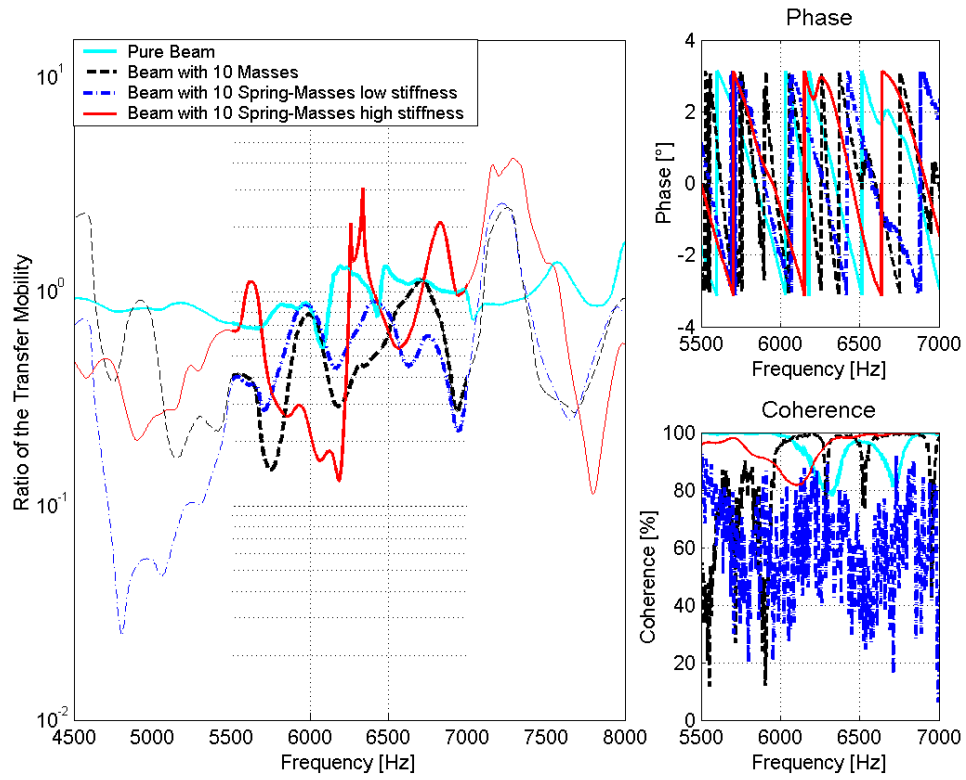


Figure 60: 5.5 kHz to 7 kHz: Measurement results from the ratio of the transfer mobility, phase and coherence of measured beams without discontinuities, with 10 masses and with 10 high and low stiffened rubber-coated masses. All discontinuities are located in the neutral layer and the ratios are normalised with the beam with only holes.

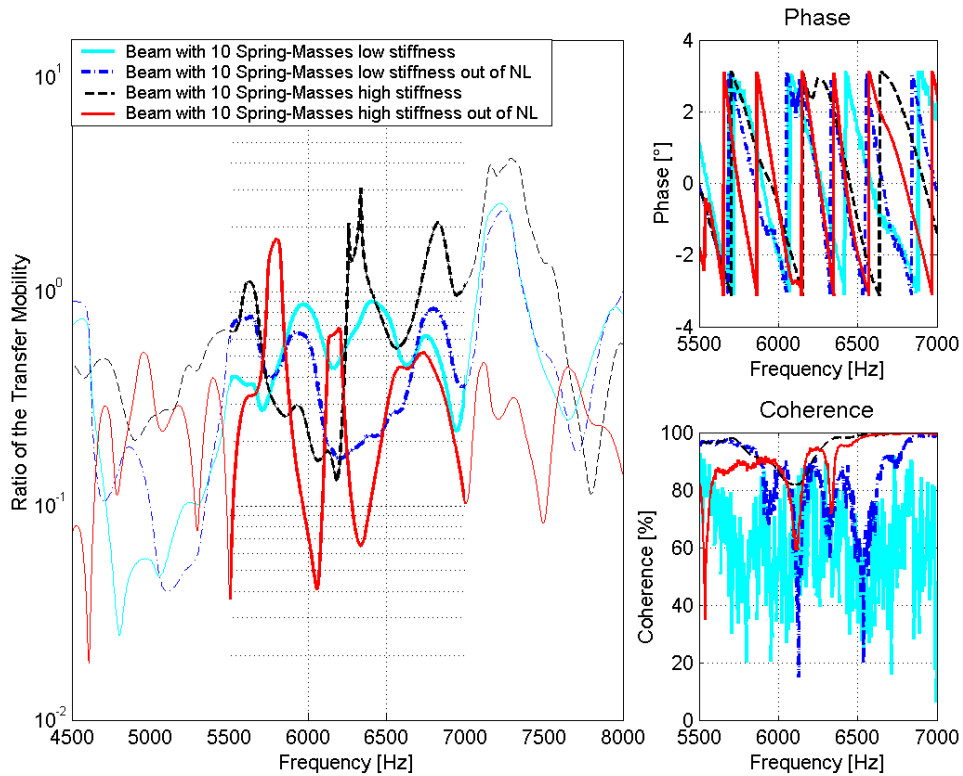


Figure 61: 5.5 kHz to 7 kHz: Measurement results from the ratio of the transfer mobility, phase and coherence of 4 beams with 10 rubber-coated masses. The discontinuities are located either in or out of the neutral layer and with high or low stiffened rubber material.

Possible resonance area of the beam with 10 rubber-coated masses with high stiffness out of the neutral layer at 5.5 kHz to 7 kHz:

In the frequency ranges just above 6 kHz and 6.3 kHz resonances of the beam with high stiffened inserts out of the neutral layer are very likely. Reduced coherences in these frequencies underline this assumption, whereas the phase only shows slight changes.

The transfer mobility at higher frequency ranges from 6 kHz on becomes fuzzy as the results seem to be dominated by many other influences. According to the numerical investigation and the pre-test measurements it is very unlikely to detect any other resonances or stop-bands in the frequency range from 6 kHz to 10 kHz. Thus these plots are not displayed in this work.

5.3.6 SUMMARY OF DISCUSSED OBSERVATIONS OF TRANSFER MOBILITY, PHASES AND COHERENCES ON MEASUREMENTS WITH BEAMS

The observations of the transfer mobility, the phases and the coherences at the measurement results on beams with 10 masses, 10 rubber-coated masses in the neutral layer and 10 rubber-coated masses out of the neutral layer give reason to make the following assumptions:

1. The 1st stop-band on a beam with 10 pure masses appears with high confidence in the frequency range from 1.5 kHz to 4 kHz as expected, although with a broader and wider attenuation range (see Figure 52 and Figure 54).
2. There is a high confidence of having the first resonance band in the frequency range from 800 Hz to 1500 Hz on the beam with 10 equally distributed low stiffened rubber-coated masses in and out of the neutral layer, respectively (Figure 51). The resonances of the beam with low stiffened inserts appear for the most part in the range as expected. Due to the measurement results and the filling procedure of the castable resin (PUR) it is very likely that the resonance of each spring-mass system vary and lead to a scattering of the resonance frequency. Some of the resonance frequencies appear in higher frequency regions, which might be attributed to thinner layers of the castable resin or shaking behaviour of the cylinders. The frequency of attenuation depends on the spring stiffness and the size of attenuation follows from the damping factor of the spring; both vary accordingly to the scattering of the layer thickness. With regard to the pre-test measurements on beam pieces this frequency range coincides with the cylindrical mass with a minimum vibration on one side (compare sub-section 5.1.2). Due to the massive scattering effects that are very likely concurrent with the given conditions in measurements, it is difficult to confirm an association.
3. There is medium confidence of having a resonance band in the frequency range from 2.5 kHz to 4 kHz on the beam with 10 high stiffened rubber-coated masses in the neutral layer (Figure 53 and Figure 55). For the most part, the resonances in the beam with high-stiffened inserts appear in higher frequency ranges as expected. Due to the observation of phases and coherences in these suspected frequency ranges, a real resonance is not always obvious. However, the attenuation of the transfer mobility and the expected resonance frequencies makes it likely to be the real resonances. Some of the resonance frequencies appear in higher frequency regions, which might be attributed to thinner layers of the castable resin. The size of the attenuation depends on the spring stiffness of the spring-mass-system and varies accordingly to the scattering of the layer thickness. According to the pre-test measurements with beam pieces it could not be identified, whether these attenuations are related to one of the three observed conditions (compare sub-section 5.1.2).
4. Under the assumption of having real resonances at the beam with high stiffened inserts, tendencies are visible, which reflect the mass controlled behaviour of the spring-mass systems below their resonances. Attenuated transfer mobility at a

possible resonance frequency range in the expected 1st stop-band underlines this assumption (Figure 53).

5. The beams with the inserts out of the neutral layer show differences to the beams with the inserts in the neutral layer. The possible resonance band of the beam with low stiffened inserts in the neutral layer coincides very well with the one having the inserts out of the neutral layer. On the beams with high stiffened inserts this effect is not visible. A lower influence of stop-bands onto the attenuation of resonant inserts, which are displaced from the neutral layer, could not be detected.
6. Some tendencies in the measurement results reinforce observations from the parametric study on the impacts of moment reactions at higher frequencies. Because various scattering effects at beams with inserts outside the neutral layer are visible, this assumption can be determined with a low confidence.

These investigations show that some of the effects can be identified with a high confidence, e.g. the 1st stop-band of the beam with pure masses or the resonances of the beam with low stiffened rubber-coated masses, respectively. Furthermore, other effects appear with a lower confidence and are revealed to be difficult to announce, e.g. the mass controlled 1st stop-band or the resonances of the beam with high stiffened rubber-coated masses. Scattering effects change or superimpose some observed phenomena, which are known from the numerical calculations.

In the following chapter all effects from the numerical investigation and measurements with a beam are listed.

6 SUMMARY OF OBSERVATIONS WITH CALCULATIONS AND MEASURED RESULTS OF BEAMS

Various phenomena in the numerical investigation of beams with inserts could have been detected. At measurements with 5 or 10 inserts, some effects observed from the calculations could have been verified. With respect to the consideration of observed phases and coherences, some of these effects occur with a high confidence, whereas others are to be handled with a lower confidence. However, some other effects could not be verified.

For an overview of the validation of the theoretically observed effects, all are summarised, and observations of the measurements are attached, if applicable. Those are depicted with an arrow “→”.

6.1 SUMMARY OF OBSERVATIONS WITH PURE MASSES EMBEDDED IN A BEAM

1. The transfer mobility of the beam with embedded pure masses illustrates the existence of stop- and pass-bands. The negative slopes follow from the reflections of the bending waves in these frequency ranges. These are the so-called stop-bands, and their occurrence is periodic due to equidistant masses (see Figure 12, Figure 13 and Figure 14).

→ Measurements with 5 or 10 masses underline the appearance of stop- and pass-bands (see Figure 45 and Figure 46).

2. The larger the distances of the masses, the broader the distances of the stop-bands in the frequency range are (see Figure 15 and Figure 44).

→ Measurements with 5 or 10 masses show broader distances in frequency of stop-bands coming along with larger distances from mass to mass (see Figure 45 and Figure 46).

3. The larger the weight of the masses, the larger the attenuations of the stop-bands are (see Figure 87).

→ N/A

4. The more masses involved and compressed within the same overall distance, the higher the attenuation - and the larger the width - of the transfer mobility in the stop-bands is (see Figure 15).

→ Measurements with 5 or 10 masses show that the attenuation of the transfer mobility in the common stop-band is increased and broadened at the beam with 10 masses (see Figure 44).

5. The more masses with identical distances to each other involved, the higher the reduction of transfer mobility in the stop-bands is. The width of the attenuations remains the same (see Figure 16).

→ N/A

6. If masses are distributed randomly along the neutral layer, the appearance of stop-bands is significantly changed (see Figure 23). Attenuation of the transfer mobility scatters according to a non-equal distribution.

→ N/A

7. If pure masses are distributed out of the neutral layer, smearing effects and reduced attenuations in the transfer mobilities can be observed at higher frequencies (see Figure 25, Figure 26, Figure 27 and Figure 28). These changes appear in the figures mentioned from approximately the 2nd stop-band on.

→ N/A

6.2 SUMMARY OF OBSERVATIONS WITH RUBBER-COATED MASSES EMBEDDED IN A BEAM

8. If the evenly distributed steel cylinders are coated with (all the same) rubber, the effects of stop- and pass-bands diminish. Attenuation is dominated by the spring-mass system, albeit in a very narrow frequency band (see Figure 17 and Figure 18).

→ Attenuation of the 1st stop-band vanishes, and the reduction in the resonances of the spring-mass systems dominates at the beam with 10 rubber-coated masses in comparison to the beam with 10 masses (see Figure 47).

9. The more rubber-coated masses involved, the higher the attenuation in the resonance is (see Figure 18).

→ N/A

10. To gain larger attenuations in transfer mobility, it makes sense to change the stiffnesses rather than the masses (see Figure 19).

→ N/A, as the used masses had all the same weight and size.

11. To receive a large attenuation at a certain frequency, the damping factor of the spring needs to be very low³³. Nevertheless, it has to be considered that the

³³ To achieve large attenuation at discrete frequencies with spring-mass-systems, the physical principle refers to the reflection of the propagating bending waves. In contrast to the well-known “vibration dampers”, the focus in this work is on the reflection - and not the absorption - of bending waves. Thus, to

attenuated frequency range is broader but lower in its magnitude with a higher damping factor of the spring (see Figure 85).

→ By coating the masses with silicon in the first trials, the anticipated effects did not appear. Much better results could have been observed by instead using the castable resin (PUR) with a lower damping factor of the spring (see Figure 47).

12. As the rubber-coated masses are mass-controlled below their resonances, the appearance of stop-bands below the resonances of rubber-coated masses is visible. At frequencies higher than the resonances the rubber-coated masses are spring-controlled, and reflections due to distance-controlled stop-bands do not appear (see Figure 20, Figure 21, Figure 22, Figure 30 and Figure 31).

→ In comparing the different behaviour (see Figure 52) between the 1st beam stop-band with 10 masses to the beams with low- and high-stiffened rubber-coated masses, this effect can be observed with a high confidence. The beam, which appears to have the resonance band above the 1st stop-band (high stiffness), reflects a reduction of the transfer mobility at this suspected stop-band, whereas the beam with low stiffness does not.

13. A stop-band impact of transfer mobility within the range of resonances (same masses, but differing spring stiffnesses) can be observed (see Figure 20, Figure 21, Figure 22, Figure 30 and Figure 31). The attenuation of transfer mobility at or close to the stop-band is reduced.

→ N/A

14. The analysis shows that the influence of stop- and pass-bands vanishes in the resonance band when the inserts are randomly distributed along the neutral layer. The transfer mobility differs the more the higher the resonances become (see Figure 24). However, if its resonances are low in frequency (see Figure 23), a randomised distribution of the rubber-coated masses along the neutral layer almost does not differ from equally distributed inserts.

→ N/A, although it is very likely that different spring-mass systems scatter in spring stiffness.

15. If rubber-coated masses are equally distributed out of the neutral layer, attenuation in the transfer mobility is decreasing at rising frequencies in comparison to the spring masses distributed in the neutral layer (see Figure 29 and Figure 30).

→ N/A

achieve large reflections it is of high interest to keep the damping factor of the springs as low as possible (see also Chapter 1 - Resonant Supports and Inserts).

16. If the rubber-coated masses are equally distributed out of the neutral layer, the stop-bands do have a minor influence on the reduced transfer mobility in the resonances in comparison to the spring-masses embedded in the neutral layer. Moment reactions dominate and reveal a reduced attenuation band at rising frequency (see Figure 30 and Figure 31).

→ N/A

17. Moment effects of rubber-coated masses in a beam have a significant impact on the transfer mobility. Their existence is dominant in comparison to reduced attenuations at a stop-band, where the higher frequency is.

→ N/A

18. If the vertical distances to the neutral layer were no longer fixed and randomly distributed, the reduction in attenuation becomes smaller (see Weith and Petersson [102]).

→ N/A

6.3 SUMMARY OF THE GENERAL OBSERVATIONS WITH INSERTS EMBEDDED IN A BEAM

19. The loss factor of the beam reduces the transfer mobility at higher frequencies. An impact on stop-bands or resonances is very low (Figure 84).

→ N/A

20. The higher the Young's modulus the more the stop-bands of a beam with pure masses embedded are shifted at higher frequencies (Figure 84).

→ Although it is not directly applicable in the measurements, one reason for the shifting in frequency of the stop-bands from measurements to calculations is very likely related to varying Young's modulus at real beams (see Figure 45 and Figure 46).

21. The higher the damping factor of the complex spring stiffness, the lower the attenuation of the transfer mobility is, though with broader side banks. It was observed that the influence of the 2nd stop-band, which overlaps at the resonances, seems to be reduced with higher damping factor of the spring (see Figure 85).

→ N/A

7 CALCULATIONS ON INFINITE PLATES WITH EQUI-SPACED RIGID OR FLEXIBLE INSERTS

7.1 INTRODUCTION TO THE STUDY ON PLATES

This investigation expands the study of embedded inserts from one-dimensional beams (Chap. 4 and 5) to two-dimensional cases with plates³⁴.

Therefore, the wave propagation in a homogeneous thin plate with pure masses and resonant inserts, which are embedded in the neutral layer, has been studied. If the analysis is made with the theory for a homogeneous thin infinite plate, the embedded masses can be seen as were they attached to the plate. When the masses are coated with rubber, the attenuation at resonance is increased considerably, whereas the stop- and pass-bands above the resonance frequency nearly vanish.

It is of interest now if the geometrical distribution of the inserts in two dimensions influence the propagation of bending waves. Thus, this poses the question, if the effects of the bending wave propagation in a beam with embedded inserts can be observed in an equivalent plate with inserts distributed in circles around the excitation point.

7.2 FORMULATION FOR A PLATE WITH INSERTS

Following Cremer and Heckl [12] employing Kirchhoff-theory, the governing set of equations is similar to the formulations of the numerical study with the beam (see section 4.2), but extended to plates and can be written as

$$v(\mathbf{X}) = \frac{\omega}{8Bk^2} \left[F_o G_F(\mathbf{X}, \mathbf{X}_S) - \sum_{v=1}^N F_v G_F(\mathbf{X}, \mathbf{X}_v) \right], \quad (29)$$

wherein index S denotes the external source and v an arbitrary position of one of the inserts.

The inserts are substituted by the forces resulting, which are applied to the infinite plate. G_F are the Green's functions pertaining to the point excited, infinite plate:

$$G_F(x, y) = H_0^{(2)}(k \cdot \sqrt{x^2 + y^2}) - H_0^{(2)}(-jk \cdot \sqrt{x^2 + y^2}). \quad (30)$$

The responses of the, possibly differing, inserts can be expressed in terms of the associated impedances as

³⁴ Main parts of the numerical study on a plate in this Chapter have been published by Weith and Petersson at the RASD conference in Southampton 2006 [98].

$$F_\mu = v(\mathbf{X}_\mu) Z_{F_\mu}; \quad 1 \leq \mu \leq N \quad (31)$$

where the force impedances of a pure mass and of a mass embedded in rubber are given by

$$Z_{F, mass} = j \cdot \omega \cdot m \quad (32)$$

and

$$Z_{F, spring-mass} = \frac{m \cdot s}{j \cdot \omega \cdot m + \frac{s}{j \cdot \omega}}, \quad (33)$$

respectively.

This means that the set of linear equations for the solution of the unknown auxiliary forces can be written as

$$\frac{F_\mu}{Z_{F_\mu}} + \frac{\omega}{8Bk^2} \left[\sum_{v=1}^N F_v G_F(\mathbf{X}_\mu, \mathbf{X}_v) \right] = F_0 \frac{\omega}{8Bk^2} G_F(\mathbf{X}_\mu, \mathbf{X}_S), \quad 1 \leq \mu \leq N. \quad (34)$$

By means of this set of N equations, the unknown auxiliary forces can be solved for and subsequently be substituted into equation (29) to obtain the complete vibration field of the plate.

7.3 NUMERICAL CALCULATIONS ON PLATES WITH INSERTS

The following calculations concern an infinite, homogeneous plate with inserts in the neutral layer distributed over the plate. Previous calculations and measurements with a beam (see Chap. 4 and 5) have shown an undesirable amplification of the transfer mobility in case of discontinuities which are embedded out of the neutral layer. For this reason moment effects are not considered in this work.

The thickness h of the plate is about 0.02m with a density ρ of 400 kg/m³. The complex Young's modulus is set to $E=5.6 \cdot 10^9 (1+\eta_{plate})$ N/m² with a loss-factor $\eta_{plate} = 0.01$ ³⁵. Each mass is calculated as a cylinder with a diameter of 0.008m and a height of 0.02m. To emphasise the effects of these inserts, each mass is multiplied by the factor 10, which

³⁵ In all calculations with plates, the thickness of the plate is set to $h=20$ mm. The error of the simple bending wave equation at Kirchhoff plates increases if the corresponding bending wave length becomes larger than 6 times that height ($\lambda > 6h$) (Cremer and Heckl [12]). Thus, transferred into a frequency, all calculated results with frequencies higher than $f=9461$ Hz are affected. Yet, as all observed frequencies in this chapter are below 9 kHz, the limited range of the Kirchhoff plate can be neglected.

results in a weight of 0.315 kg per mass. In case of rubber-coated masses with all the same stiffness, the value for the spring stiffness s is $3.5 \cdot 10^6$ N/m with a loss-factor η_{spring} of 0.01.

In the following the effects of a beam with embedded inserts will be compared with those observed for a plate with inserts ordered in circular arcs. The question arises, if the filtering effect produced by a periodic array also will be noticeable in a reflective finite environment. For multiple reflections on a finite plate with conservative boundary conditions the influence of the distributed masses mainly disappears³⁶, only the increase in mass remains. Thus, the effect of periodicity will become negligible. In consideration of losses at the boundaries of a finite plate it is assumed that the calculations on an infinite plate are asymptotically correct.

Figure 62 shows the difference of the inserts ordered in an arc and ordered in a half circle. In an infinite plate the results are the same. Thus, the calculations have shown that an opening angle of 60° is sufficient to obtain results comparable with those of a full circle respectively of a beam.

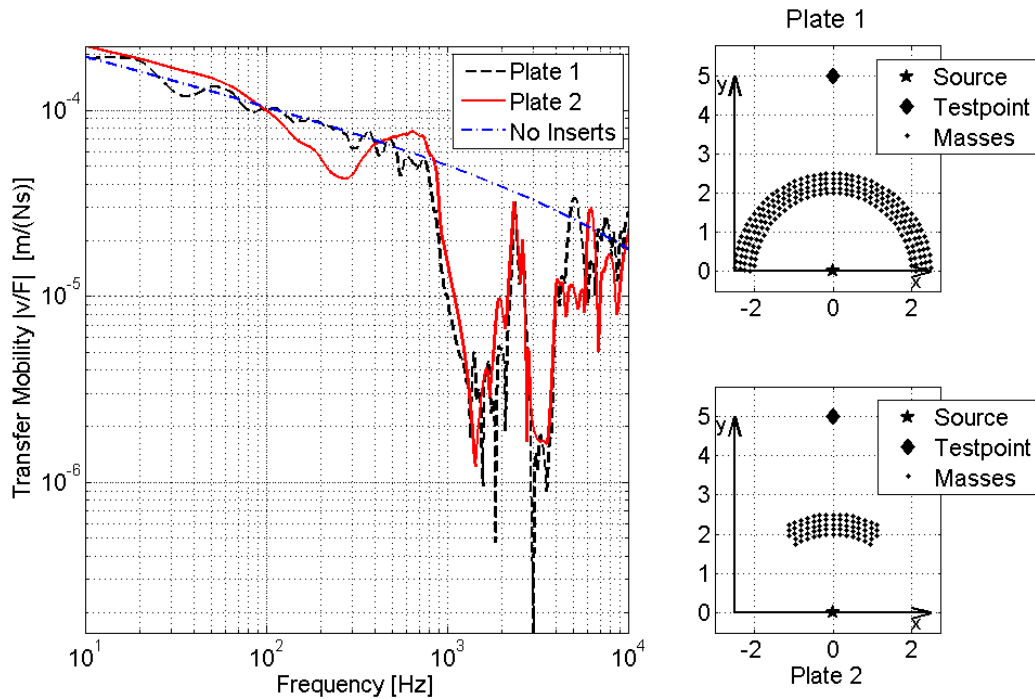


Figure 62: Transfer mobility of three plates. With 5 circular arcs (213 inserts) in an angular range of 0° to 180° , with 5 circular arcs (71 inserts) in an angular range of 60° to 120° and without inserts. The inserts are pure masses.

Therefore, it makes sense to investigate the influence of various distributions of the inserts on the plate. The incremental arc length between two sequential inserts and the

³⁶ In fact, it will be shown in Chap. 7, that measurement results on a finite plate with masses and resonant inserts distributed in circles show indifferent results.

radii of the circular arcs increase with a fixed increment. The opening angle of the arcs varies between 0° and 180° with the source point as the centre.

In Figure 63 the effects of masses are shown, starting with the arc when all are positioned along the line connection the source and receiver point. The general effects of the masses are displayed in terms of the transfer mobility from the source to the receiver.

Also the transfer mobility of an infinite homogeneous plate without inserts is included in Figure 63 for comparison. The divergence as well as the loss factor of the plate makes the curve decreasing with the frequency. If pure masses are embedded between the excitation and source point in one line (plate 1), the appearance of stop- and pass-bands above 300 Hz is observed. In the range below, the transfer mobility shows an amplification compared with the transfer mobility of a plate without inserts, possibly stems from the accumulated near field contribution and increased masses.

The attenuation of the stop-bands increases with more masses, which are distributed in circular arcs left and right of the constellation in plate 1. In the frequency range between 3 kHz and 6 kHz also, a broader band of attenuation can be observed. The comparison with an infinite homogeneous beam with pure masses in a periodic distribution indicates the same properties with the exception of the broad band of attenuation at higher frequencies. To establish if effects of scattering are the reasons for this observation, a plate is investigated next, where the number of existing circular arcs is doubled, while the distances are halved.

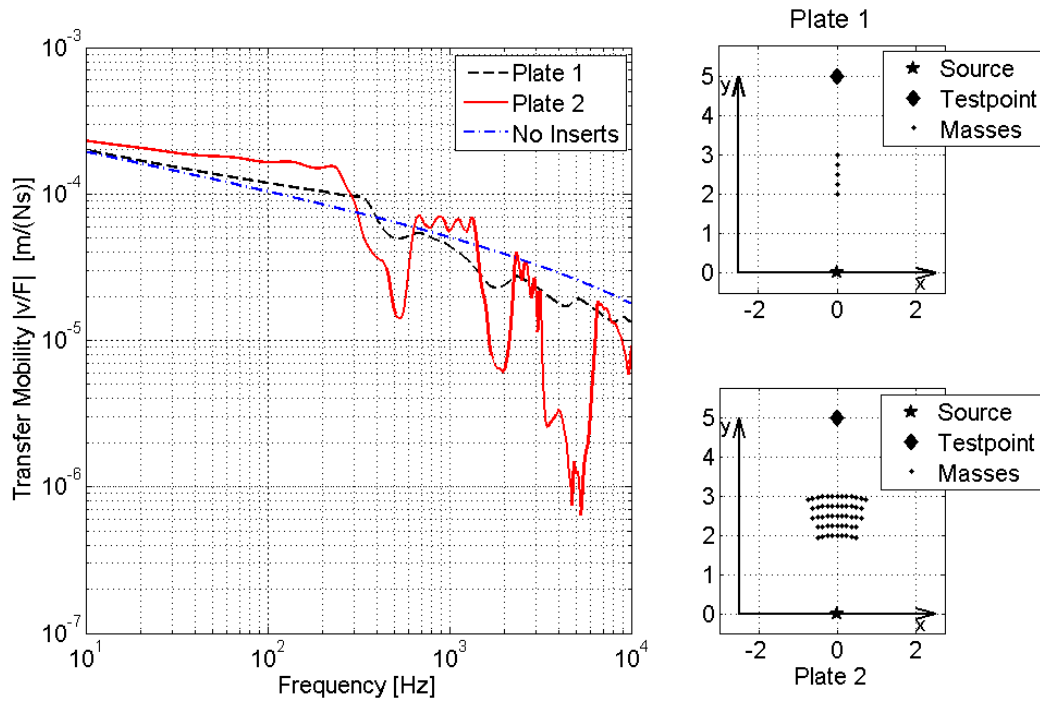


Figure 63: Transfer mobility of three plates. With 5 inserts in 1 line, with 5 circular arcs (53 inserts) and without inserts. In plate 2 the circular arcs are ordered in an angular range from 75° to 105° . The inserts are pure masses.

An observation of such a plate shows Figure 64. The first stop-band in the frequency range between 300 Hz and 600 Hz (plate 1) does not exist anymore for the new arrangement of plate 2. In contrast, the second stop-band is increased in amplitude and also markedly in bandwidth towards low frequencies. The bandwidth in the third stop-band, in turn, is smaller than that of the plate with less inserts. The effect of moving stop-bands to high frequencies with reduced distances of the inserts has been shown numerically in sub-section 4.3.1 and via measurements in sub-section 5.3.3 on beams. The bending wave length at 500 Hz is around 0.5 m. The distances from arc to arc in plate 1 is the half of it (0.25m). That means that the anti-nodes of the bending wave fits exactly with the masses and the bending wave is reflected at most.

The same effect can be seen in the frequency range from 900 Hz to 2 kHz for plate 2, where the relations between bending wave length and distances of the circular arcs are the same. Additionally, the broader band can be traced back to the various ways the bending wave use on their way through the net of inserts (scattering). For the next stop-band, the relations are the other way around again, because the distances of the inserts equal an even multiple of the bending wave length.

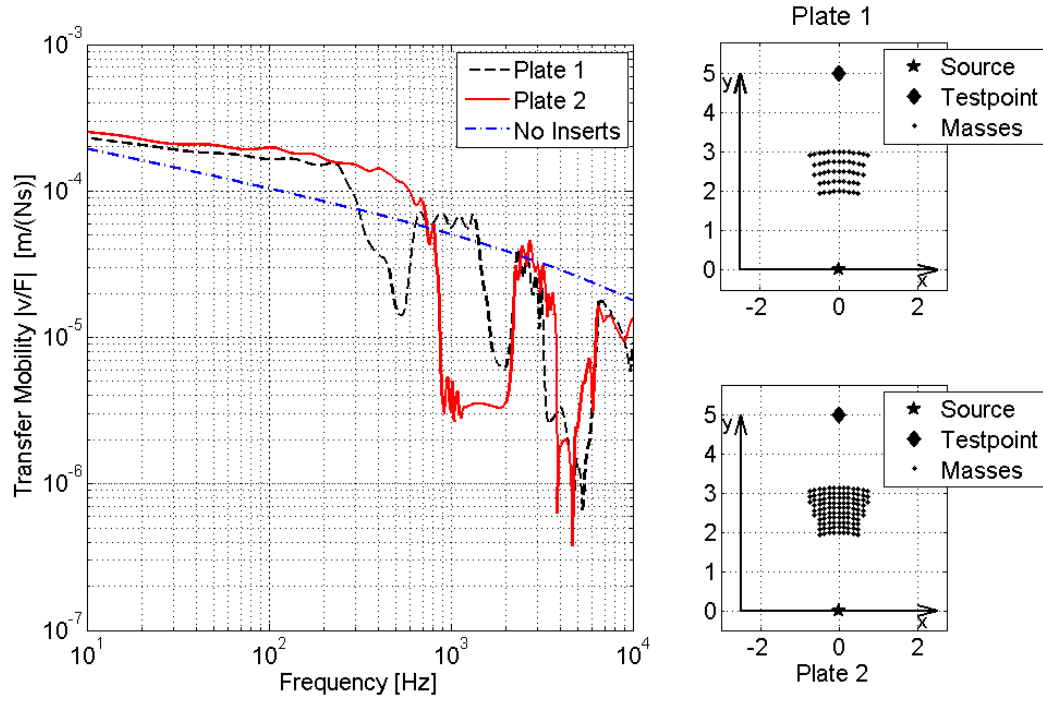


Figure 64: Transfer mobility of three plates. With 5 circular arcs (53 inserts), with 10 circular arcs (108 inserts), and without inserts. The circular arcs are ordered in an angular range from 75° to 105° . The inserts are pure masses.

In Figure 65, the circular arcs are extended to an opening angle of 60° . The increased number of masses brings along increased attenuations of the transfer mobility in the stop-bands. Another evidence for the existence of scattering effects can be observed in the form of a new trough in the transfer mobility in a low frequency range around 200 Hz. This stop-band is due to the new and longer paths the bending wave propagates in plate 2.

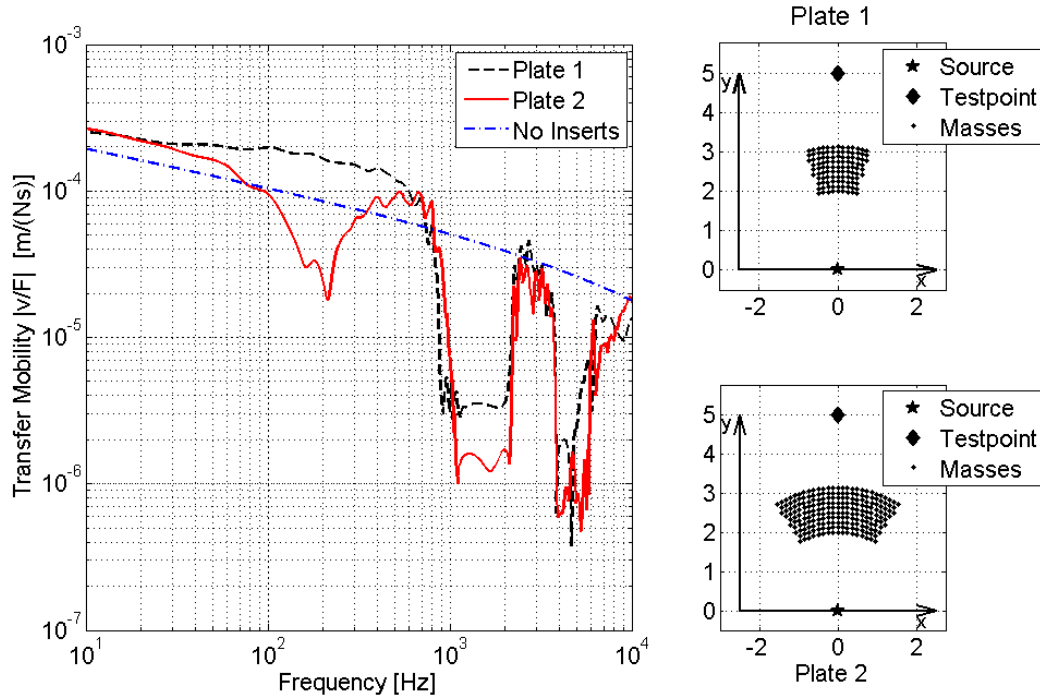


Figure 65: Transfer mobility of three plates. With 10 circular arcs (108 inserts) in an angular range of 75° to 105° , with 10 circular arcs (214 inserts) in an angular range of 60° to 120° and without inserts. The inserts are pure masses.

Figure 66 shows three different plates. The position of the receiver is different for each plate. At an angle of 120° can be observed for plate 2, that the influence of stop- and pass-bands at high frequencies is smeared in comparison with that for plate 1, but still visible. At low frequencies, below 1 kHz, the attenuation is even larger than that for an angle of 90° . This effect shows that the influence of masses can be large also remote from centre of the circular arcs. The attenuation indeed tends to zero, if the test point is out of the circular sector of the inserts. The transfer mobility of plate 3 displays this effect.

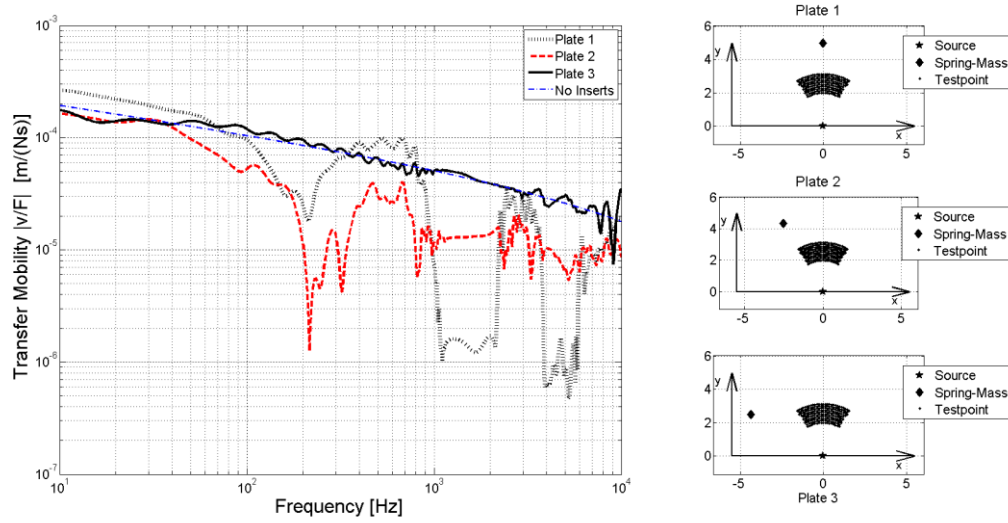


Figure 66: Transfer mobility of 4 plates. Three of them with 10 circular arcs (214 masses, test point angle 90° , 120° and 150°), and one plate without inserts. The circular arcs are ordered in an angular range from 60° to 120° . The inserts are pure masses.

If the same masses are coated with rubber, Figure 67 shows the large attenuation in the frequency range of the resonances of the inserts. This range of resonances is denoted by two vertical dotted lines. To broaden the attenuation in the resonant range, the spring stiffness can be changed in a way, such that the stiffness of each spring-mass system is increased in a logarithmical order. For clarity presentation, the stiffnesses are dimensioned as follows:

$$3.5 \cdot 10^5 (1 + j \cdot 0.01) \frac{N}{m} \leq s \leq 3.5 \cdot 10^6 (1 + j \cdot 0.01) \frac{N}{m}. \quad (35)$$

With the varying stiffnesses, an enlarged attenuation band can be observed as depicted in Figure 67. With equal stiffnesses the attenuation is significantly larger but on behalf of the bandwidth. The attenuation at resonances is growing with the stiffness. Strasberg and Feit [89] already investigated this effect, and found that it depends on the increasing impedance with frequency. At high frequencies no further stop-band can be observed. Beyond the highest resonance frequency, the influence of the rubber prevails and the transfer mobility approaches that of the plate without inserts. Above this frequency all inserts are dynamically decoupled and have no effect³⁷.

³⁷ See also the observations at the numerical study on beams in sub-section 4.3.3.

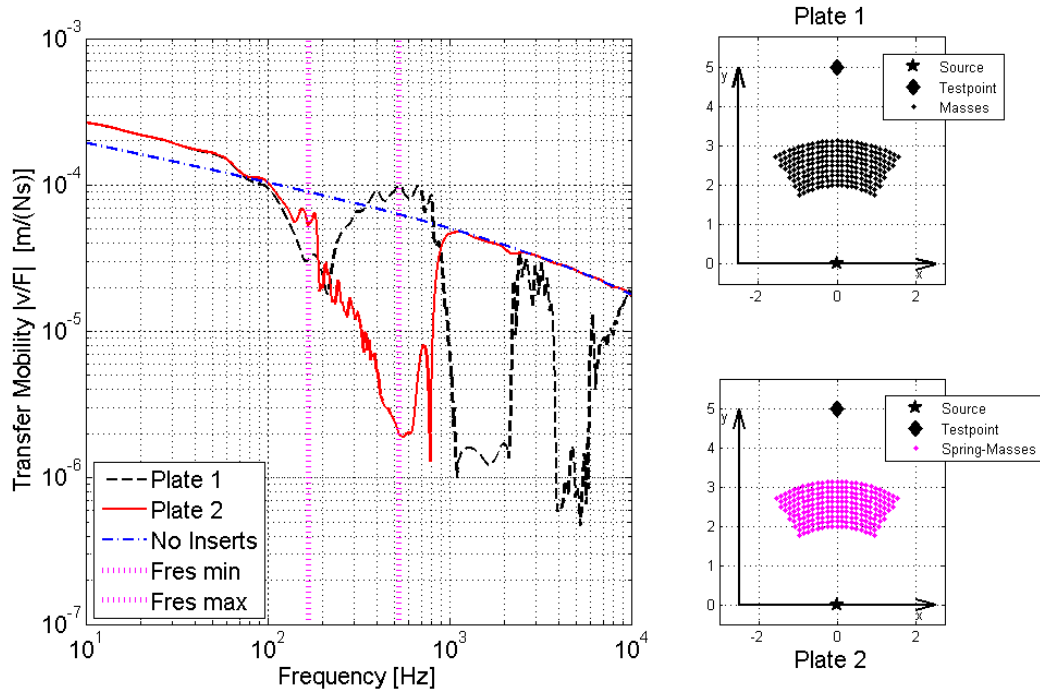


Figure 67: Transfer mobility of three plates. Plate 1 with pure masses, plate 2 with mass- and spring-systems and one plate without inserts. 10 circular arcs are ordered in an angular range from 60° to 120° and include 214 inserts each. The dotted lines display the lowest and highest resonance frequency of the spring-masses. The test point is ordered at an angle of 90° .

If the stiffnesses of the rubber-coated masses are multiplied by a factor of 100, an interesting effect can be seen within the second stop-band (Figure 68). The attenuation is reduced, although an effect of the resonances is expected. This comes from the influence of the stop-band, where the inserts in their resonances can be seen as rigid supports³⁸. Below the first resonances of the inserts, the transfer mobility of the plate with spring-mass systems coincides with that of the plate loaded by pure masses.

³⁸ Heckl, Maria [35] pointed out, that the behaviour of a support consisting of a single mass and spring is rigid in its resonance, if it is undamped. Furthermore, it has to be noted, that some of the higher stiffened inserts are still mass-controlled at frequencies below their resonances and possibly act like pure masses (see also sub-section 4.3.3).

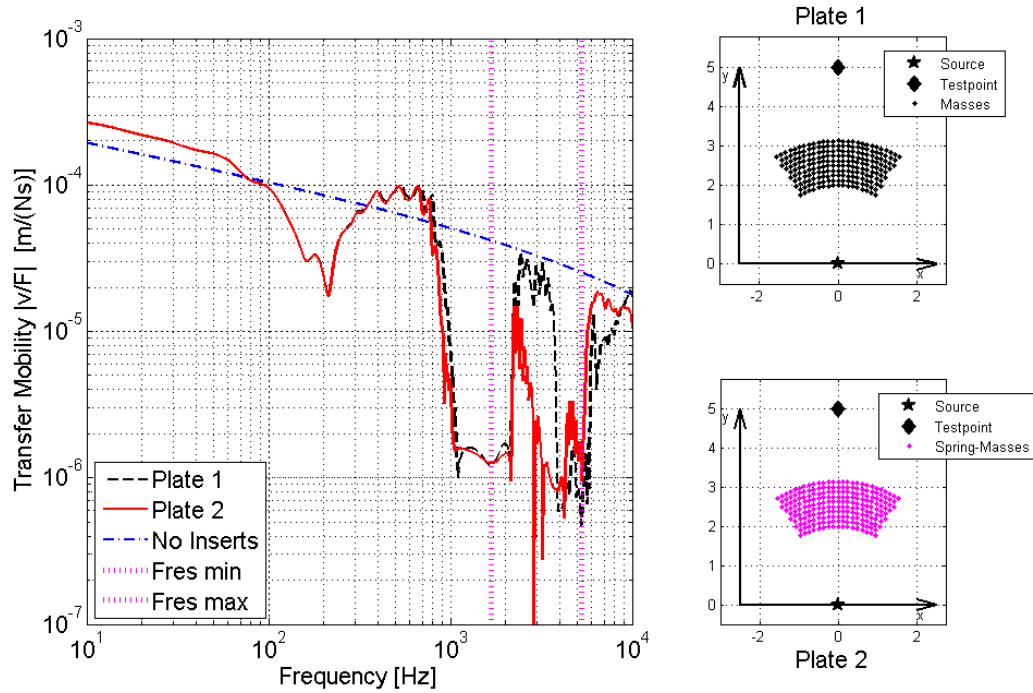


Figure 68: Transfer mobility of three plates. Plate 1 with pure masses, plate 2 with mass- and spring-systems and one plate without inserts. 10 circular arcs are ordered in an angular range from 60° to 120° and include 214 inserts each. The dotted lines display the lowest and highest resonance frequency of the spring-masses. The test point is ordered at an angle of 90° .

In order to reduce the bending wave propagation on a plate, it suggests itself to combine the effects of stop-bands and resonant attenuation. As mentioned previously, a lot of masses are required with large distances to each other to obtain a stop-band at low frequencies. On the other hand, it makes sense to use the spring-mass systems below the first appearing stop-band due to pure mass-like inserts (see Figure 67 and Figure 68). Thus, in Figure 69 is illustrated a combination of inserts with arcs of masses and spring-masses alternating.

From a comparison with the plate with pure masses, it is seen that there is only a small drop in attenuation in the second stop-band between 1 kHz and 2 kHz. At the third stop-band, the attenuation is reduced in bandwidth. Also, the attenuation at the resonant frequencies of the sprung-masses is appreciable. This combination of different inserts realise a possibility to reduce the bending wave propagation over a broader range than can be achieved with only either of the two kinds of inserts.

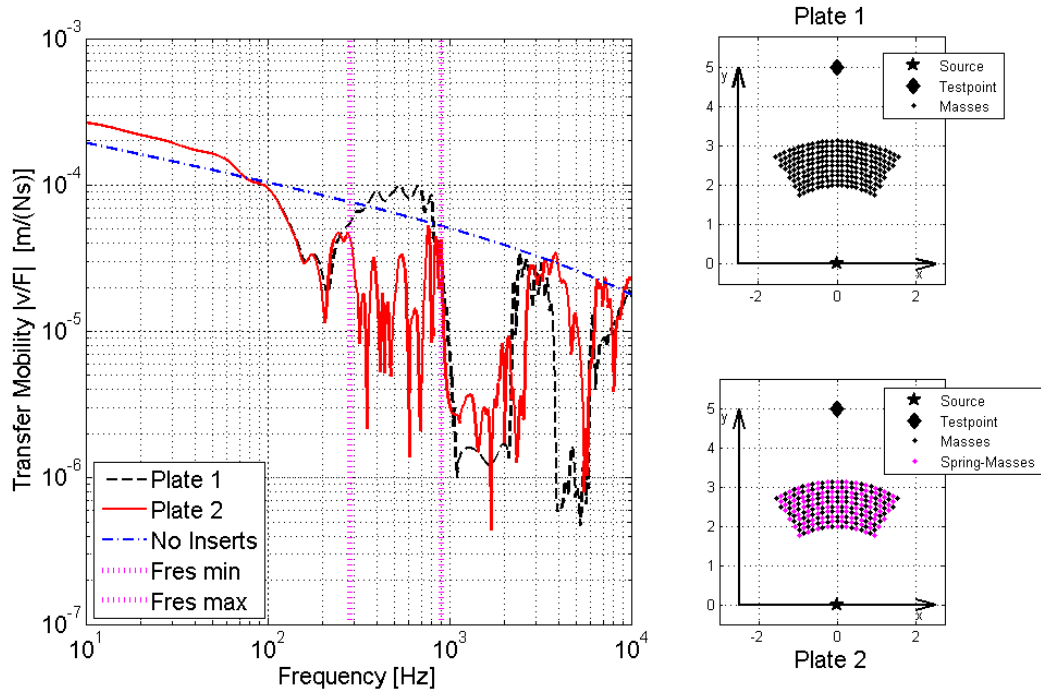


Figure 69: Transfer mobility of three plates. Plate 1 with pure masses, plate 2 with spring-mass systems and one plate without inserts. 10 circular arcs are ordered in an angular range from 60° to 120° and include 214 inserts each. The dotted lines display the lowest and highest resonance frequency of the spring-masses.

Figure 70 shows that with another distribution of the inserts, also for more high frequent and broad frequency ranges, the propagation can be influenced.

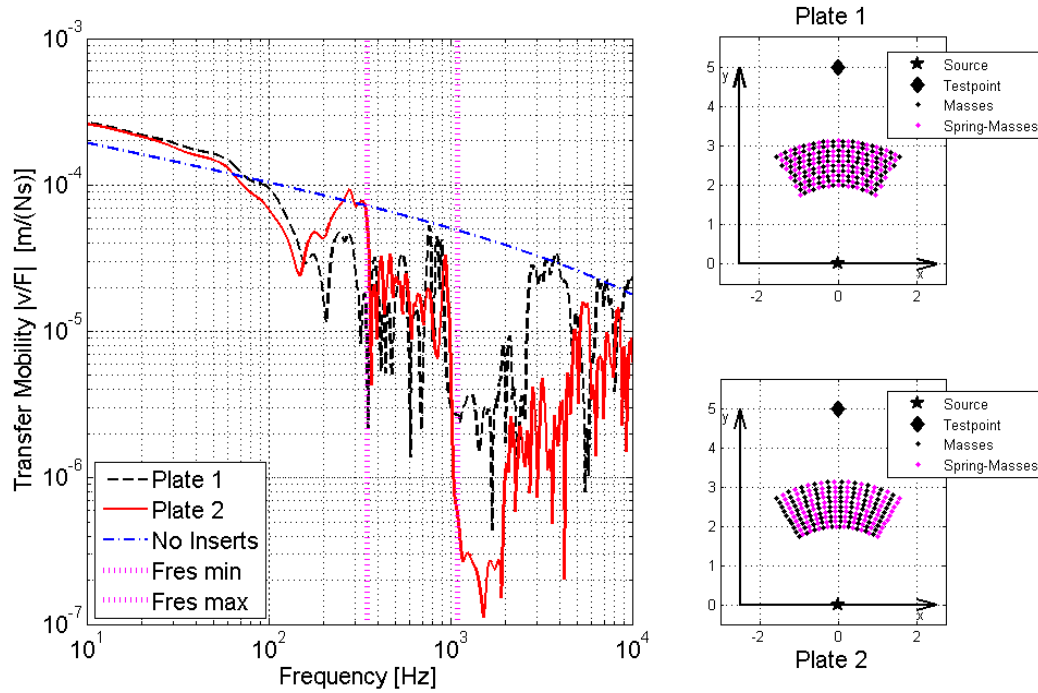


Figure 70: Transfer mobility of three plates. Plate 1 with mass- and spring-systems (214 inserts), plate 2 with mass- and spring-systems (200 inserts) and one plate without inserts. 10 circular arcs are ordered in an angular range from 60° to 120° . The dotted lines display the lowest and highest resonance frequency of the spring-masses.

7.4 SUMMARY OF CALCULATIONS ON A PLATE WITH PURE MASSES AND RESONANT INSERTS

An infinite homogeneous plate with variations of embedded masses and spring-masses has been studied. Numerical calculations demonstrate similar features as those found for the bending wave propagation in beams with embedded inserts (Chap. 4 and 5).

To exhibit the features observed for beams the masses embedded in a plate must be organised in arcs shadowing the response point from the source. The following observations could have been detected:

1. The larger the distances of the masses in radial direction, the lower the frequency of the 1st stop-band is (see Figure 62 and Figure 63).
2. The attenuation of transfer mobility with inserts ordered in an arc is slightly lower than ordering the masses in a half-circle. In an infinite plate the resulting frequencies of the stop-band are the same (see Figure 62).
3. If pure masses are embedded between the excitation and source point in one line, the appearance of stop- and pass-bands is observed (see Figure 63). The attenuation of the stop-bands increases with more masses, which are distributed in circular arcs left and right of such a line.

4. In the range below the 1st stop-band, the transfer mobility shows amplification compared with the transfer mobility of a plate without inserts, stemming from the accumulated near-field contribution (see Figure 64).
5. The attenuation in stop-band increases in amplitude with the number of masses. In the two-dimensional case of a plate, the band-width becomes broader than for a beam because of scattering effects, which make the bending waves take differing, extended paths through the net of inserts (see Figure 64).
6. If the masses are coated with rubber, similar effects as those observed for the beam appear (see Figure 17). Below the resonances of the inserts, the transfer mobility behaves as if the inserts were pure masses, and stop-bands appear (see Figure 21 and Figure 67).
7. For the range in which inserts are resonant, the higher the center frequency, the bigger the attenuation is (compare Figure 67 and Figure 68).
8. With the variation in stiffness using only rubber-coated masses, an enlarged attenuation band can be achieved, extending the stop-band region to higher frequencies. The resonances are tuned to a frequency band adjacent to the first stop- and pass-band (see Figure 68).
9. Above their resonances, stop-bands have no effect, as all resonant inserts are dynamically decoupled (see Figure 67). Beyond the highest resonance frequency, the influence of the rubber prevails, and the transfer mobility approaches that of the plate without inserts.
10. If the resonances coincide with a stop-band, the attenuation displays drop (compare Figure 20 and Figure 68). However, there is no interaction with the inserts in a pass-band.
11. The combination of different inserts (with pure and rubber-coated masses) realise a possibility to reduce the bending wave propagation over a broader range than can be achieved with only either of the two kinds of inserts (see Figure 69).
12. With another distribution of these mixed inserts, as well as for more high and broad frequency ranges, the propagation can be influenced (see Figure 70).

8 MEASUREMENTS ON A FINITE PLATE WITH MASSES AND ELASTICALLY SUPPORTED MASSES

8.1 PREPARATIONS OF THE MEASUREMENTS ON A PLATE

In the following, the measurements on a plate with masses and elastically supported masses located around the center point are displayed. In compare with the measurements with a slender wooden beam, in this case, the boundaries of the plate are not damped by sand. Those are supported on thin shelves with an overlap of 20mm of each boundary (Figure 71).

The focus with these measurements is on the investigation of a forced excitation in the center of the plate, which is enclosed by rings consisting of pure and elastically supported masses, respectively. According to the calculations in section 7.3 it is expected that the inserts act as a barrier - evoked by stop-bands or resonances - for the propagating bending waves at certain frequencies. Thus, the frequency response within the rings is supposed to be larger compared with the frequency response outside of the rings. Whether the bending waves within the rings are really shadowed under such conditions will be investigated.



Figure 71: Measurement set-up of the plate supported on thin shelves with an overlap of 20mm. The pure masses or elastically supported masses, respectively, are distributed in circles around the center point of the plate.

Therefore, the measurements are conducted with pure masses and rubber damped masses to investigate the impact of stop-bands and resonances.

A plate consisting of Plexiglas with the sizes 0.8m x 1m and a thickness of 10 mm have been used. Steel cylinder (mass= 38g) with a diameter of 20mm and a height of 15mm were stuck to both sides of the plates in circular rings.

In a pre-test, two different types of elastic material have been chosen by placing them between a steel cylinder and the excitation mass of a shaker in order to assess the most suitable rubber material. Figure 72 shows the measurement set-up.

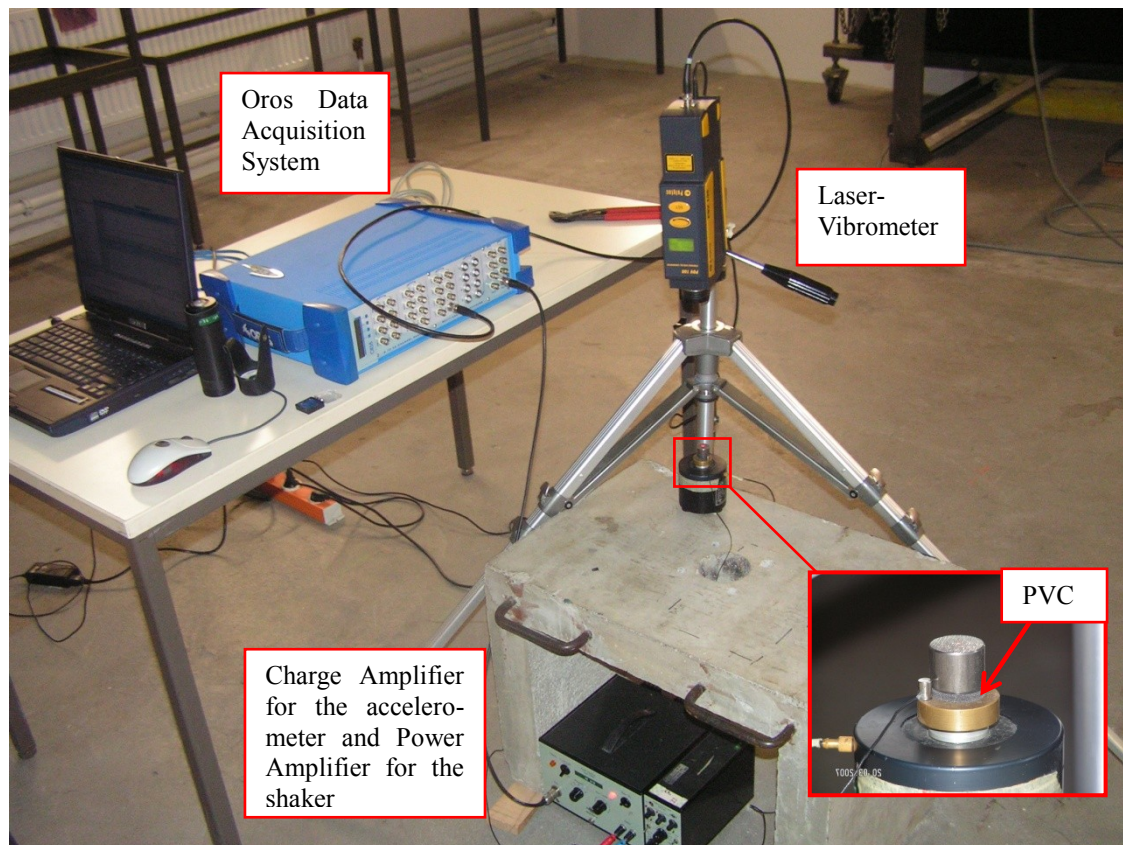


Figure 72: Measurement set-up of the pre-tests with two different rubber materials. The vibration of the shaker has been measured with an accelerometer placed on a defined mass, whereas the acceleration of the mass has been conducted with a Laser vibrometer. In the zoomed picture the shaker with its excitation mass and the accelerometer attached are visible. The rubber material (PVC) carrying the mass is stuck to the excitation mass. The accelerometer is placed on a defined mass (47g) and the acceleration of the insert has been conducted with a Laser vibrometer.

The exciting force has been measured with an accelerometer stuck to a defined cylindrical piece of metal, which was driven by the shaker with white noise. The resulting vibration of the spring-mass system has been measured with a Laser vibrometer. Two different damping materials had been used, PVC with a thickness of 2mm (Figure 72, zoomed picture) and the castable resin (Polyurethane elastomer - PUR) with a thickness of 6.5mm³⁹ (Figure 73).

³⁹ For the plates the same castable resin PUR has been used as for the measurements with the rubber-coated masses in the beams (Chap. 5). The mixture of the 2-component rubber was set to a Shore hardness of 80 ShA. Cylindrical pieces out of metal with a thickness of 6.5mm and a diameter of 22mm had been produced for this experimental set-up.

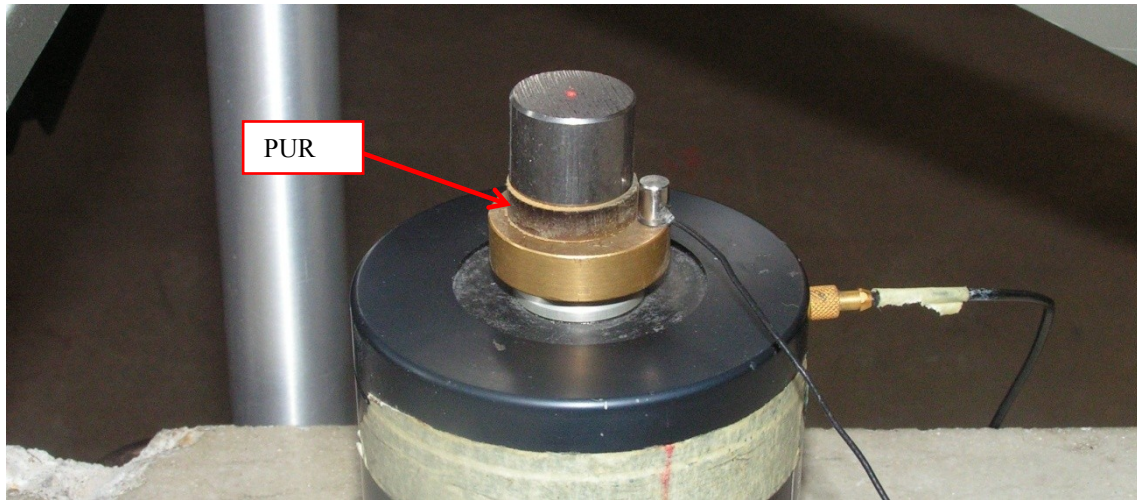


Figure 73: Measurement set-up of the pre-tests with a layer of PUR as damping material. The accelerometer has been placed on a defined mass (47g). The acceleration of the mass, which is stuck onto the elastic material (PUR) has been obtained with a Laser vibrometer.

For each rubber material three measurements had been averaged. The acceleration of the reference mass has been divided by the acceleration of the rubber damped mass. By dividing by $j2\pi f$, these ratios become proportional to the transfer mobility $(a/j2\pi f)/F$ ⁴⁰.

The resulting resonances of these “mobilities” had been measured at frequencies of about 120 Hz for PVC and about 1260 Hz for the castable resin (PUR) (Figure 74).

Assuming low frequency modes being dominant on a plate consisting of acrylic glass with finite boundaries, the elastic material PUR with a resulting higher resonance frequency has been chosen for the measurements with the plate to be able to see reasonable effects.

These rubber gums have a diameter of 22mm and a height of 6.5mm with a weight of 2.55g.

⁴⁰ The force is calculated by the mass times the acceleration. As the mass is fix, the chosen ratio is proportional to the transfer mobility.

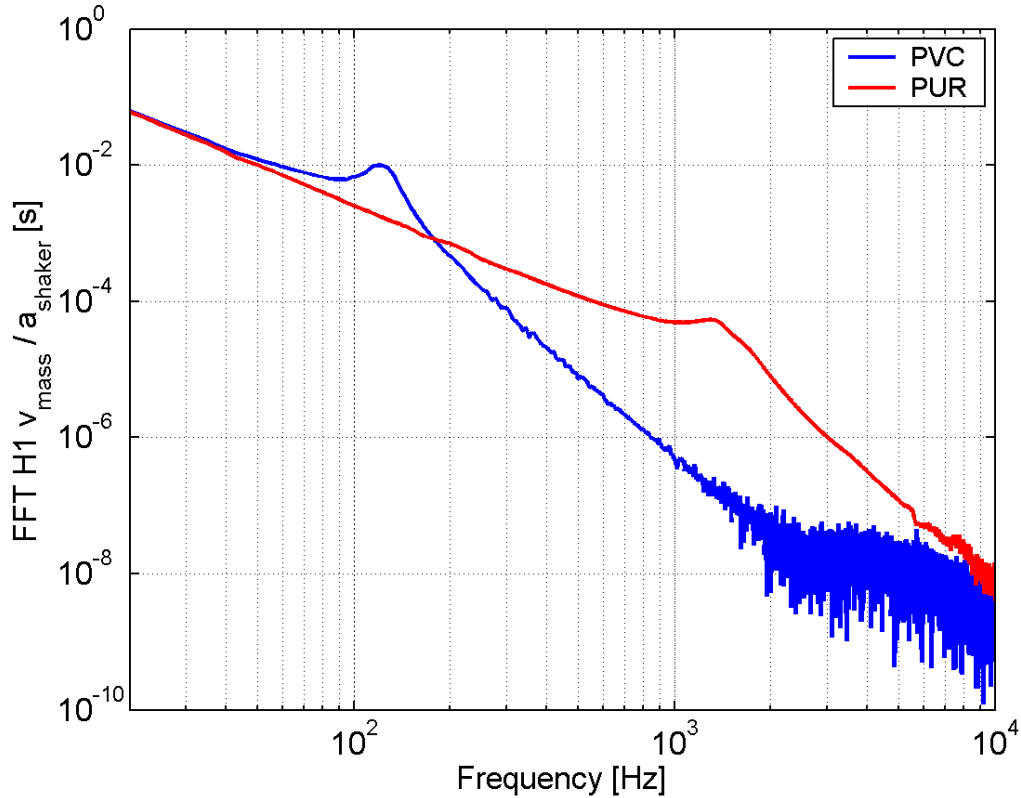


Figure 74: Frequency responses ($\text{FFT H1 } v_{\text{mass}}/a_{\text{Shaker}}$) of two elastically supported cylindrical masses with different rubber materials (PVC and PUR). The excitation of these spring-mass systems occurs with a shaker driven by white noise. The resulting resonances appear at 120 Hz for the PVC and 1260 Hz for PUR.

8.2 MEASUREMENT SET-UP OF A FINITE PLATE WITH MASSES AND ELASTICALLY SUPPORTED MASSES

In the following measurements it is interesting to observe whether the impact of stop-bands and resonances can be seen with masses or elastically supported masses attached to both sides of the plate⁴¹. Therefore a finite plate consisting of acrylic glass (Plexiglass®) has been chosen to run the measurements.⁴²

⁴¹ Assuming momentary effects are responsible for decreased reflection at stop-bands and resonances - as it could have been shown in the numerical investigation on beams (see Chap. 4) - the attachment of inserts on both sides of the plate was intended to simulate embedded inserts in the neutral layer.

⁴² As is described in Chap. 6 and Chap. 8, because the effects of stop-bands and resonance show up with high confidence in slender beams and in calculations with half-infinite plates, it became important to examine if such effects are visible in experiments with finite plates as well.

Following pictures show the measurement set-up on the plate. The excitation happened with an impulse hammer and a force transducer connected. Several accelerometers had been distributed on the plate inside and outside the rings.

For all measurements on the plate ME525 (ICP) force transducers and ME820 (ICP) accelerometers had been used.

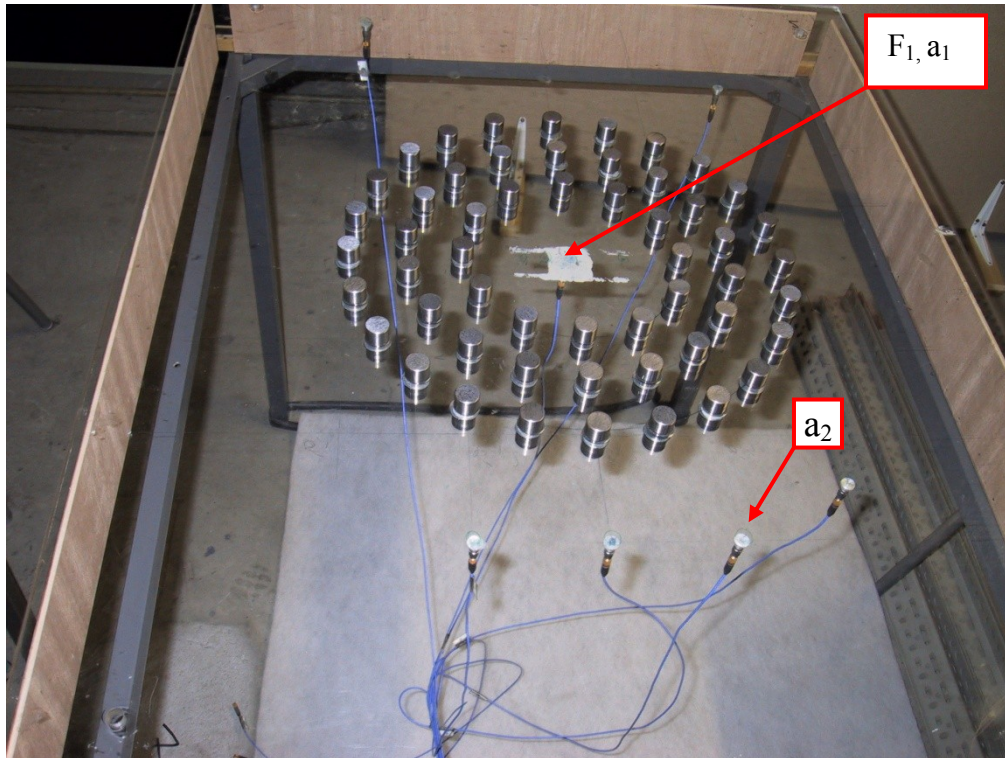


Figure 75: Plate out of acrylic glass (Plexiglass®) with three rings of pure masses, glued on both sides of the plate. One accelerometer has been placed in the middle of the rings, six others are located out of the rings. The excitation happened with an impulse hammer, including a force transducer. The boundaries of the 0.8m x 1m plate are supported on vertical shelves without being glued.



Figure 76: Plate out of acrylic glass (Plexiglass®) with three rings of pure masses, glued on both sides of the plate. View from the bottom side.

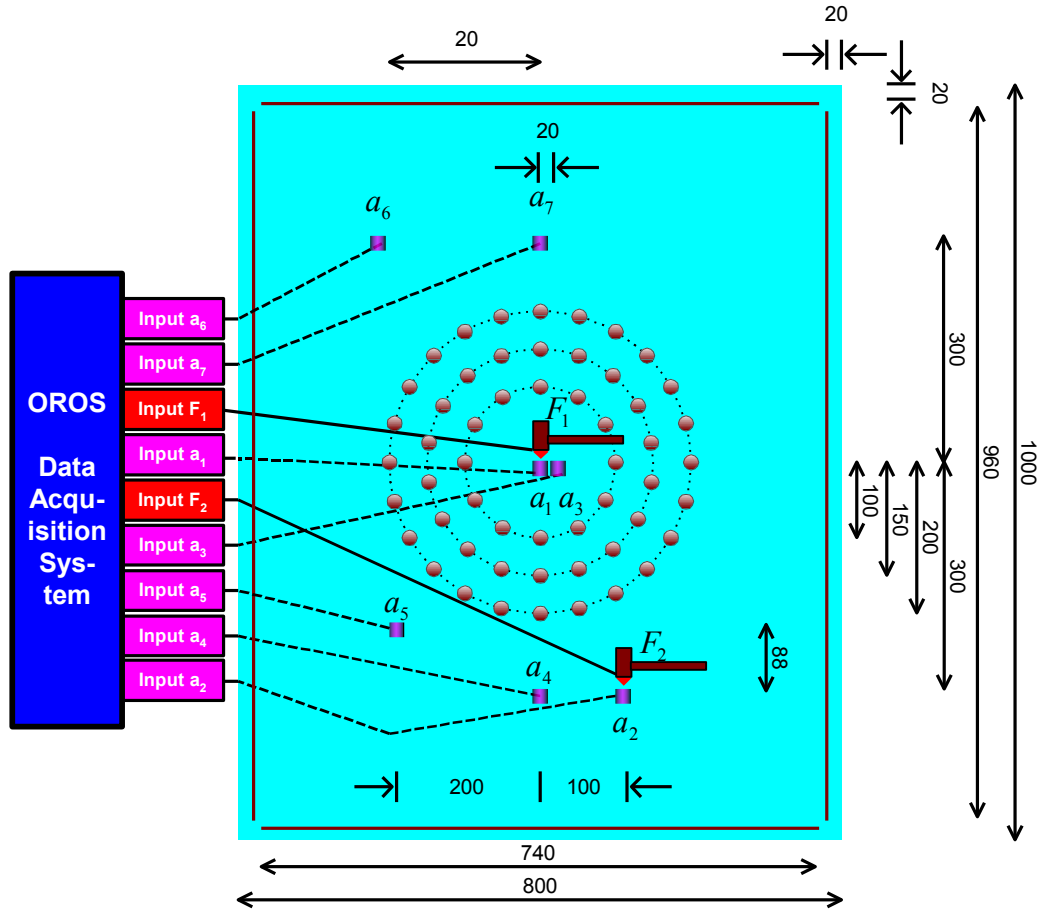


Figure 77: Measurement set-up of all measurements on the finite plate out of acrylic glass (Plexiglass®) with three rings of 12, 18 and 24 pure masses or elastically supported masses, respectively, glued on both sides of the plate. The length measures are in mm. The boundaries of the 0.8m x 1m plate are supported on vertical shelves without being glued. The excitation happened at two positions on the top side of the plate with an impulse hammer, a force transducer connected. All accelerometers have been placed on the bottom side of the plate.



Figure 78: Plate out of acrylic glass (Plexiglass®) with three rings of elastically supported masses glued on both sides of the plate. View from the top side. For this configuration one accelerometer has been placed in the center of the rings, two others shifted by 20mm each and five others have been located out of the rings. The excitation happened with an impulse hammer, including a force transducer.

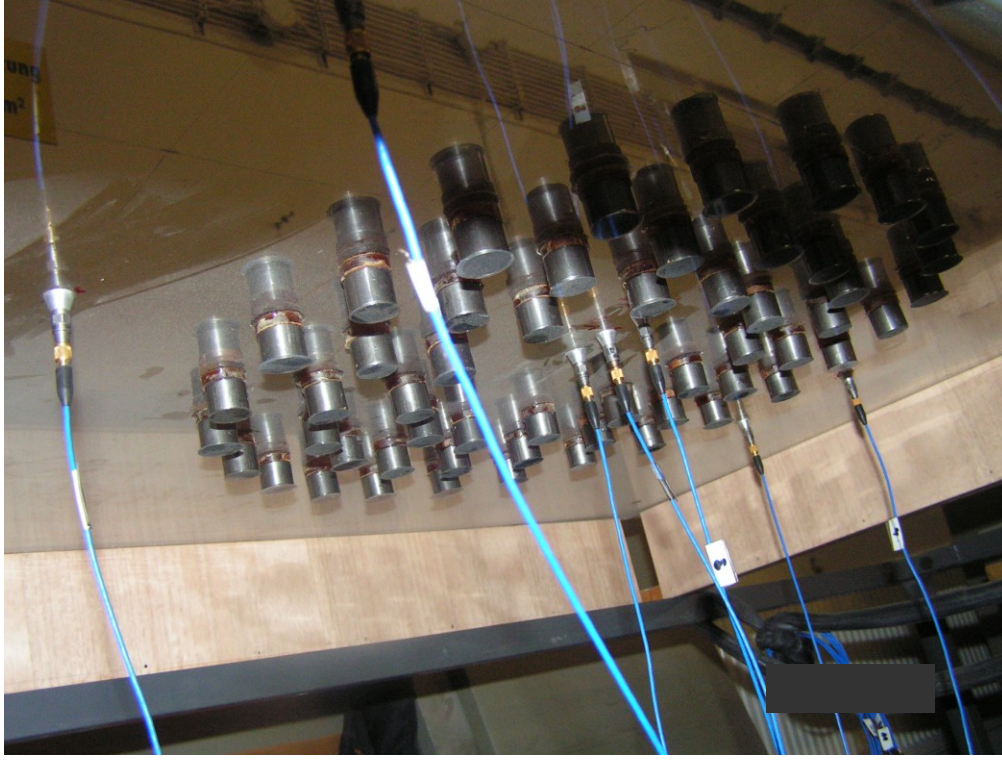


Figure 79: Plate out of acrylic glass (Plexiglass®) with three rings of elastically supported masses. View from the bottom side.

To estimate the occurring stop-band frequencies following parameters had been used:

- $h = 0.01\text{m}$ (thickness)
- $\rho = 1150\text{ kg/m}^3$
- $E_{real, plate} = 5.6 \cdot 10^9\text{ N/m}^2$ (Young's modulus of acrylic glass, see [12])
- $\eta_{plate} = 0.03$ (loss-factor of the acrylic plate)
- $\mu = 0.01$ (Poisson's ratio)

With following equations, the stop-band frequencies can be estimated with

$$\lambda_{stop-band} = dist \frac{2}{n}; \quad n = 1, 2, 3, \dots \in \mathbb{N}. \quad (36)$$

Their appearance in the frequency range follows from the bending wave equation

$$\lambda_B = \frac{2\pi}{\sqrt{\omega}} \sqrt[4]{\frac{B}{m''}} \quad (37)$$

and yields

$$f_{\lambda} = \frac{2\pi}{\lambda_B^2} \sqrt[4]{\frac{B}{m''}} \quad (38)$$

with

$$m'' = \rho h, \quad (39)$$

$$E = E_{real} (1 + j\eta_{plate}) \quad (40)$$

and

$$B = E \frac{h^3}{12(1 - \mu^2)}. \quad (41)$$

Table 4: The first four calculated stop-bands on the plate with masses are shown, which are distributed in circles around the center with radial distances of 50 mm to each other. Stop-bands occur if a half of the bending wave-length - or a multiple of it - fits with the distances of the masses. It is only the 1st stop-band, which is to be expected in the relevant frequency range from 10 Hz to 10 kHz.

Stop-bands	1 st	2 nd	3 rd	4 th
Frequency	7.87 kHz	31.48 kHz	70.83 kHz	125.9 kHz

8.3 MEASUREMENT RESULTS OF A FINITE PLATE WITH MASSES AND ELASTICALLY SUPPORTED MASSES

In the appraisal of the measurement results it was observed that a direct comparison of the transfer mobilities of the pure plate with one of the plates with supports attached could not be applied due to the impact of increased mass of the plate with additional supports.

Thus, the ratio of the point mobility v_1/F_1 to the transfer mobility v_2/F_1 is displayed, which finally yields the ratio of the inner to the outer velocity (equation (42))⁴³:

⁴³ In the following, this “point mobility” in the center of the rings with the force F_1 and the velocity v_1 , calculated with the accelerometer a_1 exactly underneath this position, will be called “transfer mobility” in the context of the “ratios of the transfer mobilities”.

$$\text{Transfer mobility, Ratio}_{inner/outer} = \frac{\frac{a_1}{j2\pi f}}{\frac{a_2}{j2\pi f}} = \frac{F}{F} = \frac{v_1}{v_2} \quad (42)$$

In all measurements, the masses or elastically supported masses are glued to the plate on both sides.

At first, a comparison of a pure plate, a plate with one ring of masses and a plate with three rings of masses, each attached to both sides of the plate, has been conducted. It can be seen in Figure 80, that the vibration within the rings is larger compared to the vibration outside the rings over the entire frequency range from 200 Hz on. The black line at the value 1 denotes vibrations, which are of the same magnitude inside and outside the rings. Values larger than 1 indicate higher vibrations within the rings.

Furthermore, it can be seen in Figure 80 that the vibrations of the plate with one and three mass-rings are different to the vibrations of the pure plate at frequencies from 1 kHz on.

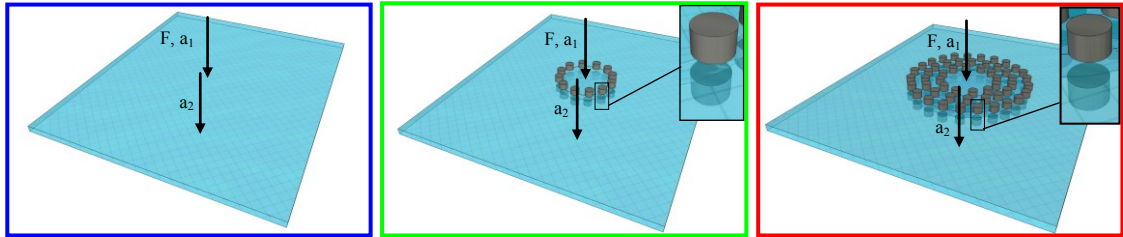
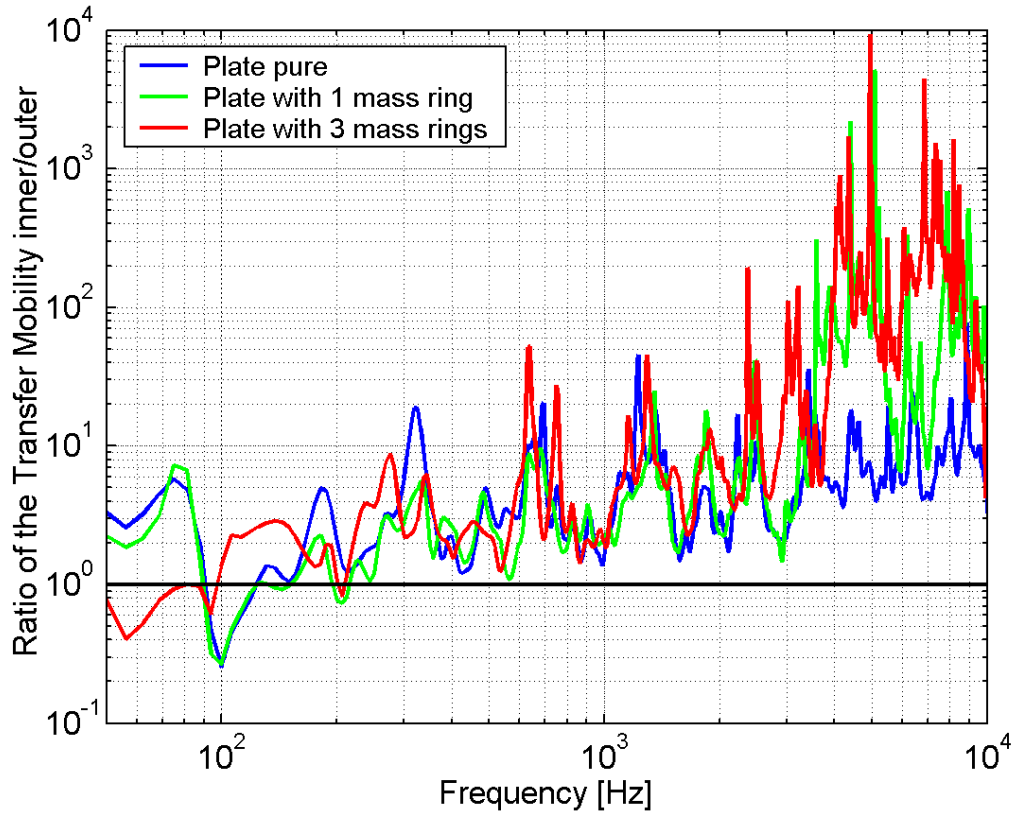


Figure 80: Non-smoothed ratio of the transfer mobility in the center of the plate from three plates. The plate on the left side is without masses, the plate in the middle with 1 mass-ring and the plate on the right side with three mass-rings. The masses are glued from both sides of the plate.

In a zoomed plot (Figure 81) of the same configurations in a frequency range from 500 Hz to 10 kHz, the smoothed ratios of the inner to the outer transfer mobilities of the plates with one mass ring and three mass rings show increased vibrations at a frequency range from 3 kHz to 5 kHz (see the black dotted circle). It is very unlikely that these differences are related to existing stop- and pass-bands, as the first stop-band is not expected below 7.87 kHz according to the calculations from Table 4. The orange dotted circle denotes the difference at a frequency range from 6 kHz to 7 kHz of one mass ring and three mass rings. Assuming scattering effects between the calculation and the measurement, these differences are possibly related to the stop-band, which reflects the propagating bending waves excited in the middle of the plate.

Considering the individual weight of each mass and each rubber, the overall weight of the Plexiglas plate is increased. The following table (Table 5) shows the impact of these additional inserts⁴⁴.

Table 5: Measured weights of the plate and the inserts.

Type of plate	Number of masses 38g/mass	Number of rubbers 2.55g/rubber	Weight [kg]	Related to
Pure plate	0	0	9.5	Figure 80 Figure 81
1 ring of masses glued on both sides	24	0	0.91	Figure 80 Figure 81
Three rings of masses glued on both sides	108	0	4.10	Figure 80 Figure 81
Three rings of elastically supported masses glued on both sides	108	108	4.38	Figure 82 Figure 83

It is well known that additional masses, independent of their distribution, alter the vibration and the mode pattern of a finite plate and are accompanied by significant scattering. Thus, there are several possible reasons for an increased ratio of the transfer mobility with additional masses.

However, because no radial distances exist with only one ring of masses on a plate, stop-bands should not appear. In other words, the comparison with the plate with three rings should show differences, if they exist.

⁴⁴ It is obvious that three rings of masses or elastically supported masses increase the weight of the plate by almost 50%. The impact of such a large weight increase needs to be considered in the discussion of measurement results, as it will very likely change the entire vibration behaviour significantly, though it is difficult to know in which dimensions exactly.

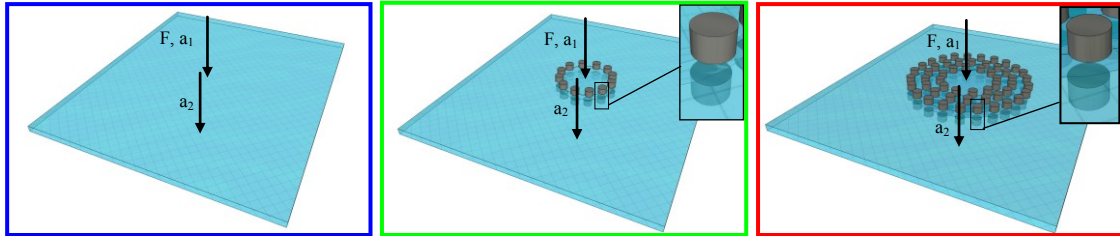
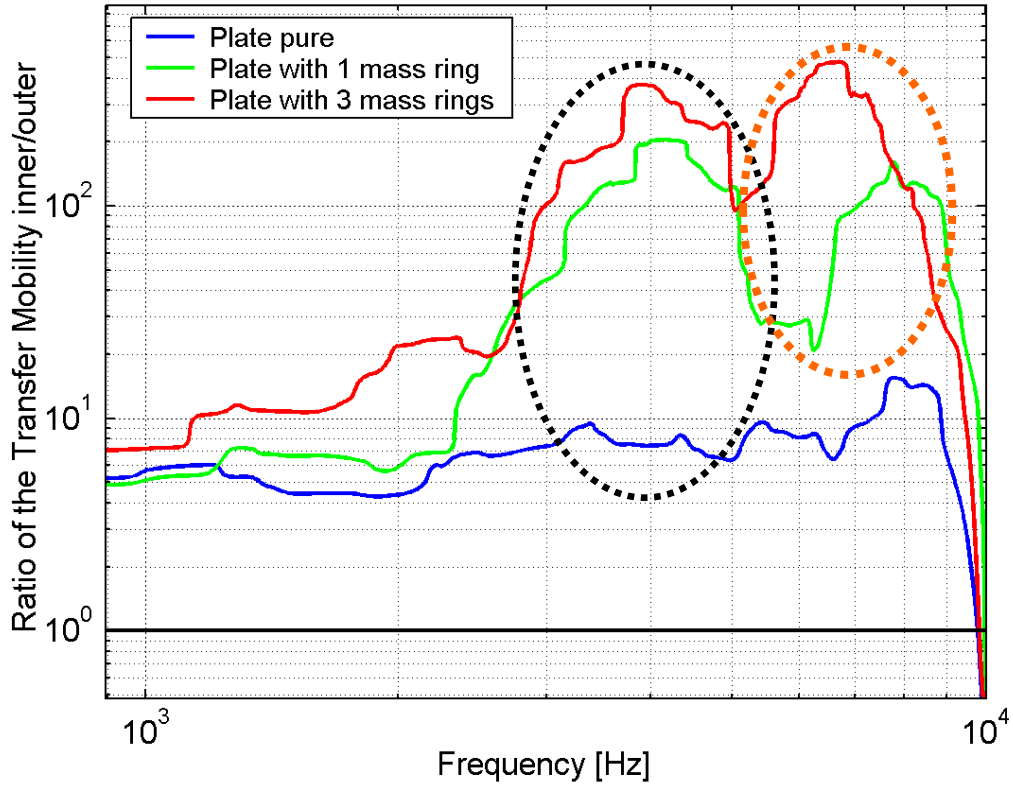


Figure 81: Smoothed ratio of the transfer mobility in the center of the plate from three plates. Zoomed plot at a frequency range from 500 Hz to 10 kHz. The plate on the left side is without masses, the plate in the middle with 1 mass-ring and the plate on the right side with three mass-rings. The masses are glued from both sides of the plate.

The ratio of the transfer mobility from a plate with three rings of elastically supported masses is shown in the following two plots (Figure 82 and Figure 83). The excitation happened in the center point and outside the rings.

The ratios of the transfer mobilities of a force excitation within and outside the rings were compared using various accelerometers placed in both areas (inside and outside).

In comparing these ratios with the two accelerometers within the rings, low differences are observed (compare dotted and non-dotted curves in Figure 82). Thus, the vibrations at or adjacent to the centre of the plate are almost identical at all measurements.

At frequencies higher than 4 kHz, all vibrations are increased within the rings, independent of the location of the introduced forces⁴⁵. The excited bending waves seem to be trapped in that frequency range.

The results of the two forces, one positioned within and the other outside the rings, show that below 4 kHz the vibrations are the highest close to or at the excitation point (see Figure 82, red curve, “F₂ a₁/a₂”).

According to the pre-test measurements (Figure 74) the resonances of the rubber-damped masses are expected to be at about 1.26 kHz, which denotes the interesting frequency range for these measurements with rubber-coated masses. In fact, increased vibration levels can be seen at a frequency just below 1 kHz (Figure 82, orange dotted circle), which is possibly caused by the resonances of the elastically supported masses.

Assuming variations in stiffness of the cylindrical rubber inserts lower resonance frequencies are possible, which lead to an increased vibration level within the rings.

However, the red curves (Figure 82, black dotted circle with F₂: a₁/a₂ and a₃/a₂) depict higher vibrations outside the rings and do not follow the assumption of having the resonance effect of the rubber-damped masses.

Thus, although there are tendencies toward resonance effects, all of these observations underline the influence of finite conditions and adding weight to the plate (see Table 5). With regard to the calculations on beams and plates (see Figure 20, Figure 21 and Figure 67), the plate with elastically supported masses should be decoupled at frequencies higher than the resonances. That means that the appearance of an increased transfer mobility at higher frequencies may indicate a relation to effects other than those from stop-bands.

⁴⁵ Except of the accelerometer a₇.

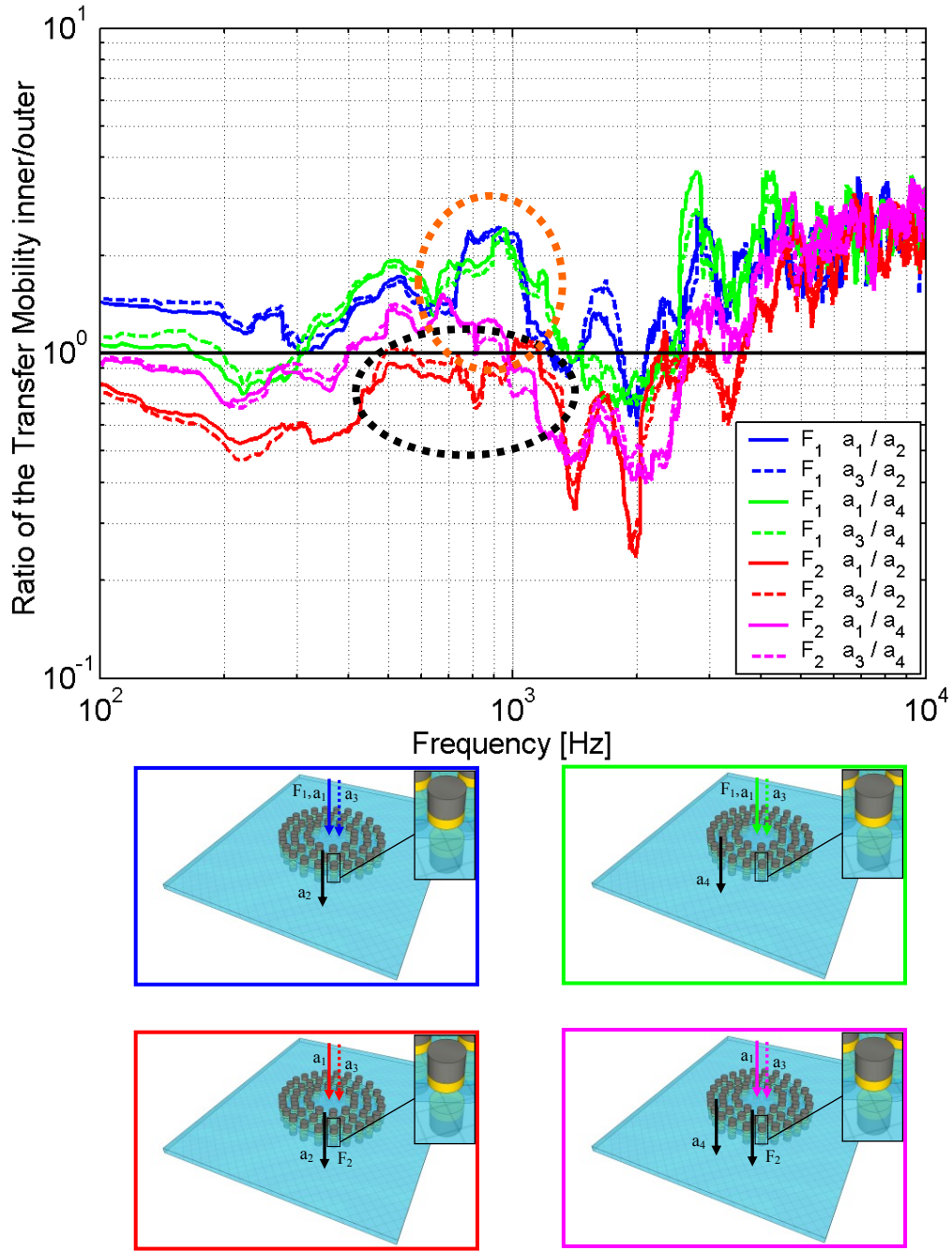


Figure 82: Smoothed ratios of the transfer mobility on different positions of the plate with elastically supported masses. The excitation happened in the center point and outside of the rings.

In a further step, additional accelerometers, located outside the rings will be considered (orange dotted circle of Figure 83). In the frequency range between 400 Hz to about 1 kHz, all vibration levels are higher than those outside the rings even when the plate is excited outside the rings.

Including the results of Figure 82, 7 of 8 test point positions underline the assumption of resonance effects in the frequency range of about 400 Hz to 1 kHz, which result in reduced bending wave vibrations within the ring.

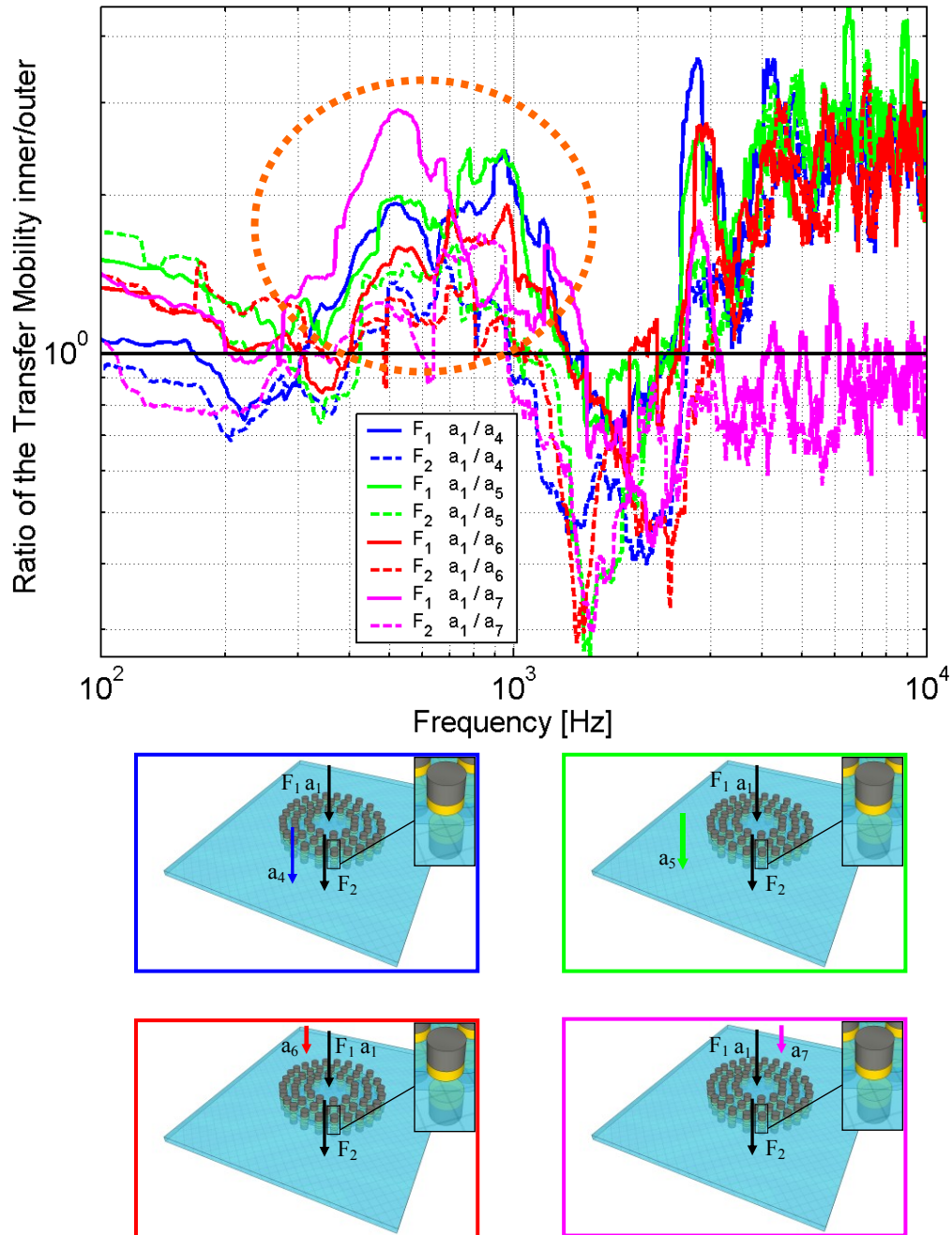


Figure 83: Smoothed ratios of the transfer mobility on different positions of the plate with elastically supported masses. The excitation happened in the center point and outside of the rings.

However, in a higher frequency range between 1 and 3 kHz the opposite behaviour can be observed. Almost all curves show an increased vibration level outside the rings (Figure 82 and Figure 83).

At frequencies higher than 3 kHz, all curves (except the magenta ones of Figure 83, a_7) show increased vibration levels. As discussed, it was not expected that stop-band influences would occur at the plate with elastically supported masses in this frequency region, as the masses should be decoupled above the resonances of the spring-mass systems. Therefore, this observation at higher frequencies might be related to the increased weight of the plate with inserts.

In the following section all of these observed effects are summarised.

8.4 SUMMARY OF THE MEASUREMENTS ON A THIN, FINITE PLATE

All these observations on a finite plate show that the measurements are accompanied by much scattering and many uncertainties. The results are often overlapped by several side conditions that are neither easy to detail nor to distinguish. The impact of having reflecting boundaries and the effects of additional masses on the entire plate increase the risk of scattering effects.

Nevertheless, some of the measurement results indicate that the radial distances of the rings of masses or the resonances of elastically supported masses do have a reflecting impact onto propagating bending waves, which were excited in the center of the plate or outside the rings. At these measurement results, the transfer mobility shows attenuation within the rings at or close to the expected stop-band frequency or resonances.

On the other hand, none of these measurements on the finite plate really prove an influence from stop-bands or resonances. Alone, bonding some additional masses onto a plate significantly changes the vibrations. All results, which are assigned to be related to stop-band or resonant impacts, could be accidentally determined conclusions. Even a direct comparison with a pure plate will be superimposed with the unknown influence of the additional masses, which change the entire vibrational behaviour.

Furthermore, the modal behaviour of this finite plate might have a large impact to the results as the positions of the forces and accelerometers possibly match with nodes and anti-nodes of the mode pattern.

To achieve real proof, a much larger plate with highly damped boundaries should be used. Furthermore, several measurements with the rings of circles shifted to several positions on the plate should be applied. If, accordingly, the vibrations within the circles were measured with higher amplitude compared to outside the rings - and if these were independent of the excitation point - we could be closer to an approval.

However, there are tendencies that resonances and stop-band-effects exist with the measurement set-up used.

9 CONCLUDING REMARKS

The effects of periodically and non-equally distributed inserts in a wave guide have been studied.

Calculations and measurements in a wooden beam have shown that stop- and pass-bands appear when steel cylinders are evenly distributed in the neutral layer, but they vanish when the masses are coated with rubber. Instead, the resonance of the spring-mass systems plays a dominant role in attenuation. The transfer mobility reveals a pronounced trough, and it is possible to broaden and move the attenuation in frequency by changing the stiffnesses.

If resonances coincide with a stop-band, attenuation is reduced and new effects have been investigated when the inserts are in addition displaced from the neutral layer.

Numerical calculations on a half-infinite homogeneous plate with variations of embedded masses, or spring-masses demonstrate similar features as those found for bending wave propagation in beams with embedded inserts.

Stop- and pass-bands arise if pure masses are periodically distributed. To exhibit the features observed for beams, the masses embedded in a plate must be organised into arcs shadowing the response point from the source. The larger the distances of the inserts, the lower the frequency of the first stop-band is. The attenuation in stop-band increases in amplitude with the number of masses. In the two-dimensional case of a plate, the band-width becomes broader than for a beam because of scattering effects, which make the bending waves take differing, extended paths through the net of inserts. Even for the inserts placed along the connecting line between source and receiver can attenuation at low frequencies be achieved.

If the masses are coated with rubber, similar effects as those observed for the beam appear. Below the resonances of the inserts, the transfer mobility behaves as if the inserts were pure masses, and stop-bands appear. For the range in which the inserts are resonant, the higher the centre frequency, the bigger the attenuation is. Also, inserts do not affect propagating bending waves above their highest resonance frequency.

Based on observations, it is suggested to combine the effects of periodically distributed masses with resonantly reacting spring-mass inserts. It is observed that it is possible to widen the range of attenuation at low and high frequencies by distributing inserts in various alternating ways within circular arcs around the excitation point. The resonances are tuned to a frequency band adjacent to the first stop- and pass-bands. Since the drop in attenuation is limited to the removal of every second mass, a replacement with corresponding spring-masses, which yields a broadened band of attenuation, is suggested.

Measurement results on a finite plate with rigid or flexible supports - ordered in circles and attached to both sides of the plate - indicate that propagating bending waves are shadowed in the frequency ranges of stop-bands or resonances. However, these measurements on a finite plate cannot be used for any kind of approval, as the

attachment of masses very likely significantly changes the entire vibration behaviour of the plate and overlay any other effects.

Nevertheless, this work demonstrates various possibilities for reducing the bending wave propagation on beams and plates that have highly damped ends or boundaries without markedly increasing the total mass or substantially altering other properties.

Furthermore, based on the obtained 1-D and 2-D numerical results and the experimental findings on the beam, it can be assumed that the methods shown herein allow a practical application to isolate bending waves even on finite panels, such as doors and walls.

10 OUTLOOK

According to the effects shown in this work, there are options available that make it interesting for further investigations:

- It could have been noticed that variation at the measurements with the beams is very likely related to non-isotropic conditions and torsion drilled beams. Thus, a future step could be the corroboration of the described effects using isotropic material on a beam.
- In the observations of this work, moment reactions come along with a reduced attenuation in stop-bands and resonances. Thus, instead of using cylindrical inserts, which are embedded in the neutral layer of a beam or attached to both sides of a plate, rubber-coated spheres are suggested. These can be embedded in the neutral layer and fully covered by the isotropic material without significantly changing necessary mechanical parameters.
- As shown in the numerical and experimental study on beams, the original idea of reducing the vibrations with some inserts looks promising. However, by only using embedded masses, their distances need to be too large for making stop-bands effective in the interesting frequency range. But, further investigation with rubber-coated spheres embedded in the neutral layer of a beam might allow for an adjustment at lower frequency ranges. The unknown size will be the impact of finite conditions at beams, which was not investigated in this work. However, reflections in the evenly distributed spring-mass systems even occur in beams with finite ends. Thus, excited beams or bars, which are clamped or open at their ends, are recommended to be tested with embedded spring-mass systems.
- It will be a challenge to reduce vibrations on finite plates such as lightweight structures (e.g., cabin doors in a ship). Main modes of excitation of bending waves are related to airborne sound on the entire surface or to structure-borne sound over the boundaries. Any additional inserts will change the bending-wave propagation on a finite plate due to the increased masses. According to the measurement results in this work on a finite plate, a satisfactory impact of stop-bands or resonances is difficult to approve, and, accordingly, it is uncertain if it really exists. Therefore, additional measurements with a larger plate and damped boundaries are necessary to verify the stop-band and resonance impact on plates. Several measurements with the rings of circles shifted to different positions on the plate should be applied.
- Although not explicitly shown in this work, numerical analyses also support the possibility of influencing the directivity of the wave field with defined patterns of the distributed inserts. It is worth checking whether smart distributions of inserts lead to bending waves that propagate mainly to a highly damped region within the finite plate, for instance. The overall vibrations might be larger damped than without such directing patterns.

For sure, there exist many other ideas to be researched in conjunction with the effects presented in this work. That means the possibilities for resonant inserts are far from exhausted, and much work remains to clarify the associated effects.

Finally, it should be stated that the basic observations with the mixture of masses and rubber-coated masses, distributed in several ways in different structures, will hopefully animate other researchers to continue in this field.

11 ATTACHMENTS

11.1 ADDITIONAL PARAMETER STUDY OF AN INFINITE HOMOGENOUS BEAM WITH INSERTS

Following parameters are additionally investigated. These are useful for a better understanding of the behaviour of the transfer mobility and in addition of the understanding of the measurements.

- η_{beam} (loss factor of the beam)
- E_{beam} (complex Young's modulus)
- η_{spring} (loss factor of the rubber coating)
- m_{mass} (mass of the inserts)

11.1.1 LOSS FACTOR OF THE BEAM AND YOUNG'S MODULUS

In Figure 84 the influence of the loss factor of the beam η_{beam} and the Young's modulus E_{beam} is depicted. While an increased beam loss factor only changes the magnitude, the E-Module has an impact on the frequency of the stop-bands (and the pass-bands). The higher the Young's modulus, the more the stop-bands of a beam with pure masses embedded are shifted to higher frequencies. The beams used for the measurements in this work (see section 5.2) are neither ideally isotropic nor homogeneous. Therefore the likelihood that a shifted stop-band frequency is within the beam parameters needs to be considered.

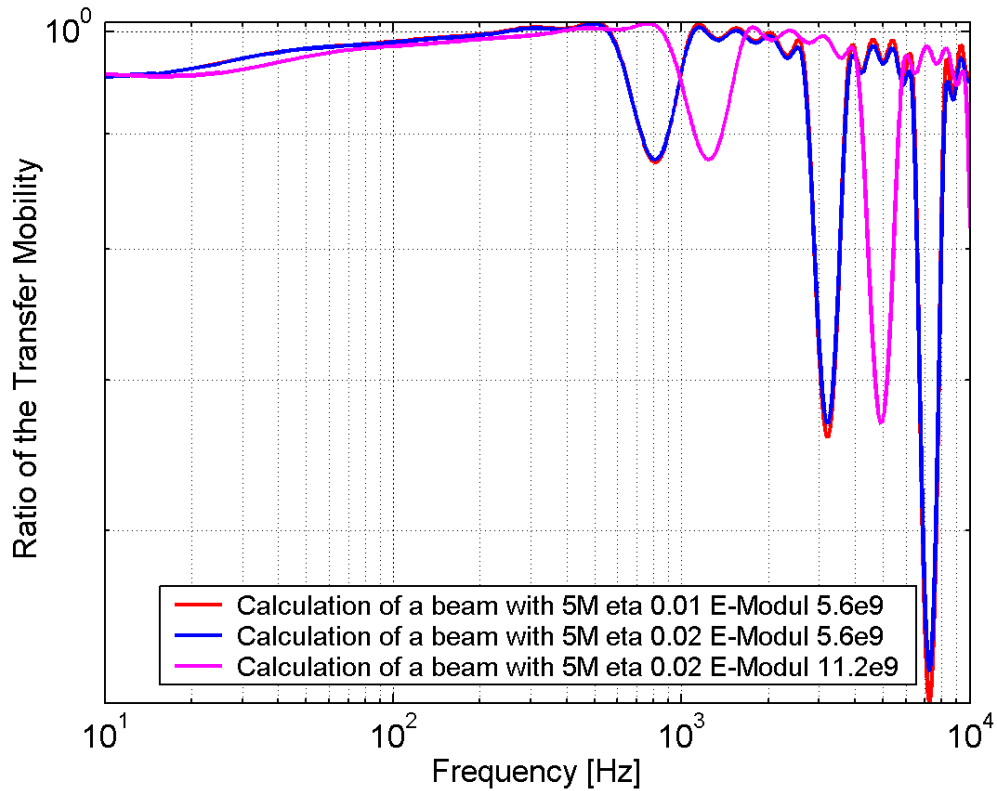


Figure 84: Calculated transfer mobilities of a beam with 5 masses in distances of 0.2m with a doubled loss factor of the beam η_{beam} and a doubled Young's modulus E_{beam} . An increased loss factor leads to a slightly higher attenuation in the stop-bands and a slightly reduced attenuation between the stop-bands. An increased Young's modulus affects the frequency range of the stop-bands.

11.1.2 LOSS FACTOR OF THE RUBBER COATING

In Figure 85 the damping factor of the complex spring stiffness has been increased by a factor of 10 (from η_{spring} 0.02 to 0.2). As expected for spring-mass systems the attenuation in the resonance is decreased, but with broader side banks. An interesting effect can be seen in the frequency range at the 2nd stop-and-pass-band, which shows a lower reduction of the spring-mass system with higher damping factor of the spring. The influence of the 2nd stop-band, which overlaps at the resonances, seems to be reduced with higher damping factor of the spring. However, a shifted resonance frequency by a changed damping factor of the spring is not visible.

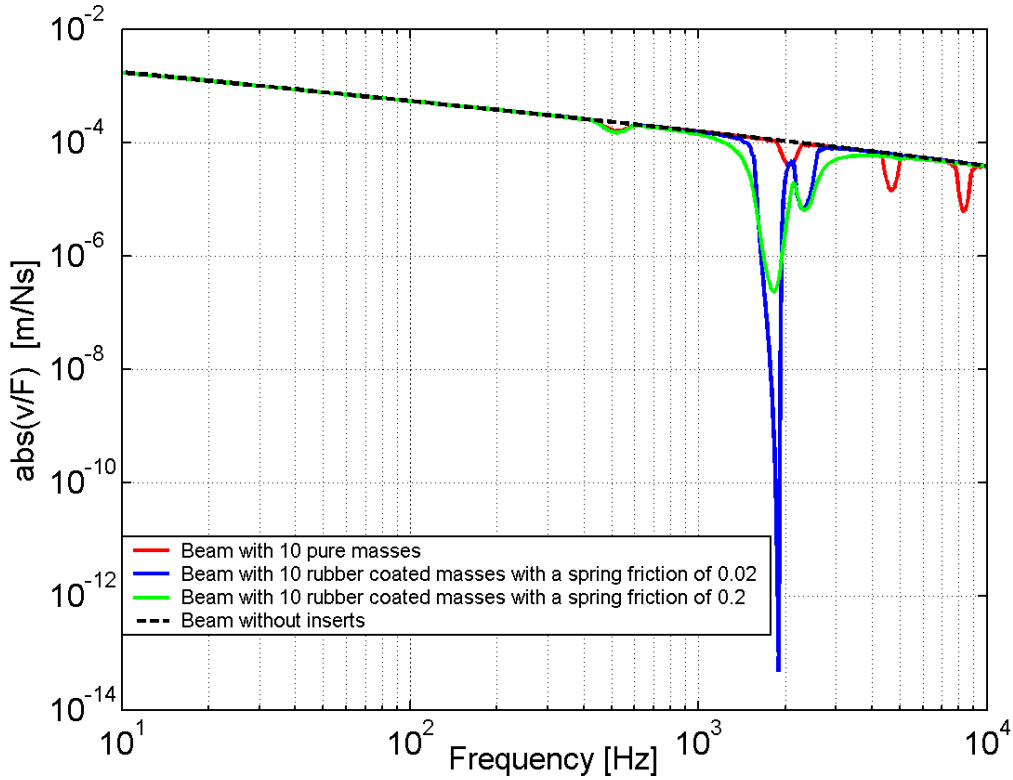


Figure 85: Transfer mobility of an infinite beam with 10 pure masses and 10 rubber-coated masses with different damping factors of the complex spring stiffness. All of them are embedded in the neutral layer.

Furthermore, it is also of interest, which damping factor of the spring are to be expected at spring-mass systems embedded in the real beams. According to the pre-test measurements (sub-section 5.1.1, Figure 34) the damping factor of the spring of the beam piece with the high stiffened rubber-coated masses at a Shore hardness of 80 ShA will be determined.

Therefore, the Nyquist plot of the beam piece with the high stiffened rubber-coated masses at a Shore hardness of 80 ShA has been used (

Figure 86). By calculating the poly-fitted curve of the circle, which includes the resonance of the mass- and spring-system, the damping factor of the spring can be evaluated with Karl et al. [45] or Möser [74] involving geometrical equations from Bronstein [9]:

$$\eta_{spring} = \frac{\omega_2^2 - \omega_1^2}{2\omega_0 \left[\omega_2 \tan\left(\frac{\alpha_2}{2}\right) + \omega_1 \tan\left(\frac{\alpha_1}{2}\right) \right]} \quad (43)$$

Hereby, α_1 and α_2 are the angles of the resonance frequency ω_0 to the center point and the frequencies ω_1 and ω_2 . The value of $\eta_{Spring, meas} = 0.124$ of these measurements is

much higher than the values chosen in most of the calculations ($\eta_{\text{Spring,calc}} = 0.02$). In the calculations, each mass-and spring system has been clearly defined, while the pre-test measurements show a scattering of the attenuations in the resonances (Figure 36), which can be anticipated in the beams with distributed spring-mass systems as well.

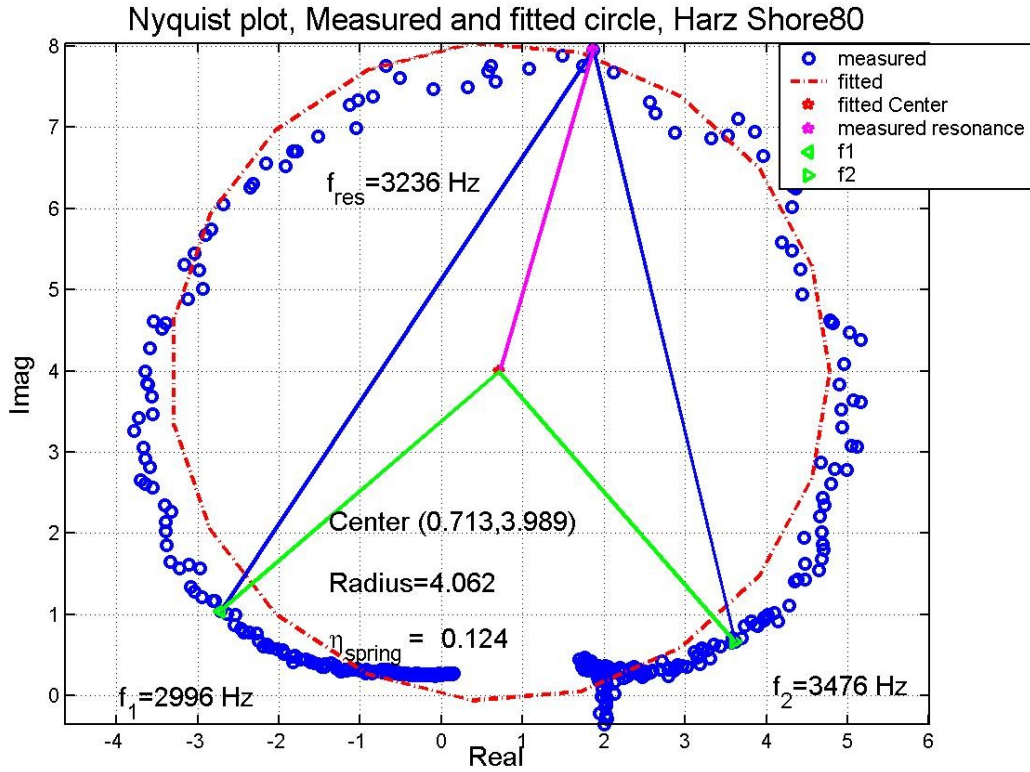


Figure 86: Nyquist plot of a measured beam piece with a high stiffened rubber-coated mass (80 ShA). The real and imaginary parts are calculated with the cross spectra of the accelerometer on the top of the beam to the mean of the accelerometers on both sides of the rubber-coated mass. The fitted circle at the resonance of the measured transfer mobility succeed in the damping factor of the spring $\eta_{\text{spring}} = 0.124$, using equation (43). The resonance frequency is 3.24 kHz.

11.1.3 IMPACT OF THE WEIGHT OF MASSES ONTO THE ATTENUATIONS IN THE TRANSFER MOBILITY

In the following plot the weight of the masses of a beam with 10 equally distributed masses has been reduced by a factor of 2. As expected, the attenuations of the transfer mobility are reduced while stop-band frequencies remain the same (Figure 87).

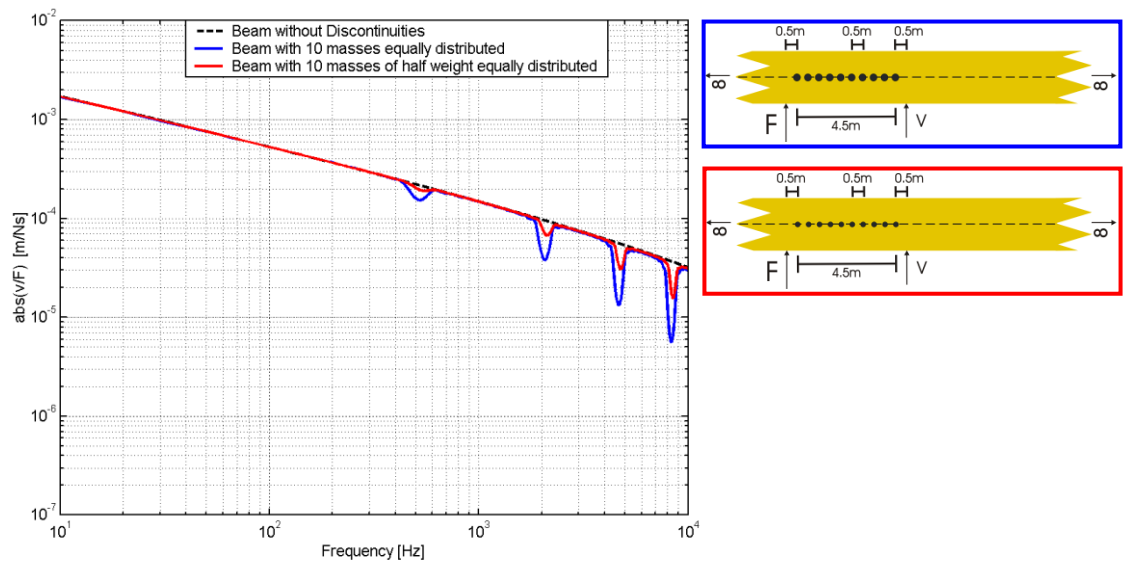


Figure 87: Transfer mobility of an infinite beam with 10 embedded masses in the neutral layer of default weight and 10 masses with half of the weight. As depicted in the sketches on the right side 10 masses are equally distributed over a length of 4.5m.

11.2 ERROR INVESTIGATION

The accuracy of numerical investigation is limited at high frequencies by the employment of the simple bending wave equation. This has to be taken into consideration for the results at higher frequencies.

In addition, the comparison of the calculations and measurements for a beam with pure masses show that the attenuation of first appearing stop-band do not agree in magnitude. A reason therefore can be found in the use of a wooden beam. Wood is not isotropic and thus some parameters such as the Young's modulus or the loss factor are not the same over the entire length of the beam. It is also not clear to what extend the bending waves are converted into longitudinal or torsional waves when the former are reflected at the inserts.

Apart from the usual measurement errors, e.g. calibration and acquisition system errors, following effects might have an influence to the results:

NUMERICAL INVESTIGATION

- In all calculations and measurements with beams, the vertical height of the beam is about $h=80\text{mm}$. The error of the simple bending wave equation from Euler-Bernoulli increases if the corresponding bending wave-length grows larger than 6 times that height ($\lambda>6h$). Thus, transferred into a frequency, all calculated results with frequencies higher than $f=2359\text{Hz}$ need to be considered under this condition.
- Furthermore, the use of an Euler-Bernoulli-beam does not consider shear stresses. That means that wave transformation from vertical bending waves to torsional, longitudinal or horizontal bending waves is not reflected in the measurement results, although scattering in the results of the measurements are very likely related to such transformations.

MEASUREMENTS ON A BEAM

- Stiffness and loss factor of the polyurethane (PUR) changes by the time.
- Non-isotropic inhomogeneous beams were used for the measurements.
- Scattering effects appear due to the sensible filling procedure of polyurethane (PUR).
- Beams in measurements are slightly screwed along the x-axis and vary in density.
- Due to the very large effort of measuring the transfer mobility of a beam, the decision was made using one of the beams with only holes as a baseline. Thus, not every beam has been measured in its form with only holes and therefore the ratios of the transfer mobilities are affected by different conditions of each beam.

MEASUREMENTS ON A PLATE

- Measurements of the plate with inserts stuck to both sides of the rings do not avoid moment effects, as mass heights very likely play a role. These moment reactions are even higher when masses are attached to the rubber.
- As previously mentioned, the effects of additional masses and reflections at the boundaries very likely supersede any other effects and therefore possibly falsify conclusions.

12 REFERENCES

- [1] Alagoz, S., A sonic crystal diode implementation with a triangular scatterer matrix, *Applied Acoustics* 76, 402–406, 2014
- [2] Alsaif, K. and Foda, M., Vibration suppression of a beam structure by intermediate masses and springs, *Journal of Sound and Vibration*, 256(4), 629-645, 2002
- [3] Amabili, M., Pellegrini, M. Righi, F. and Vinci, F. Effect of concentrated masses with rotary inertia on vibrations of rectangular plates, *Journal of Sound and Vibration*, 295, 1- 12, 2006
- [4] Avitable, P., Experimental Mode Analysis – A simple Non-Mathematical Presentation, University of Massachusetts Lowell, Sound and Vibration, January 2001
- [5] Bansal, A., Free waves in periodically disordered systems: Natural and bounding frequencies of unsymmetric systems and normal mode localization, *Journal of Sound and Vibration*, 207(3), 365-382, 1997
- [6] Blanc, A., Control of Sound Radiation from Structures with Periodic Smart Skins, Thesis submitted to the Faculty of the Virginia Polytechnic Institute and State University, July 2001
- [7] Bouzit, D. and Pierre, C., An experimental investigation of vibrational localisation in disordered multi-span beams, *Journal of Sound and Vibration*, 187(4), 649-669, 1995
- [8] Brillouin, L., Wave propagation in periodic structures, Electric filters, and crystal lattices, 2nd edition, Dover publications, McGraw-Hill Book Company, 1946
- [9] Bronstein, I., Semendjajew, K., Musiol, G. and Mühlig, H., Taschenbuch der Mathematik, Harri Deutsch Verlag, 2000
- [10] Chen, S., Wang, G., Wen, G., Wen, X., Wave propagation and attenuation in plates with periodic arrays of shunted piezo-patches, *Journal of Sound and Vibration*, 332, 1520–1532, 2013
- [11] Cheng, Z. and Shi, Z., Vibration attenuation properties of periodic rubber concrete panels, *Construction and Building Materials*, 50, 257–265, 2014
- [12] Cremer, L. and Heckl, M., Körperschall, 2nd Edition, Springer, Heidelberg, New York, 1995
- [13] Cremer, L. and Leilich, H., Arch. d. elektr. Übertr., Zur Theorie der Biegekettenleiter, 7(6), 261, 1953
- [14] Dayou, J., Global control of structural vibration using multiple-tuned tunable vibration neutralizers, *Journal of Sound and Vibration*, 258(2), 345-357, 2002

- [15] Ding, L., Zhu, H. and Yin, T. Wave propagation in a periodic elastic-piezoelectric axial-bending coupled beam *Journal of Sound and Vibration*, 332, 6377–6388, 2013
- [16] Dobson, D. C., An efficient method for band structure calculations in 2D photonic crystals, *Journal of computational physics*, 149, 363-376, 1999
- [17] Dyer, I., Moment impedances of plates, *Journal of Acoustic Society of America*, Volume 32, Number 10, 1960
- [18] Dyer, I., Response of plates to a decaying and convecting random pressure field, *Journal of Acoustic Society of America*, Volume 31, Number 7, 1959
- [19] Ewins, D., *Theory and Practice, Journal of Modal Testing*, Research Studies Press Ltd., Letchworth, England, 1986
- [20] El-Raheb, M. and Wagner, P., Effects of end cap and aspect ratio on transmission of sound across a truss-like periodic double panel, *Journal of Sound and Vibration*, 250(2), 299-322, 2002
- [21] Friis, L. and Ohlrich, M., Coupling of flexural and longitudinal wave motion in a periodic structure with asymmetrically arranged transverse beams, *Journal of the Acoustical Society of America*, 118, 3010, 2005
- [22] Gao, Q., Wu, F., Zhang, H., Zhong, W., Howson, W. and Williams, F., Exact solutions for dynamic response of a periodic spring and mass structure, *Journal of Sound and Vibration*, 331, 1183–1190, 2012
- [23] Gei, M., Wave propagation in quasiperiodic structures: stop/pass band distribution and prestress effects, *International Journal of Solids and Structures*, 47, 3067–3075, 2010
- [24] Gürgöze, M., Alternative formulations of the characteristic equation of a Bernoulli-Euler beam to which several viscously damped spring-mass systems are attached in-span, *Journal of Sound and Vibration*, 223(4), 666-677, 1999
- [25] Gürgöze, M., Longitudinal vibrations of rods coupled by several spring-mass systems, *Journal of Sound and Vibration*, 234(5), 895-905, 2000
- [26] Gürgöze, M., Proportionally damped systems subjected to damping modifications by several viscous dampers, *Journal of Sound and Vibration*, 255(2), 407-412, 2002
- [27] Gürgöze, M., Viscously damped mechanical systems subject to several constraint equations, *Journal of Sound and Vibration*, 229(5), 1264-1268, 2000
- [28] Gürgöze, M., On the alternative formulations of the frequency equation of a Bernoulli-Euler beam to which several spring-mass systems are attached in span, *Journal of Sound and Vibration*, 217(3), 585-595, 1998

- [29] Gürgöze, M., On the Eigenfrequencies of a cantilever beam with attached tip mass and a spring-mass system, *Journal of Sound and Vibration*, 190(2), 149-162, 1996
- [30] Hawwa, M., Reflection of flexural waves in geometrically periodic beams, *Journal of Sound and Vibration*, 199(3), 453-461, 1997
- [31] Heckl, M., Investigation on the Vibration of Grillages and Simple Beam Structures, *Journal of the Acoustical Society of America*, Volume 36, Number 7, May 1964
- [32] Heckl, M., Körperschallausbreitung auf Balken mit vielen Störstellen, *Acustica*, Vol. 81, 1995
- [33] Heckl, M., Körperschalldämpfung bei Balken durch seitlich angebrachte Widerstände, *Acustica*, 45(4), 1980
- [34] Heckl, M., Wave propagation on beam-plate systems, *Journal of the Acoustical Society of America*, Volume 33, Number 5, May 1961
- [35] Heckl, M. (Maria), Coupled waves on a periodically supported Timoshenko beam, *Journal of Sound and Vibration*, 252(5), 849-882, 2002
- [36] Hettler, S., Akustische Modellierung von Leichtbauteilen mit internen Resonatoren, *DAGA*, 617-618, 2005
- [37] Hettler, S., Leistner P. and Thompson, D., A modal approach to lightweight partitions with internal resonators, *Forum Acusticum*, 2027-2032, 2005
- [38] Hettler, S., Vibroacoustic behaviour of sandwich structures with spatially distributed resonators, PhD-Thesis, Lehrstuhl für Bauphysik der Universität Stuttgart, Fraunhofer Institut für Bauphysik, Stuttgart, 2013
- [39] Hiersekorn, M., Delsanto, P. Batra, N. and Matic, P., Modelling and simulation of acoustic wave propagation in locally resonant sonic materials, Special session: ultrasonic modelling - invited papers, 2003
- [40] Hodges, C., Woodhouse, J., Vibration isolation from irregularity in a nearly periodic structure: Theory and measurements, *Journal of Sound and Vibration*, 74(3), 894-905, 1983
- [41] Howe, M. and Heckl, M., Sound radiation from plates with density and stiffness discontinuities, *Journal of Sound and Vibration*, Volume 21, Issue 2, Pages 193-203, 1972
- [42] Ibrahim, R., Recent advances in nonlinear passive vibration isolators, *Journal of Sound and Vibration*, 314, 371-452, 2008
- [43] Irretier, H., Schwingungstechnik, Script, Institut für Mechanik, Universität Kassel, 6. Auflage 2006

- [44] Jolly, M. and Sun, J., Passive tuned vibration absorbers for sound radiation reduction from vibrating panels, *Journal of Sound and Vibration*, 191(4), 577-583, 1996
- [45] Karl, L., Haegemann, W., Pyl, L. and Degrande, G., Measurement of material damping with bender elements in triaxial cell, Department of Civil Engineering, Structural Mechanics Division, K.U. Leuven, Belgium, CiteSeer_x, 2008
- [46] Karabutov, A., Kozhusko, V., Pelivanov, I. and Mityurich, G., Interference of opposing longitudinal acoustic waves in an isotropic absorbing plate and a periodic structure with defects, *Acoustical physics*, Vol. 47, No. 6, 721-726, 2001
- [47] Kessissoglou, N. J., An analytical and experimental investigation on active control of the flexural wave transmission in a simply supported ribbed plate, *Journal of Sound and Vibration*, 240(1), 73-85, 2001
- [48] Kohrs, T. and Petersson, B.A.T., Wave beaming and wave propagation in lightweight plates with truss-like cores, *Journal of Sound and Vibration*, 321, 137-165, 2009
- [49] Kushwaha, M. and Djafari-Rouhani, D., Sonic stop-bands for periodic arrays of metallic rods: Honeycomb structure, *Journal of Sound and Vibration*, 218(4), 697-709, 1998
- [50] Langley, R. S., A variational principle for periodic structures, *Journal of Sound and Vibration*, 135(1), 135-142, 1989
- [51] Langley, R., The frequency band-averaged wave transmission coefficient of a periodic structure, *Journal of the Acoustical Society of America*, 100(1), 304-311, 1996
- [52] Langley, R. and Smith, J., Statistical energy analysis of periodically stiffened damped plate structures, *Journal of Sound and Vibration*, 208(3), 407-426, 1997
- [53] Lee, J.-H., Kim, J., Analysis of Sound transmission through periodically stiffened panels by space-harmonic expansion method, *Journal of Sound and Vibration*, 251(2), 349-366, 2002
- [54] Lin, H. and Tsai, Y., Free vibration analysis of a uniform multi-span beam carrying multiple spring-mass systems, *Journal of sound and vibration*, 302, 442-456, 2007
- [55] Liu, Z., Zhang, X., Mao, Y., Zhu, Y., Yang, Z., Chan, C. and Sheng, P., Locally Resonant Sonic Materials, *Science*, Vol 289, 1734-1736, 2000
- [56] Ljunggren, S., Line mobilities of infinite plates, *Journal of the Acoustical Society of America*, 86(4), 1419-1431, 1989

- [57] Lucklumaa, R., Zubtsova, M., Ke, M., Henningc, B. and Hempeld, U., 2D Phononic Crystal Sensor with Normal Incidence of Sound, *Procedia Engineering*, 25, 787 – 790, 2011
- [58] Luongo, A. and Romeo, F., Real wave vectors for dynamic analysis of periodic structures, *Journal of Sound and Vibration*, Volume 279, issue 1-2, 309-325, 2005
- [59] Lyapunov, V., Flexural-wave propagation in a plate with periodic obstructions, *Soviet Physics-Acoustics*, Vol. 18, No. 2, 1972
- [60] Ma, C., Parker, R., and Yellen, B., Optimization of an acoustic rectifier for uni-directional wave propagation in periodic mass–spring lattices, *Journal of Sound and Vibration*, 332, 4876–4894, 2013
- [61] Mace, B. R., Periodically stiffened Fluid-loaded plates, II: response to line and point forces, *Journal of Sound and Vibration*, 73(4), 487-504, 1980
- [62] Mangaraju, V. and Sonti, V. Wave attenuation in periodic three-layered beams: analytical and FEM study, *Journal of Sound and Vibration*, 276, 541–570, 2004
- [63] Marathe, A. and Chatterjee, A., Wave attenuation in nonlinear periodic structures using harmonic balance and multiple scales, *Journal of Sound and Vibration*, February 16, 2005
- [64] Mangaraju, V. and Sonti, V. Wave attenuation in periodic three-layered beams: analytical and FEM study, *Journal of Sound and Vibration*, 276, 541–570, 2004
- [65] Martínez-Rodrigo, M. and Museros, P., Optimal design of passive viscous dampers for controlling the resonant response of orthotropic plates under high-speed moving loads, *Journal of Sound and Vibration*, 330, 1328–1351, 2011
- [66] Martínez-Sala, R., Rubio, C., Garcia-Rafí L., Sánchez-Pérez, J., Sánchez-Pérez, E. and Llinares, J., Control of noise by trees arranged sonic crystals, *Journal of Sound and Vibration*, 291, 100-106, 2006
- [67] Maysenhölder, W., Transmission Loss of Plates with Internal Resonators Modelled by Harmonic Oscillators with Frequency Dependent Complex Mass and Spring Stiffness, *Euronoise*, Naples, paper ID: 57, 2003
- [68] Mead, D. J., A general theory of harmonic wave propagation in linear periodic systems with multiple coupling, *Journal of Sound and Vibration*, 27(2), 235-260, 1973
- [69] Mead, D. J., Free wave propagation in periodically supported infinite beams, *Journal of Sound and Vibration*, 11(2), 181-197, 1970
- [70] Mead, D. J., *Passive vibration control*, Wiley, Chichester, Weinheim, New York, Brisbane, Singapore, Toronto, 1988

- [71] Mead, D. J., Wave propagation in continuous periodic structures: Research contributions from Southampton 1964–1995, *Journal of Sound and Vibration*, 190(3), 495–524, 1996
- [72] Mermertas, V. and Gürgöze, V., Preservation of the fundamental natural frequencies of rectangular plates with mass and spring modifications, *Journal of Sound and Vibration*, 276, 440–448, 2006
- [73] Modulor-Katalog 2004, Kapitel J Modellieren, Auflage Oktober 2003
- [74] Möser, M., *Messtechnik der Akustik*, Springer, Heidelberg, New York, 2010
- [75] Möser, M. and Kropp, W., *Körperschall - Physikalische Grundlagen und technische Anwendungen*, Begründet von Lothar Cremer und Manfred Heckl, 3. aktualisierte Auflage, Springer, Heidelberg, New York, 2010
- [76] Möser, M., *Technische Akustik*, 8. aktualisierte Auflage, Springer Verlag, 2010
- [77] Muravskii, G., On frequency independent damping, *Journal of Sound and Vibration*, 274, 653–668, 2004
- [78] Newton, „Principia“, Book II, 1686
- [79] Nijman E., Simple analytical models for tough mid-frequency range problems, *Proceeding of 3rd Styrian Noise, Vibration & Harshness Congress*, 2005
- [80] Pennec, Y., Vasseur, J., Djafari-Rouhani, B., Dobrzyński, L. and Deymier, P., Two-dimensional phononic crystals: Examples and applications, *Surface Science Reports*, 65, 229–291, 2010
- [81] Pesko, F., *Schwingungen punktweise belasteter Systeme unter Berücksichtigung der Kopplung verschiedener Wellenarten*, Institut für Technische Akustik Berlin, Prof. Cremer zum 75. Geburtstag gewidmet, 1980
- [82] Petersson, B.A.T, *Advanced Noise & Vibration Control Supplement for Lectures*, Institut für Technische Akustik, TU Berlin, 2001
- [83] Petersson, B.A.T, *Influence of structural periodicity perturbations on transfer mobilities*, TNO-report, TPD-HAG-RPT-950093, 1995
- [84] Picó, R., Sánchez-Morcillo, V., Pérez-Arjona, I., and Staliunas, K., Spatial filtering of sound beams by sonic crystals, *Applied Acoustics*, 73, 302–306, 2012
- [85] Ramsey, K., *Effective Measurements for Structural Dynamics Testing*, *Sound and Vibration*, 24-35, November 1975

-
- [86] Ratle, A. and Berry, A. Use of genetic algorithms for the vibroacoustic optimization of a plate carrying point-masses, *Journal of Acoustic Society of America*, 104(6), 3385-3397, 1998
- [87] Romero-García, V., Krynkin, A., Garcia-Raffi, L., Umnova, O. and Sánchez-Pérez, J., Multi-resonant scatterers in sonic crystals: Locally multi-resonant acoustic metamaterial, *Journal of Sound and Vibration*, 332, 184–198, 2013
- [88] Schwan, L. and Boutin, C., Unconventional wave reflection due to “resonant surface”, *Wave Motion* 50, 852–868, 2013
- [89] Strasberg, M. and Feit, D., Vibration damping of large structures induced by attached small resonant structures, *Journal of Acoustic Society of America*, 99(1), 335-344, 1996
- [90] Stütz, M., Wellenausbreitung in periodischen Systemen, Studienarbeit am Institut für Technische Akustik der TU Berlin, 2005
- [91] Thompson, D., A continuous damped vibration absorber to reduce broad-band wave propagation in beams, *Journal of Sound and Vibration*, 311, 824–842, 2008
- [92] Thompson, D., The theory of a continuous damped vibration absorber to reduce broad-band wave propagation in beams, ISVR Technical Memorandum No 968, 2007
- [93] Thompson, D., Mechanical impedances for thin plates, *Journal of Acoustic Society of America*, Volume 32, 10, 1302 – 1305, 1960
- [94] Waag, U, Schneider, L., Stephani, G, Gerick, A and Bernhard, E. Metallische Hohlkugelstrukturen – Eigenschaftspotential zur Schall- und Energieabsorption, VDI-Berichte Nr. 1595, 2001
- [95] Wang, G., Wen, J., Wen, X., Yu, D. and Liu, Y. Locally resonant forbidden bands of flexural elastic wave in slender beams, 12th International Congress on Sound and Vibration, 2005
- [96] Wang, G., Quasi-one-dimensional periodic structure with locally resonant band gap, *Journal of applied mechanics*, Vol. 73, 167, 2006
- [97] Wang, Y. The transient dynamics of a moving accelerating/decelerating mass traveling on a periodic-array non-homogeneous composite beam, *European Journal of Mechanics A/Solids*, 28, 827–840, 2009
- [98] Weith, W. and Petersson, B.A.T., Bending wave propagation in plates with embedded resonant inserts, 9th International Conference on Recent Advances in Structural Dynamics, No. 104, Southampton, Proceedings 2006
- [99] Weith, W. and Petersson, B.A.T., Körperschall-Reduktion in periodischen Mikrostruktur-Kompositen, DAGA 2005

-
- [100] Weith, W. and Petersson, B.A.T., Manipulation von Biegewellen in Platten mit anti-resonanten Mikro-Struktur-Kompositen, DAGA 2006
- [101] Weith, W. and Petersson, B.A.T., Periodic effects of resonant inserts in microstructure-composites, Proceedings of Noise and Vibration: Emerging Methods (NOVEM), 2005
- [102] Weith, W. and Petersson, B.A.T., Wave propagation in periodic microstructure composites. Proceed. 11th International Congress of Sound & Vibration, 3637-3644, 2004
- [103] Wu, J. and Chou, H., A new approach for determining the natural frequencies and mode shapes of a uniform beam carrying any number of sprung masses, Journal of Sound and Vibration, 229(3), 451-468, 1999
- [104] Wu, J. and Chen, D., Dynamic Analysis of a uniform cantilever beam carrying a number of elastically mounted point masses with dampers, Journal of Sound and Vibration, 229(3), 549-578, 2000
- [105] Xiao, Y. Wen, J. and Wen, X., Broadband locally resonant beams containing multiple periodic arrays of attached resonators, Physics Letters, A 376, 1384–1390, 2012
- [106] Xiao, Y. Wen, J., Yu, D., Wen, X., Flexural wave propagation in beams with periodically attached vibration absorbers: Band-gap behavior and band formation mechanisms Journal of Sound and Vibration, 332, 867–893, 2013
- [107] Xu, M., Zhang, X. and Zhang, W., Space-harmonic analysis of input power flow in a periodically stiffened shell filled with fluid, Journal of Sound and Vibration, 222(4), 531-546, 1999
- [108] Yu, D., Liu, Y. Zhao, H., Wang, G. and Qiu, J., Flexural vibration band gaps in Euler-Bernoulli beams with locally resonant structures with two degrees of freedom, Physical Review B 73, 064301, 2006
- [109] Yu, D., Wen, J., Shen, H., Xiao, Y. and Wen, X., Propagation of flexural wave in periodic beam on elastic foundations, Physics Letters, A 376, 626–630, 2012
- [110] Yuan, B., Humphrey, V., Wen, J. and Wen, X., On the coupling of resonance and Bragg scattering effects in three-dimensional locally resonant sonic materials, Ultrasonics, 53, 1332–1343, 2013
- [111] Yun, Y. and Mak, C., Experimental study of coupled vibration in a finite periodic dual-layered structure with transverse connection, Applied Acoustics, 72, 287–296, 2011
- [112] Zheng, H. and Bert, C., A differential quadrature analysis of vibration for rectangular stiffened plates, Journal of Sound and Vibration, 241(2), 247-252, 2001

- [113] Zhang, V. Lefebvre, J. and Gryba, T., Resonant transmission in stop bands of acoustic waves in periodic structures, *Ultrasonics*, 44, e899–e904, 2006
- [114] Zhang, X. and Liu, T. G., Vibrational power flow analysis of damaged beam structures, *Journal of Sound and Vibration*, 242(1), 59-68, 2001
- [115] Zoues, R. and Rand, R. Transition curves for the quasi-periodic Mathieu equation, *Journal of applied mathematics*, Society for Industrial and Applied Mathematics, Vol. 58, No. 4, pp. 1094-1115, 1998
- [116] Zubtsov, M., Lucklum, R., Ke, M., Oseev, A., Grundmann, R., Henning, B. and Hempel, U., 2D phononic crystal sensor with normal incidence of sound, *Sensors and Actuators, A* 186, 118– 124, 2012

13 LIST OF TABLES

Table 1: The distances from mass to mass as depicted in Figure 15	35
Table 2: Calculated frequencies of the first four stop-bands for beams with different distances from mass to mass.....	38
Table 3: Six configurations with beams and inserts have been measured	62
Table 4: The first four calculated stop-bands on the plate with masses are shown, which are distributed in circles around the center with radial distances of 50 mm to each other.	119
Table 5: Measured weights of the plate and the inserts.	122

14 LIST OF FIGURES

Figure 1: Infinite beam with evenly distributed rigid supports.	24
Figure 2: Infinite beam with evenly distributed embedded masses within the beam (in this case out of the neutral layer).	24
Figure 3: Infinite beam with evenly distributed embedded masses in the neutral layer.	25
Figure 4: Infinite beam with evenly distributed rubber-coated masses in the neutral layer.	25
Figure 5: Infinite beam with evenly distributed rubber-coated masses with increasing stiffnesses in the neutral layer.	25
Figure 6: Infinite beam with evenly distributed rubber-coated masses with increasing stiffnesses displaced from the neutral layer.	26
Figure 7: Embedded masses in the neutral layer.	29
Figure 8: Rubber-coated balls in the neutral layer.	30
Figure 9: Masses out of the neutral layer.	30
Figure 10: Rubber-coated balls at a distance from the neutral layer.	31
Figure 11: An infinite homogenous slender beam with inserts in the neutral layer.	32
Figure 12: Transfer mobility of an infinite beam with 5 embedded masses in the neutral layer.	33
Figure 13: Transfer mobility of an infinite beam with 10 embedded masses in the neutral layer.	34
Figure 14: Transfer mobility of an infinite beam with 20 embedded masses in the neutral layer.	34
Figure 15: Transfer mobility of an infinite beam with 5, 10 and 20 embedded masses in the neutral layer.	35
Figure 16: Transfer mobility of an infinite beam with 5, 10 and 20 embedded masses in the neutral layer with all the same distances.	36
Figure 17: Transfer mobility of an infinite beam with rubber-coated masses embedded in the neutral layer.	39

LIST OF FIGURES

Figure 18: Transfer mobility of an infinite beam with 5, 10 and 20 rubber-coated masses embedded in the neutral layer.	40
Figure 19: Transfer mobility of an infinite beam with 5 rubber-coated masses with variable masses and stiffnesses embedded in the neutral layer.	41
Figure 20: Transfer mobility of an infinite beam with 20 pure masses and 20 rubber-coated masses embedded in the neutral layer.....	42
Figure 21: Transfer mobility of an infinite beam with 20 pure masses and 20 rubber-coated masses embedded in the neutral layer.....	43
Figure 22: Transfer mobility of infinite beams with 10 pure masses and 10 rubber-coated masses embedded in the neutral layer.....	44
Figure 23: Transfer mobility of infinite beams with 10 pure masses and 10 rubber-coated masses with very low stiffnesses embedded in the neutral layer.	45
Figure 24: Transfer mobility of infinite beams with 10 pure masses and 10 rubber-coated masses with very high stiffnesses embedded in the neutral layer.	46
Figure 25: Transfer mobility of an infinite beam with 10 pure masses embedded in and out of the neutral layer.....	47
Figure 26: Transfer mobility of an infinite beam with 20 pure masses embedded in and out of the neutral layer.....	48
Figure 27: Transfer mobility of an infinite beam with 10 and 20 pure masses embedded out of the neutral layer with distances of 0.5m to each other.	48
Figure 28: Transfer mobility of an infinite beam with 20 pure masses embedded in and out of the neutral layer.....	49
Figure 29: Transfer mobility of an infinite beam with 10 pure masses out of the neutral layer, 10 rubber-coated masses in and 10 rubber-coated masses out of the neutral layer.....	50
Figure 30: Transfer mobility of an infinite beam with 20 pure masses out of the neutral layer, 20 rubber-coated masses in and 20 rubber-coated masses out of the neutral layer.....	51
Figure 31: Transfer mobility of an infinite beam with 20 pure masses and 20 rubber-coated masses out of the neutral layer, with different equally distributed distances.....	52

LIST OF FIGURES

Figure 32: Measurement set-up with a small piece of the wooden beam, filled with a rubber-coated mass, which was vertically driven by a shaker.....	54
Figure 33: Frequency response of three beam pieces with embedded rubber-coated masses.	55
Figure 34: Three beam pieces with embedded rubber-coated masses. The Nyquist plot shows the real and imaginary part of the mean of the accelerations on the sides of the masses to the acceleration of the top of the beam piece.....	56
Figure 35: Velocity of a beam piece with masses embedded in rubber coating with the Shore hardness of ShA 40.....	57
Figure 36: Velocity of 4 beam pieces with masses embedded in rubber coating with a Shore hardness of ShA 80 each.	58
Figure 37: Basic measurement set-up of a slender beam with discontinuities embedded in the neutral layer.....	61
Figure 38: Measurement set-up of a slender beam. Both ends of the beam are embedded into sand to reduce reflections.	63
Figure 39: Measurement equipment of a slender beam with the excitation point of the shaker in 1.25m distance to one end of the beam.....	64
Figure 40: The 5 th and 6 th position of rubber-coated masses out of the neutral layer on a slender beam.	64
Figure 41: Transfer mobility of 5 measurements carried out on a pure beam within one test sequence.....	65
Figure 42: Transfer mobilities of the mean of 5 measurements carried out on a pure beam and on the same beam with 10 holes.	66
Figure 43: Calculated ratio of the transfer mobility of a beam with 5 masses (distances 0.4m) and a calculated beam with 10 masses (distances 0.2m), normalised with the same beam without any inserts.....	67
Figure 44: Measured transfer mobility of a beam with 5 and 10 masses (distances 0.2 m and 0.4 m), normalised with the same beam with only holes.....	68
Figure 45: Ratio of the transfer mobility of beams with 5 masses (distances 0.4m).....	69
Figure 46: Ratio of the transfer mobility of a beam with 10 masses (distances 0.2m).....	70

Figure 47: Ratio of the transfer mobility of a beam with 10 masses (distances 0.2m) and 10 spring-masses, respectively.	72
Figure 48: 400 Hz to 10 kHz: Measurement results from the ratio of the transfer mobility, phase and coherence of measured beams without discontinuities, with 10 pure masses and with 10 low stiffened (sketch in the bottom left) and 10 high stiffened (sketch in the bottom right) rubber-coated masses.	75
Figure 49: 400 Hz to 10 kHz: Measurement results from the ratio of the transfer mobility, phase and coherence of 4 beams with 10 rubber-coated masses with low stiffness (sketches in the top) and high stiffness (sketches at the bottom), distributed in and out of the neutral layer (all ratios are normalised with the beam with only holes).	76
Figure 50: 400 Hz to 2 kHz: Measurement results from the ratio of the transfer mobility, phase and coherence of measured beams without discontinuities, with 10 masses and with 10 high and low stiffened rubber-coated masses.	77
Figure 51: 400 Hz to 2 kHz: Measurement results from the ratio of the transfer mobility, phase and coherence of 4 beams with 10 rubber-coated masses.	78
Figure 52: 1.5 kHz to 3 kHz: Measurement results from the ratio of the transfer mobility, phase and coherence of measured beams without discontinuities, with 10 masses and with 10 high and low stiffened rubber-coated masses.	79
Figure 53: 1.5 kHz to 3 kHz: Measurement results from the ratio of the transfer mobility, phase and coherence of 4 beams with 10 rubber-coated masses.	81
Figure 54: 2.5 kHz to 4 kHz: Measurement results from the ratio of the transfer mobility, phase and coherence of measured beams without discontinuities, with 10 masses and with 10 high and low stiffened rubber-coated masses.	82
Figure 55: 2.5 kHz to 4 kHz: Measurement results from the ratio of the transfer mobility, phase and coherence of 4 beams with 10 rubber-coated masses.	83
Figure 56: 3.5 kHz to 5 kHz: Measurement results from the ratio of the transfer mobility, phase and coherence of measured beams without discontinuities, with 10 masses and with 10 high and low stiffened rubber-coated masses.	84

Figure 57: 3.5 kHz to 5 kHz: Measurement results from the ratio of the transfer mobility, phase and coherence of 4 beams with 10 rubber-coated masses.....	85
Figure 58: 4.5 kHz to 6 kHz: Measurement results from the ratio of the transfer mobility, phase and coherence of measured beams without discontinuities, with 10 masses and with 10 high and low stiffened rubber-coated masses.....	86
Figure 59: 4.5 kHz to 6 kHz: Measurement results from the ratio of the transfer mobility, phase and coherence of 4 beams with 10 rubber-coated masses.....	87
Figure 60: 5.5 kHz to 7 kHz: Measurement results from the ratio of the transfer mobility, phase and coherence of measured beams without discontinuities, with 10 masses and with 10 high and low stiffened rubber-coated masses.....	88
Figure 61: 5.5 kHz to 7 kHz: Measurement results from the ratio of the transfer mobility, phase and coherence of 4 beams with 10 rubber-coated masses.....	89
Figure 62: Transfer mobility of three plates. With 5 circular arcs (213 inserts) in an angular range of 0° to 180°, with 5 circular arcs (71 inserts) in an angular range of 60° to 120° and without inserts. The inserts are pure masses.....	98
Figure 63: Transfer mobility of three plates. With 5 inserts in 1 line, with 5 circular arcs (53 inserts) and without inserts. In plate 2 the circular arcs are ordered in an angular range from 75° to 105°. The inserts are pure masses.....	100
Figure 64: Transfer mobility of three plates. With 5 circular arcs (53 inserts), with 10 circular arcs (108 inserts), and without inserts. The circular arcs are ordered in an angular range from 75° to 105°.....	101
Figure 65: Transfer mobility of three plates. With 10 circular arcs (108 inserts) in an angular range of 75° to 105°, with 10 circular arcs (214 inserts) in an angular range of 60° to 120° and without inserts.	102
Figure 66: Transfer mobility of 4 plates. Three of them with 10 circular arcs (214 masses, test point angle 90°, 120° and 150°), and one plate without inserts. The circular arcs are ordered in an angular range from 60° to 120°.....	103
Figure 67: Transfer mobility of three plates. Plate 1 with pure masses, plate 2 with mass- and spring-systems and one plate without inserts. 10	

circular arcs are ordered in an angular range from 60° to 120° and include 214 inserts each.....	104
Figure 68: Transfer mobility of three plates. Plate 1 with pure masses, plate 2 with mass- and spring-systems and one plate without inserts. 10 circular arcs are ordered in an angular range from 60° to 120° and include 214 inserts each.....	105
Figure 69: Transfer mobility of three plates. Plate 1 with pure masses, plate 2 with spring-mass systems and one plate without inserts. 10 circular arcs are ordered in an angular range from 60° to 120° and include 214 inserts each.....	106
Figure 70: Transfer mobility of three plates. Plate 1 with mass- and spring-systems (214 inserts), plate 2 with mass- and spring-systems (200 inserts) and one plate without inserts. 10 circular arcs are ordered in an angular range from 60° to 120.	107
Figure 71: Measurement set-up of the plate supported on thin shelves with an overlap of 20mm. The pure masses or elastically supported masses, respectively, are distributed in circles around the center point of the plate.....	110
Figure 72: Measurement set-up of the pre-tests with two different rubber materials.....	111
Figure 73: Measurement set-up of the pre-tests with a layer of PUR as damping material.	112
Figure 74: Frequency responses (FFT1 H1 $v_{\text{mass}}/a_{\text{Shaker}}$) of two elastically supported cylindrical masses with different rubber materials (PVC and PUR).	113
Figure 75: Plate out of acrylic glass (Plexiglass®) with three rings of pure masses, glued on both sides of the plate.	114
Figure 76: Plate out of acrylic glass (Plexiglass®) with three rings of pure masses, glued on both sides of the plate.	115
Figure 77: Measurement set-up of all measurements on the finite plate out of acrylic glass (Plexiglass®) with three rings of 12, 18 and 24 pure masses or elastically supported masses, respectively, glued on both sides of the plate.	116
Figure 78: Plate out of acrylic glass (Plexiglass®) with three rings of elastically supported masses glued on both sides of the plate.	117

Figure 79: Plate out of acrylic glass (Plexiglass®) with three rings of elastically supported masses.	118
Figure 80: Non-smoothed ratio of the transfer mobility in the center of the plate from three plates.	121
Figure 81: Smoothed ratio of the transfer mobility in the center of the plate from three plates.	123
Figure 82: Smoothed ratios of the transfer mobility on different positions of the plate with elastically supported masses.	125
Figure 83: Smoothed ratios of the transfer mobility on different positions of the plate with elastically supported masses.	126
Figure 84: Calculated transfer mobilities of a beam with 5 masses in distances of 0.2m with a doubled loss factor of the beam η_{beam} and a doubled Young's modulus E_{beam}	134
Figure 85: Transfer mobility of an infinite beam with 10 pure masses and 10 rubber-coated masses with different damping factors of the complex spring stiffness.	135
Figure 86: Nyquist plot of a measured beam piece with a high stiffened rubber-coated mass (80 ShA).	136
Figure 87: Transfer mobility of an infinite beam with 10 embedded masses in the neutral layer of default weight and 10 masses with half of the weight.	137